

การเตรียมฟิล์มซูเปอร์ไม่ชอบน้ำยวดึงด้วยการเคลือบจุ่มในภาวะที่มีอนุภาคนาโน



นางสาว สุนิสา จินดาสุวรรณ

ศูนย์วิทยทรัพยากร
จุฬาลงกรณ์มหาวิทยาลัย

วิทยานิพนธ์นี้เป็นส่วนหนึ่งของการศึกษาตามหลักสูตรปริญญาวิทยาศาสตรดุษฎีบัณฑิต

สาขาวิชาวัสดุศาสตร์ ภาควิชาวัสดุศาสตร์

คณะวิทยาศาสตร์ จุฬาลงกรณ์มหาวิทยาลัย

ปีการศึกษา 2551

ลิขสิทธิ์ของจุฬาลงกรณ์มหาวิทยาลัย

PREPARATION OF SUPER HYDROPHOBIC FILMS BY DIP COATING IN THE PRESENCE
OF NANO-PARTICLES



Miss Sunisa Jindasuwan

ศูนย์วิทยทรัพยากร

A Dissertation Submitted in Partial Fulfillment of the Requirements
for the Degree of Doctor of Philosophy Program in Materials Science

Department of Materials Science

Faculty of Science

Chulalongkorn University

Academic year 2008

Copyright of Chulalongkorn University

510030

Thesis Title	PREPARATION OF SUPER HYDROPHOBIC FILMS BY DIP COATING IN THE PRESENCE OF NANO-PARTICLES
By	Miss Sunisa Jindasuwan
Field of Study	Materials Science
Advisor	Pornapa Sujaridworakun, D.Eng
Co-Advisor	Associate Professor Supatra Jinawath, Ph.D. Siththisuntorn Supothina, Ph.D.

Accepted by the Faculty of Science, Chulalongkorn University in Partial
Fulfillment of the Requirements for the Doctoral Degree

S. Hannongbua
..... Dean of the Faculty of Science
(Professor Supot Hannongbua, Ph.D.)

THESIS COMMITTEE

Sirithan J.
..... Chairman
(Assistant Professor Sirithan Jiemsirilars, Ph.D.)

Pornapa Sujaridworakun
..... Advisor
(Pornapa Sujaridworakun, D.Eng)

Supatra
..... Co-Advisor
(Associate Professor Supatra Jinawath, Ph.D.)

S. Supothina
..... Co-Advisor
(Siththisuntorn Supothina, Ph.D.)

Dujreutai Pongkao Kashima
..... Examiner
(Dujreutai Pongkao Kashima, D.Eng)

Angkhana
..... External Examiner
(Angkhana Jaroenworarluck, D.Eng)

สุนิสา จินดาสุวรรณ : การเตรียมฟิล์มซูเปอร์ไม่ชอบน้ำด้วยวิธีการเคลือบจุ่มในภาวะที่มีอนุภาคนาโน. (PREPARATION OF SUPER HYDROPHOBIC FILMS BY DIP COATING IN THE PRESENCE OF NANO-PARTICLES) อ.ที่ปรึกษาวิทยานิพนธ์หลัก : อ.ดร.พรนภา สุจิตวรกุล, อ.ที่ปรึกษาวิทยานิพนธ์ร่วม : รศ.ดร.สุพัตรา จินาวัฒน์, ดร.สิทธิสุนทร สุโพธิณะ, 119 หน้า.

จากสมบัติทำความสะอาดตัวเองของใบบัวนำไปสู่การประยุกต์ใช้งานในด้านต่างๆ การเตรียมพื้นผิวที่ไม่ชอบน้ำด้วยวิธีเหมือนพื้นผิวใบบัวสามารถเตรียมได้จากการปรับปรุงสมบัติเคมีพื้นผิวร่วมกับการเพิ่มความขรุขระของพื้นผิว โดยเมื่อความขรุขระเพิ่มขึ้นและพลังงานพื้นผิวลดลงทำให้สมบัติไม่ชอบน้ำเพิ่มขึ้น

ในงานวิจัยนี้ จะทำการเตรียมฟิล์มใสที่มีสมบัติไม่ชอบน้ำด้วยวิธีบนพื้นผิวกระจก โดยเตรียมจากสองวิธี คือ วิธีประกอบฟิล์มชั้นต่อชั้นและวิธีไฮบริดอินทรีย์/อนินทรีย์โดยมีวัสดุที่ให้ความขรุขระอยู่ในรูปของอนุภาคและสารแขวนลอย โดยวิธีแรกจะเตรียมฟิล์มจากพอลิเอทิลีนโกลด์ พอลิอัลลิลลามีนไฮโดรคลอไรด์/พอลิอะคริลิกแอซิด โปเลียเออร์ อนุภาคของซิลิกา และสารละลายไซเลน ส่วนวิธีที่สองจะเตรียมฟิล์มจากการผสมพอลิเมอร์เมทริกซ์กับสารละลายไซเลนและวัสดุที่ให้ความขรุขระ สภาวะที่ดีที่สุดจากวิธีประกอบฟิล์มชั้นต่อชั้นและวิธีไฮบริดอินทรีย์/อนินทรีย์ให้ฟิล์มที่มีมุมสัมผัสสูงสุดที่ 174 และ 166 องศา มีพลังงานพื้นผิวต่ำที่ 1 และ 4 มิลลิจูลต่อตารางเมตรตามลำดับ ฟิล์มที่เตรียมได้จากทั้งสองวิธีมีความใส การยึดเกาะดี และมีความเสถียรต่อการใช้งานดี

ศูนย์วิทยทรัพยากร จุฬาลงกรณ์มหาวิทยาลัย

ภาควิชา.....วัสดุศาสตร์..... ลายมือชื่อนิสิต.....สุนิสา จินดาสุวรรณ.....
สาขาวิชา.....วัสดุศาสตร์..... ลายมือชื่ออ.ที่ปรึกษาวิทยานิพนธ์หลัก.....พรนภา สุจิตวรกุล.....
ปีการศึกษา.....2551..... ลายมือชื่ออ.ที่ปรึกษาวิทยานิพนธ์ร่วม.....สุพัตรา จินาวัฒน์.....
ลายมือชื่ออ.ที่ปรึกษาวิทยานิพนธ์ร่วม.....สิทธิสุนทร สุโพธิณะ.....

487 38619 23 : MAJOR MATERIALS SCIENCE

KEYWORDS : SUPERHYDROPHOBIC / FILMS / DIP COATING / PARTICLES

SUNISA JINDASUWAN : PREPARATION OF SUPER HYDROPHOBIC FILMS
BY DIP COATING IN THE PRESENCE OF NANO-PARTICLES. ADVISOR :
PORNAPA SUJARIDWORAKUN, D.Eng, CO-ADVISOR : ASSOC.PROF.
SUPATRA JINAWATH, Ph.D., SITTHISUNTORN SUPOTHINA, Ph.D., 119 pp.

Self-cleaning property of the lotus leaf is attractive for practical application. To create a superhydrophobic surface as observed at surface of the lotus leaf, modification of surface chemistry is always combined with surface roughness enhancement. Increasing surface roughness and decreasing surface free energy lead to an increase of hydrophobicity.

In this present study, the transparent superhydrophobic films were coated on glass surface by two methods: layer-by-layer deposition of the polyelectrolyte multilayer and dip coating of the organic/inorganic hybrid films. Both types of film consisted of oxide particles as surface roughening materials which were employed either as a particulate or sol form. In the first method, the films were prepared by coating of the polyelectrolyte PAH/PAA bilayers, followed by silica and semi-fluorinated silane layers. In the latter, the films were prepared by mixing the semi-fluorinated silane and surface roughening material with the polymer matrix. The highest contact angle of 174 and 166 degrees, and low surface free energy at 1 and 4 mJ/m² were obtained from the polyelectrolyte multilayer and hybrid films, respectively. Both types of film were transparent, and had good adhesion and good stability.

Department : Materials Science

Field of Study : Materials Science

Academic Year : 2008

Student's Signature : *Sunisa Jindasunan*

Advisor's Signature : *Pornapa Sujaridworakun*

Co-Advisor's Signature : *J. P.*

Co-Advisor's Signature : *S. Supothina*

ACKNOWLEDGEMENTS

I would like to gratefully acknowledge Office of the higher education commission for a scholarship during my doctoral study. I would like to express my sincere gratitude to Dr. Sitthisuntorn Supothina and Dr.Pornapa Sujaridworakun for their helpful guidance, suggestion and encouragement throughout this study. I am grateful to Associate Professor Supatra Jinawath for useful comments. I would like to thank the National Metal and Materials Technology for providing financial support and instruments. Finally, I would like to thank to my family, my teachers, my friends and my colleagues; Miss On-uma Nimiitrakoolchai and Miss Ramida Ratanakam for their helpful and valuable assistance throughout the entire course of research, and Mr. Nithi Atthi for a Minitab program for the Taguchi's DOE study.



ศูนย์วิทยทรัพยากร
จุฬาลงกรณ์มหาวิทยาลัย

CONTENTS

	Page
ABSTRACT (THAI)	iv
ABSTRACT (ENGLISH)	v
ACKNOWLEDGMENT.....	vi
CONTENTS.....	vii
LIST OF TABLES.....	x
LIST OF FIGURES.....	xi
CHAPTER I: INTRODUCTION.....	1
CHAPTER II: LITERATURE REVIEW.....	4
2.1 Wettability and contact angles.....	4
2.2 Contact angle models.....	7
2.3 Structures of natural superhydrophobic surfaces.....	10
2.4 Literature reviews.....	13
CHAPTER III: EXPERIMENTAL PROCEDURES.....	26
3.1 Film deposition by layer-by-layer method.....	26
3.1.1 Reagents.....	27
3.1.2 Film deposition.....	27
3.1.2.1 Effect of etching condition.....	28
3.1.2.2 Effect of particulate type.....	28
3.1.2.3 Effect of number of PAH/PAA bilayer.....	29
3.2 Hybrid organic/inorganic films.....	29
3.2.1 Organic/inorganic hybrid film containing oxide particulate.....	29
3.2.1.1 Reagents.....	29
3.2.1.2 Film deposition.....	30
3.2.1.3 Optimization of parameter by Taguchi method.....	31
3.2.2 Organic/inorganic hybrid film containing oxide sol.....	32
3.2.2.1 Reagents.....	32
3.2.2.2 Film deposite.....	33

	Page
3.2.2.3 Effect of TIP:PDMS ratio.....	33
3.3 Characterization.....	34
3.3.1 Thermal property.....	34
3.3.2 Surface topology and film's thickness.....	34
3.3.3 Surface morphology.....	35
3.3.4 Film's hydrophobicity.....	35
3.3.5 Film adhesion.....	35
3.3.6 Optical properties.....	36
3.3.7 Film stability.....	36
3.3.8 Surface free energy.....	36
CHAPTER IV: RESULTS AND DISCUSSION.....	39
4.1 Surface characterization of glass substrate.....	39
4.2 Film deposition via layer-by-layer method.....	41
4.2.1 Effect of etching condition.....	41
4.2.2 Effect of particulate type	48
4.2.3 Effect of number of polyelectrolyte bilayers.....	61
4.2.4 Film adhesion.....	69
4.2.5 Surface free energy.....	71
4.3 Film formation by organic/inorganic hybrid method.....	81
4.3.1 Organic/inorganic hybrid films containing oxide particulate.....	81
4.3.1.1 Optimization of parameter by Taguchi method.....	81
4.3.1.2 Film topography.....	84
4.3.1.3 Film stability.....	85
4.3.1.4 Film adhesion.....	86
4.3.1.4 Surface free energy.....	88
4.3.2 Organic/inorganic hybrid films containing oxide sol	88
4.3.2.1 Effect of TIP:PDMS ratio.....	89
4.3.2.2 Effect of heat treatment.....	89
4.4 Comparison polyelectrolyte multilayer and hybrid organic/inorganic films.....	93

	Page
CHAPTER V: CONCLUSIONS.....	95
SUGGESTION FOR FUTURE WORK.....	97
REFERENCES.....	98
APENDICES.....	106
APENDIX A Classification of adhesion test results.....	107
APENDIX B Adhesion test results from tape test.....	109
BIOGRAPHY.....	119



ศูนย์วิทยทรัพยากร
จุฬาลงกรณ์มหาวิทยาลัย

LIST OF TABLES

Table	Page
3.1	Factors and the correspondent level of the factors..... 31
3.2	Designed controlling factors with different levels by Taguchi's DOE..... 32
3.3	Surface free energy and dispersion and polar components of liquid..... 37
4.1	Summary of the water contact angle and surface roughness of each layer..... 47
4.2	Contact angle and surface roughness (scanning area 5 μm x 5 μm) of the films containing different type and amount of SiO_2 nanoparticles..... 54
4.3	Summary of the water contact angle and surface roughness of etched polyelectrolyte bilayer..... 64
4.4	Adhesion test result from tape test..... 69
4.5	Values of contact angle and Owen – Wendt's method surface energy of the films containing different type and content of SiO_2 particle..... 73
4.6	Values of contact angle and Chibowski's method surface energy of the films containing different type and content of SiO_2 particle..... 74
4.7	Values of contact angle, surface energy of solid and surface free energy between solid and liquid obtained from the films containing different type and content of SiO_2 particle..... 80
4.8	Optimized condition Taguchi DOE analysis..... 82
4.9	Values of contact angle and surface roughness of the films obtained at different heating temperature..... 92
4.10	Comparison of the polyelectrolyte multilayer and hybrid films. The listed values are at the optimum condition for each coating method..... 94
A.1	Classification of adhesion test results..... 108

LIST OF FIGURES

Figure		Page
2.1	Drop configurations for measurement of contact angle (a) equilibrium drop (b) advancing and (c) receding drop.....	5
2.2	Water droplets on different wettability characteristic solid surfaces.....	6
2.3	Schematic illustrations of Young, Wenzel and Cassie's models.....	8
2.4	A microscopic SEM image of a lotus leaf showing the two-scale roughness.....	11
2.5	Slip of water droplet from (a) an inclined hydrophobic surface where the water drop crawls over the dust particles and (b) an inclined superhydrophobic surface where the dust particles are collected and taken away: self cleaning.....	12
2.6	SEM images of superhydrophobic surfaces made by roughening PDMS-based materials (a) PDMS surface treated by CO ₂ -pulsed laser (b) lotus-like surface by nanocasting (c) PS-PDMS/PS electrospun fiber mat and the droplet on it and (d) PS-PDMS surface cast from a 5 mg/ml solution in dimethylformamide in humid air.....	15
2.7	SEM images of TiO ₂ /PDMS hybrid films with various PDMS content (a) 0 (b) 40 and (c) 60%wt.....	17
2.8	FE-SEM micrographs of (a) top-view and (b) cross-section of 47% v/v silica.....	18
2.9	SEM images of films prepared by one-step method with various weight of SiO ₂ A200 (a) 14.4% (b) 37.6% (c) 75.2% and SiO ₂ H70 (d) 14.4% (e) 37.6% and (f) 75.2%.....	19
2.10	(a) Photograph of water droplet and (b) AFM image of the superhydrophobic SiO ₂ nanoparticle films.....	21
2.11	(a) AFM image of PAH/PAA-coated ZrO ₂ multilayer film with 5 nm ZrO ₂ nanoparticles and SEM images of films with deposit cycles (b) 5 (c) 10 and (d) 20, respectively.....	23

Figure	Page
2.12	Surface free energy of PMMA/filler films calculated from contact angle hysteresis..... 24
3.1	Flow chart of film deposition by a LBL method..... 28
3.2	Flow chart of film deposition for the organic/inorganic hybrid film containing oxide particle..... 30
3.3	Flow chart for deposition of organic/inorganic film containing oxide particle derived from suspension..... 33
4.1	AFM topographical mapping and water droplet image of bare glass substrate..... 39
4.2	SEM images of 3 polyelectrolyte bilayers etched with HCl solution (a) pH 1.0 for 3 h (b) 2.3 for 3 h and (c) pH 1.0 for 1.5 h followed by pH 2.3 for 1.5 h..... 42
4.3	AFM topographical mapping and water droplet image of polyelectrolyte 3 bilayers (a) before and after etching with HCl Solution having a pH of (b) 1.0 (c) pH 2.3 for 3 h and (d) combination between pH1.0 and 2.3 each 1.5 h..... 43
4.4	AFM topographical mapping and water droplet image of deposited nanosilica Aerosil [®] 200 on etched polyelectrolyte 3 bilayers by HCl solution (a) pH 1.0 (b) pH 2.3 for 3 h and (c) combination between pH 1.0 and 2.3 each 1.5 h..... 44
4.5	a) Before and (b) after deposition of Aerosil [®] 200 and silane treatment 45
4.6	TEM images of (a) Aerosil [®] 200 (b) Aeroperl [®] 300/30 and (c) Aeroperl [®] 806/30..... 50
4.7	(a) SEM image of the etched polyelectrolyte bilayers and (b-d) SEM images of the water-repellent films by which surface roughness was created by dipping into Aerosil [®] 200 suspension at a solid content of 0.05, 1 and 5 %wt, respectively..... 51
4.8	SEM image of the water-repellent films by which surface roughness was created by dipping into Aeroperl [®] 300/30 suspension at a solid

Figure	Page
	content of (a) 0.05 (b) 1 and (c) 5 %wt..... 52
4.9	Drawing of water droplet on (a) film containing Aerosil® 200 and (b) Aeroperl® 300/30..... 54
4.10	2-Dimensional (left) and 3-dimensional (right) topographical images of the films containing (a) 0.05 (b) 1 and (c) 5 %wt of Aerosil® 200..... 55
4.11	2-Dimensional (left) and 3-dimensional (right) topographical images of the films containing (a) 0.05 (b) 1 and (c) 5 %wt of Aeroperl® 300/30... 56
4.12	2-Dimensional (left) and 3-dimensional (right) topographical images of the films containing (a) 0.05 (b) 1 and (c) 5 %wt of Aeroperl® 806/30... 57
4.13	Transmittance of bare glass substrate and the glass substrate coated with films containing 0.05, 1 and 5 %wt of (a) Aerosil® 200 (b) Aeroperl® 300/30 and (c) Aeroperl® 806/30..... 59
4.14	SEM images of etched films containing PAH/PAA with (a) 1 (b) 3 (c) 10 and (d) 20 bilayers..... 62
4.15	AFM height images of the film containing PAH/PAA (a) 2 bilayers and (b) 4 bilayers at thickness 36 and 51 nm, respectively..... 64
4.16	Relationship between hydrophobicity and number of PAH/PAA bilayers..... 65
4.17	Relationship between wavelength and percent transmittance of glass substrate, 1, 3, 5, 10 and 20 bilayers..... 66
4.18	Relationship between number of bilayers and film stability..... 67
4.19	Film containing Aeroperl® 806/30 at 5%wt before tape test..... 69
4.20	Film containing Aeroperl® 806/30 at 5%wt after tape test..... 69
4.21	Relationship between (a) hydrophobicity and roughness and (b) hydrophobicity and surface energy from Owen-Wendt method of film containing Aerosil® 200, Aeroperl® 300/30 and Aeroperl® 806/30..... 74
4.22	Relationship between (a) hydrophobicity and roughness and (b) hydrophobicity and surface energy from Chibiowski method of films containing Aerosil® 200, Aeroperl® 300/30 and Aeroperl® 806/30..... 75

Figure		Page
4.23	Diagram of work between liquid/liquid and solid/liquid.....	76
4.24	Schematic illustration of surface free energy between vapor liquid and solid.....	78
4.25	Main effects plot for S/N ratios to contact angle (A: cotiox, B: Aerosil [®] 200, C: Aeroperl [®] 300/30, D: Aeroperl [®] 806/30 and E: TiO ₂ 25)	82
4.26	AFM topographical mapping of hybrid organic/inorganic film prepared from best condition.....	83
4.27	AFM height images of the hybrid film containing 5%wt Aerosil [®] 200 at thickness 692.5 nm.....	84
4.28	Relation between contact angle and keeping duration.....	85
4.29	Film containing Aerosil [®] 200 at 5 %wt before tape test.....	86
4.30	Film containing Aerosil [®] 200 at 5 %wt after tape test.....	86
4.31	Effect of TIP:PDMS molar ratio on surface hydrophobicity	88
4.32	TGA profile of the sample prepared from the precursor having the TIP:PDMS ratio 1.0:1.5.....	89
4.33	AFM topographical images of the PDMS-based hybrid films coated on glass substrate heat-treated at 60 – 200 °C.....	90
B.1	Film containing Aerosil [®] 200 at 0.05 wt% before tape test.....	109
B.2	Film containing Aerosil [®] 200 at 0.05 wt% after tape test.	109
B.3	Film containing Aerosil [®] 200 at 1 wt% before tape test.	110
B.4	Film containing Aerosil [®] 200 at 1 wt% after tape test.	110
B.5	Film containing Aerosil [®] 200 at 5 wt% before tape test.	111
B.6	Film containing Aerosil [®] 200 at 5 wt% after tape test.	111
B.7	Film containing Aeroperl [®] 300/30 at 0.05 wt% before tape test.....	112
B.8	Film containing Aeroperl [®] 300/30 at 0.05 wt% after tape test.....	112
B.9	Film containing Aeroperl [®] 300/30 at 1 wt% before tape test.....	113
B.10	Film containing Aeroperl [®] 300/30 at 1 wt% after tape test.....	113
B.11	Film containing Aeroperl [®] 300/30 at 5 wt% before tape test.....	114
B.12	Film containing Aeroperl [®] 300/30 at 5 wt% after tape test.....	114

Figure		Page
B.13	Film containing Aeroperl [®] 806/30 at 0.05 wt% before tape test.....	115
B.14	Film containing Aeroperl [®] 806/30 at 0.05 wt% after tape test.....	115
B.15	Film containing Aeroperl [®] 806/30 at 1 wt% before tape test.....	116
B.16	Film containing Aeroperl [®] 806/30 at 1 wt% after tape test.....	116
B.17	Film containing Aeroperl [®] 806/30 at 5 wt% before tape test.....	117
B.18	Film containing Aeroperl [®] 806/30 at 5 wt% after tape test.....	117



ศูนย์วิทยทรัพยากร
จุฬาลงกรณ์มหาวิทยาลัย

CHAPTER I

INTRODUCTION

1.1 Background

Many surfaces in nature such as the surface of butterfly wings and plant leaves are highly water-repellent and superhydrophobic, and therefore exhibit self-cleaning property [1-4]. Lotus leaf is the most famous example among the natural superhydrophobic surfaces. Inspired by the water-repellent natural surfaces, synthetic superhydrophobic surfaces having water contact angle larger than 150 degrees have been extensively explored by chemists and materials scientists during the past decade. Water-repellent property of the superhydrophobic surface can be applied to glass windows of automobile and building, micro-fluidic channel, anti-biofouling coating, anti-rusting and functional films [3-5].

Basically, water-repellency of the surface is governed by two factors. The first one is a chemical factor of the solid surface and the liquid with a very low surface energy. The other is a geometrical factor with an increase in the surface roughness [3-17]. It is well known that water contact angle on a smooth hydrophobic surface does not exceed 120 degrees [6, 10-11, 17]. Therefore, reduction of surface chemistry is always combined with surface roughness enhancement to achieve the superhydrophobicity.

Low surface energy can be achieved by coating the surface of interest with low surface energy substances or by mixing them with other coating materials. Examples of low surface energy substances include fluorocarbons, fluorinated polymers such as polytetrafluoroethylene, perfluoroalkylsilane, paraffin wax, alkyltrialkoxysilane, polysiloxane, and polydimethylsiloxane [3-5, 12-27].

The superhydrophobic surfaces can be fabricated by various methods, including chemical vapor deposition, electrodeposition, phase separation, plasma

polymerization, lithographic patterning, electrospraying, sol-gel coating, organic/inorganic hybrid coating and electrostatic self-assembly [4-5, 9-10, 17, 27-36]. However, some of these methods are either expensive, substrate limited, required the use of harsh chemical treatments, or not easily scaled-up to create large-area uniform coatings [35].

In this research, two types of the superhydrophobic films - layer-by-layer deposited polyelectrolyte multilayer and organic/inorganic hybrid – were prepared. All the films were deposited on glass substrates by dip coating method. Films' properties such as hydrophobicity, morphology, topology, optical property, thickness, film adhesion, film stability and surface energy were extensively studied. Relationships between the hydrophobicity, surface roughness and surface energy are discussed.

1.2 Objectives of Research

1.2.1 To fabricate the polyelectrolyte multilayer and organic/inorganic hybrid superhydrophobic films by dip coating method.

1.2.2 To investigate the parameters affecting the superhydrophobic property.

1.3 Scope of Research

Two types of the superhydrophobic films were fabricated: layer-by-layer polyelectrolyte multilayer and organic/inorganic hybrid films. The films were deposited on glass slide substrate by dip coating technique. For the polyelectrolyte multilayer film, effects of film preparation parameters such as etching condition, number of polyelectrolyte multilayer, type and content of oxide particulate on the film's property were extensively studied. For the organic/inorganic hybrid film, preparation parameters were optimized using a Taguchi's design of an experiment method. Films' properties

such as water contact angle as a measure of hydrophobicity, optical transmittance, surface roughness, stability, thickness, adhesion, surface energy were characterized.

1.4 Benefit of Research

The knowledge obtained from this research will enable ones to fabricate the water-repellent films by mimicking surface feature of natural superhydrophobic surface. It can be applied to not only glass substrate but also other solid surfaces. In addition, since the film deposition method developed in this work is a simple dip coating, the film can be coated on variety of shapes and sizes with no restriction on line of sight. Moreover, all chemicals employed are commercially available, and it is therefore feasible to scale up the process, especially for the organic/inorganic hybrid film.



CHAPTER II

LITERATURE REVIEW

Since the degree of superhydrophobicity is determined by contact angle, therefore in the beginning of this chapter, a theory of wettability and contact angle is described. There are three kinds of contact angle models; Young, Wenzel and Cassie's model. Next, the discovery of natural superhydrophobic phenomena is described following by a literature review on the development of the superhydrophobic surfaces.

2.1 Wettability and contact angle

Wettability remains as a research subject at the border between physics and chemistry [5]. It is crucial in many practical applications. Wettability may be quantitatively defined by reference to the contact angle of a water droplet on the surface (figure 2.1(a)). Contact angle has been widely studied for at least 200 years and well understood in many aspects. For a planar surface, the equilibrium contact angle can be measured very simply from the profile of droplet resting on the surface [37]. In practice, there are two types of contact angle values; static and dynamic contact angles.

The static contact angle may be determined by drawing a tangent to the profile at the point of three-phase contact after the droplet profile has been enlarged either by image projection or photography. It may also be measured directly using a telescope fitted with a goniometer eyepiece, or indirectly by measuring the angle at which light from a point source is reflected from the surface of a liquid droplet at its point of contact with the solid [38-39].

Another aspect to be considered when measuring contact angle is dynamic contact angle. It was measured during the growth (advancing contact angle) and shrinkage (receding contact angle) of a water droplet. The difference between advancing and receding contact angle is defined as contact angle hysteresis. The

observation of different values of contact angle may be depending upon whether the liquid droplet is advanced or withdrawn across the solid surface. Contact angle hysteresis arises from solid surfaces seldom being either smooth or chemically homogeneous [40-41]. The common methods of determining the advancing and receding angles are shown in Figure 2.1(b) and (c). In Figure 2.1(b) and (c) the liquid is advanced or withdrawn across the surface by increasing or decreasing the size of the liquid droplet, which is typically by a syringe. As discussed by Rance [42], it is best to let the needle remain in the droplet during measurements to avoid unnecessary vibration or distortion of the droplet. This does not affect the contact angle.



Figure 2.1 Droplet configurations for measurement of contact angle (a) equilibrium droplet (b) advancing and (c) receding droplet. L = liquid, V = vapor.

Depending on the value of the contact angle, surface properties are determined as hydrophilic (contact angle < 90 degrees) or hydrophobic (contact angle > 90 degrees). Partial wetting corresponds to contact angle < 90 degrees. For contact angle > 90 degrees the solid is not wetted by the liquid. Contact angle at 90 degrees is the transition between partial wetting and non-wetting case [43]. Surfaces with water contact angle higher than 150 degrees are superhydrophobic or ultrahydrophobic (with very little contact angle hysteresis) (Figure 2.2). As contact angle increases, the area of the liquid-solid interface shrinks and the interaction between the droplet and the solid surface weakens. This can eventually cause the droplet roll off or slide down the surface when a small force is applied, or the surface is slightly tilted.

The contact angle is also most widely employed to estimate solid surface free energy. Sharma and Rao [44] listed the main approaches for the estimation of surface free energy such as the Zisman [45], the Fowkes [46], Owens and Wendt [47] geometric mean approach, Wu [48] harmonic mean, Van Oss et. al. [49] the acid-base approach and the equation of state approach derived by Neumann et. al. [50] and Li and Neumann [51]. The Owens and Wendt approach (also known as the Owens-Wendt-Rabel-Kaelbe model) is commonly used to estimate surface free energies of complex surfaces (Castilho Pereira et. al. [52], Jacobasch et. al. [53]). It is efficient for comparison of various surfaces, which is importance for practical applications (Michalski et. al. [54]).



Figure 2.2 Water droplets on solid surfaces of different wettability characteristic.

Basically, the superhydrophobic surface is governed by two factors. The first is the chemical factor of the solid surface and the liquid with a very low surface energy. The other is the geometrical factor with increased surface roughness [3-17]. For the formation of superhydrophobic films, modification of surface chemistry is always combined with surface roughness enhancement.

For low surface energy substances, fluorine is the most effective element because of its small atomic radius and the biggest electronegativity among all atoms, so that a covalent bond could be formed with carbon to generate low surface energy of the surface [7, 17]. Hare et. al. reported that the surface energy increases when fluorine is replaced by other elements such as H and C, in the order of $-\text{CF}_3 < -\text{CF}_2\text{H} < -\text{CF}_2- < -$

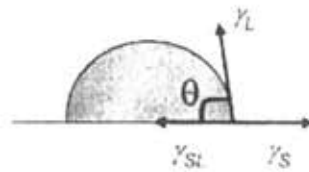
CH_3 < $-\text{CH}_2-$, and predicted that the closest hexagonal packing of $-\text{CF}_3$ groups on the surface would give the lowest surface energy of the materials [55]. Therefore, fluorocarbon polymers make excellent hydrophobic films and coatings. However, the adhesion between the substrate and the fluoro-based hydrophobic coating is formed by van der Waals force and it is very weak when such films are directly attached to the substrates. Thus, it is necessary to copolymerize with other monomers to offset this drawback. Many low surface energy materials were used such as fluorocarbon, fluorinated polymer, polytetrafluoroethylene, perfluoroalkylsilane, tetraethoxysilane, paraffin wax, alkyltrialkoxysilane, polysiloxane, and polydimethylsiloxane [3-5, 12-27].

Surface roughness can also change the contact angle as the chemicals do but through a different mechanism. It is well known that water contact angles on smooth hydrophobic surfaces are generally not exceeding 120 degrees. Contact angles of long chain hydrocarbon and fluorocarbon self-assembled monolayer are only 112 and 115 degrees, respectively [56]. However, the situation is quite different when the surface is rough [57]. An increased roughness results in an increased surface area and increased apparent surface energy. The contact angle needs to increase accordingly to balance the enlarged surface energy between the solid substrate and liquid droplet.

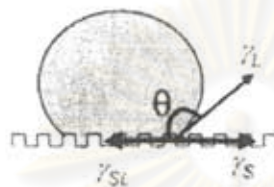
The methods that have been developed so far to enhance roughness of solid surfaces include mechanical abrasion, the addition of fillers, etching, wax solidification, anode oxidation, hot water immersion, chemical vapor deposition, phase separation, molding, printing, pyrolysis and lithography [4-5, 9-10, 17, 27-36].

2.2 Contact angle models

Wetting between solid and liquid is first described by Young [59]. However, it is suitable for a flat, smooth surface. Two models, the Wenzel's model and Cassie's model, have been put forward to explain the impact of surface roughness on wettability. Both Wenzel and Cassie droplets can be formed on the same roughness depending on how a droplet is formed [58]. The three models are shown in Figure 2.3.

Young's Eq.

$$\cos \theta = \frac{\gamma_s - \gamma_{sl}}{\gamma_l}$$

Wenzel's Eq.

$$\begin{aligned} \cos \theta &= \frac{r(\gamma_s - \gamma_{sl})}{\gamma_l} \\ &= r \cos \theta \end{aligned}$$

$$r = \frac{\text{Real Sa}}{\text{Apparent Sa}}$$

Cassie's Eq.

$$\cos \theta' = f \cos \theta + (1-f) \cos 180^\circ$$



$$= f \cos \theta + f - 1$$

f : Area fraction of solid surface

Figure 2.3 Schematic illustrations of Young, Wenzel and Cassie's models [5].

In the first model, the wettability of a flat surface expressed by contact angle of a water droplet is given by Young's equation. Young's paper describing his equation appeared in 1805 [59]. The contact angle (θ) is defined by

$$\cos \theta = \frac{\gamma_{sv} - \gamma_{sl}}{\gamma_{lv}} \quad (2.1)$$

where θ is contact angle, γ_{sv} , γ_{sl} and γ_{lv} are the interfacial surface tensions with solid, liquid and gas, respectively. Young's angle is a result of thermodynamic equilibrium of the free energy at the solid-liquid-vapor interphase. However, this equation can be applied only to a flat surface.

It is now known that there are typically two states in which a droplet can reside on a given rough surface [58]. The droplet either sits on the peaks of the surface roughness or it wets the grooves, depending on how it is formed. The droplet that sits on the peaks has air pockets along its contact with the substrate. The contact angle of the droplet that wets the grooves is given by Wenzel's model while the contact angle of a droplet that sits on the roughness peaks is given by Cassie's model.

Several models describing the contact angle at the rough solid surface have been proposed so far. Wenzel proposed a theoretical model describing the contact angle at the rough surface [60]. He modified Young's equation as follows

$$\cos \theta^w = r \cos \theta \quad (2.2)$$

where θ^w corresponds to the apparent contact angle, r represents the roughness factor and θ refers to Young's angle. The roughness factor is defined by the actual surface area divided by the projected surface area. In the Wenzel's regime, the contact angle and its hysteresis increase as the roughness factor increases for a hydrophobic surface.

The decrease in the contact angle hysteresis is attributed to the switch from the Wenzel to the Cassie state because of the increased air fraction leading to the water droplet on top of the protrusions, and is therefore in contact with both solid and air pockets trapped between the protrusions [61]. In the Cassie's model, the apparent contact angle is the sum of all the contributions of the different phases as described by

$$\cos \theta^c = f_1 \cos \theta_1 + f_2 \cos \theta_2 \quad (2.3)$$

where θ^c is the apparent contact angle, f_1 and f_2 are surface fraction of phase 1 and 2, respectively; θ_1 and θ_2 are contact angle of phase 1 and phase 2, respectively. For a rough surface containing only one type of asperities, given f is the solid fraction, then the air fraction is $(1 - f)$. With $\theta = 180$ degrees for air, the resulting contact angle can be calculated by the following equation

$$\cos \theta^c = f(1 + \cos \theta) - 1 \quad (2.4)$$

Thus, for the Cassie's model, the apparent contact angle is a sole function of solid fraction for a given surface with contact angle. Therefore, to obtain a superhydrophobic surface, the contribution of the solid part should be as small as possible or a solid material with very high contact angle should be used. In practice, the Cassie's model can not predict accurately the wetting behavior of a pre-designed surface. However, it is often used to compare it with a practical result in order to confirm the presence of the Cassie state.

In summary, both theories can predict the contact angle of a rough surface only qualitatively. Furthermore, it is not evident which theory should be used and when. Therefore, it would be very important to obtain some guidelines for predicting the surfaces behavior, which is critical in designing superhydrophobic surfaces. Thus, many research interests have been devoted to modeling superhydrophobic surfaces.

2.3 Structures of natural superhydrophobic surface

Many surfaces in nature are highly hydrophobic and exhibit self-cleaning property [1-4]. Examples include the wings of butterflies and the leaves of some plants. Inspired by water-repellent natural surfaces, superhydrophobic surfaces having a water contact angle larger than 150 degrees have been extensively studied by chemists and materials scientists during the past decade. Their potential applications are automobile glass, building materials, microfluid channels, antibiofouling paint, anti-rusting and functional films [3-5].

Lotus leaves are one of the most famous examples among the natural superhydrophobic surfaces [1, 4]. The water contact angle of a lotus leaf is 161 ± 2.7 degrees with contact angle hysteresis of only 2 degrees. Picture of the lotus leaf obtained by Barthlott and Neihuis is shown in Figure 2.4 [1]. The structure of the lotus leaf consists of a combination of a two-scale roughness; one around $10 \mu\text{m}$ (roughness structure) and the other around 100 nm (fine structure). These surfaces are also referred to as hierarchical micro- and nano-structure. The hydrophobicity of the lotus leaf arises

from the epicuticular wax secreted by the lotus itself. The wax has a contact angle of 110 degrees, not highly hydrophobic. However, the lotus leaf still exhibits a superhydrophobic property. It is presumed that this combination of roughness and wax contribute to the superhydrophobicity of the lotus leaf. The rolling off of water droplets and collecting the contaminants from the lotus leaf is dubbed as the "lotus effect". The lotus leaf therefore always exhibits a very low degree of contamination which is regarded as self cleaning.

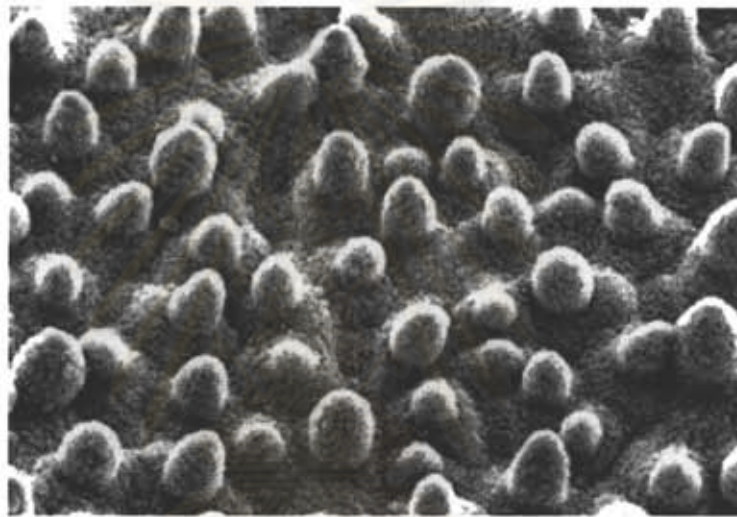


Figure 2.4 A microscopic SEM image of a lotus leaf showing the two-scale roughness.

The self cleaning effect is evident for the lotus leaf. The underlying mechanism has been thoroughly studied. At the interface between a viscous fluid and a solid surface, usually, a nonslip boundary condition dominates [62]. Slip on the boundary can occur on the scale of a few tens of nanometers, which is not appreciated for macroscopic flow. However, when the droplet moves down a tilted rough superhydrophobic surface, due to the high contact angle (minimized contact between the fluid and surface), effective macroscopic slip occurs on scales consistent with the characteristic size of the surface features. For the droplet of water rolling off a lotus leaf, the droplet behaves as an elastic ball rather than a fluid (Figure 2.5). In case of a normal hydrophobic surface, because of the nonslip boundary condition, the water droplet falls across the dirt particles and the dirt particles are mainly displaced to the sides of the

droplet and re-deposited behind the droplet. Especially hydrophobic particles tend to remain on such surface (Figure 2.5(a)). In the case of water-repellent rough surfaces, the solid/water interface is minimized. Water forms a spherical droplet, and collects the particles from the surface (Figure 2.5(b)).

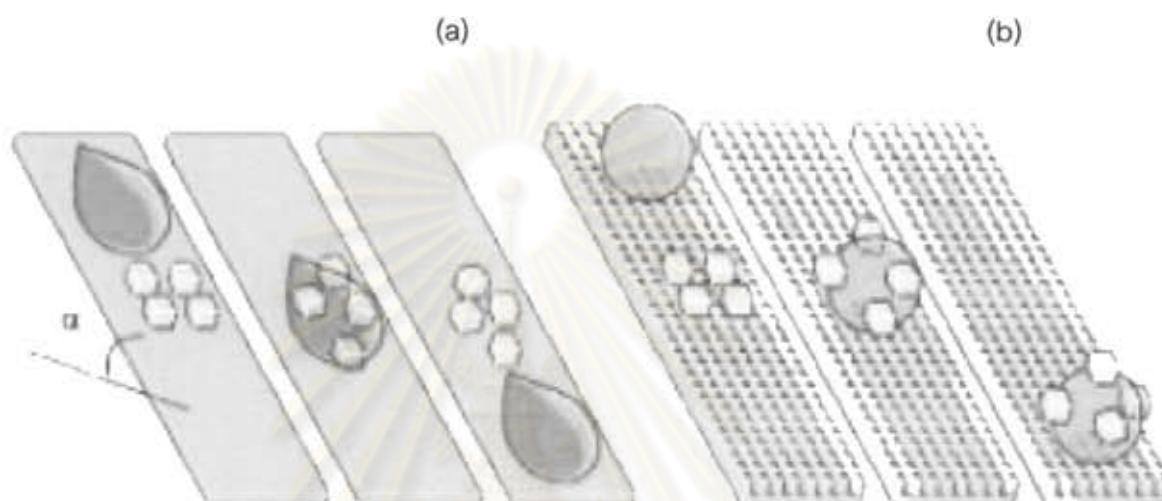


Figure 2.5 Slip of a water droplet from a) an inclined hydrophobic surface where the water drop crawls over the dust particles and b) an inclined superhydrophobic surface where the dust particles are collected and taken away: self-cleaning.

ศูนย์วิทยทรัพยากร
จุฬาลงกรณ์มหาวิทยาลัย

2.4 Literature reviews

As mentioned in section 2.3, the best known example of superhydrophobic surface is the lotus leaf. Barthott and Neinhuis discovered the context between the chemical and structural nature of the lotus leaf surface and its strong water repellent and self cleaning properties [1]. Numerous studies have confirmed that this combination of surface roughness and low surface free energy materials leads to water contact angle higher than 150 degrees. Controlling the wetting of the surfaces is an importance problem relevant to many areas of technology. The interest in self-cleaning surfaces is being driven by the desire to make non-wettable surfaces for potential applications.

The first artificial superhydrophobic surface was demonstrated in the mid-1990s by Onda et. al. [63]. This article reported a super-water-repellent surface made of alkylketene dimmer. Water droplet on this surface has a contact angle as large as 174 degrees. A wide variety of methods have been developed by mimicking this effect. The methods include a chemical vapor electrodeposition, electric deposition, phase separation, plasma polymerization, lithographic patterning, electrospray, sol-gel synthesis, organic/inorganic hybrid method and layer-by-layer deposition method [4-5, 9-10, 17, 27-36]. Most of the methods disclosed to date, however, are either expensive, substrate limited, require the use of harsh chemical treatments, or cannot be easily scaled-up to create large-area uniform coatings [35]. Water repellent coatings have been achieved by different methods using hydrophobic materials such as fluorocarbon, fluorinated polymer, polytetrafluoroethylene, perfluoroalkylsilane, tetraethoxysilane, other silanes, paraffin wax, alkyltrialkoxysilane, polysiloxane, polydimethylsiloxane and other chemicals [3-5, 12-27].

Techniques to make the superhydrophobic surfaces can be simply divided into two categories: making a rough surface from a low surface energy material and modifying a rough surface with a material of low surface energy. In this section, recent publications on the field of superhydrophobicity are reviewed, and their major results are presented.

For the first categorized techniques, the superhydrophobic surfaces are generated via producing rough surface from inherently low surface materials [3-5, 12-27]. A well-known material with low surface energy is polydimethylsiloxane (PDMS). Because of its intrinsic deformability and hydrophobic property, the PDMS can readily be made into superhydrophobic surfaces using various methods. For example, Khorasani et. al. treated the PDMS using CO₂-pulsed laser as an excitation source [64]. The water contact angle for the treated PDMS was as high as 175 degrees which was believed to be due to both the porosity and chain ordering on the PDMS surface (Figure 2.6(a)). Similarly, Jin et. al. used a laser etching method to make a rough surface of PDMS elastomer containing micro-, submicro- and nanocomposite structure [65]. Such a surface exhibited a superhydrophobicity with water contact angle higher than 160 degrees and sliding angle lower than 5 degrees. Sun et. al. recently reported a nanocasting method to make superhydrophobic PDMS surface [66]. They first made a negative PDMS template using lotus leaf as an original template and then used the negative template to make a positive PDMS template, a replica of the original lotus leaf. The positive PDMS template (Figure 2.6(b)) had the same surface structures and superhydrophobic as the lotus leaf. Given the difference in composition and consequent surface energy between the lotus leaf (paraffinic wax crystals, -CH₂-, 30-32 mJ/m²) and the PDMS replica (-CH₃-, 20 mJ/m²), the similarity of the hydrophobic obtained is surprising.

Another way to exploit the low surface energy of PDMS is to use a block copolymer such as poly(styrene-*b*-dimethylsiloxane) (PS-PDMS). For instance, Ma et. al. made a superhydrophobic membrane in the form of a nonwoven fiber mat by electrospinning a PS-PDMS block copolymer blended with PS homopolymer (Figure 2.6(c)) [67]. The superhydrophobic with water contact angle of 163 degrees was attributed to the combination of enrichment of PDMS component on fiber diameters (150 nm to 400 nm). The flexibility, breathability and free-standing feature of the membrane are of particular interesting in areas such as textile and biomedical applications. More recently, Zhao et. al. prepared a superhydrophobic surface by casting a micellar

solution of PS-PDMS in humid air based on the cooperation of vapor-induced phase separation and surface enrichment of PDMS block (Figure 2.6(d)) [68].

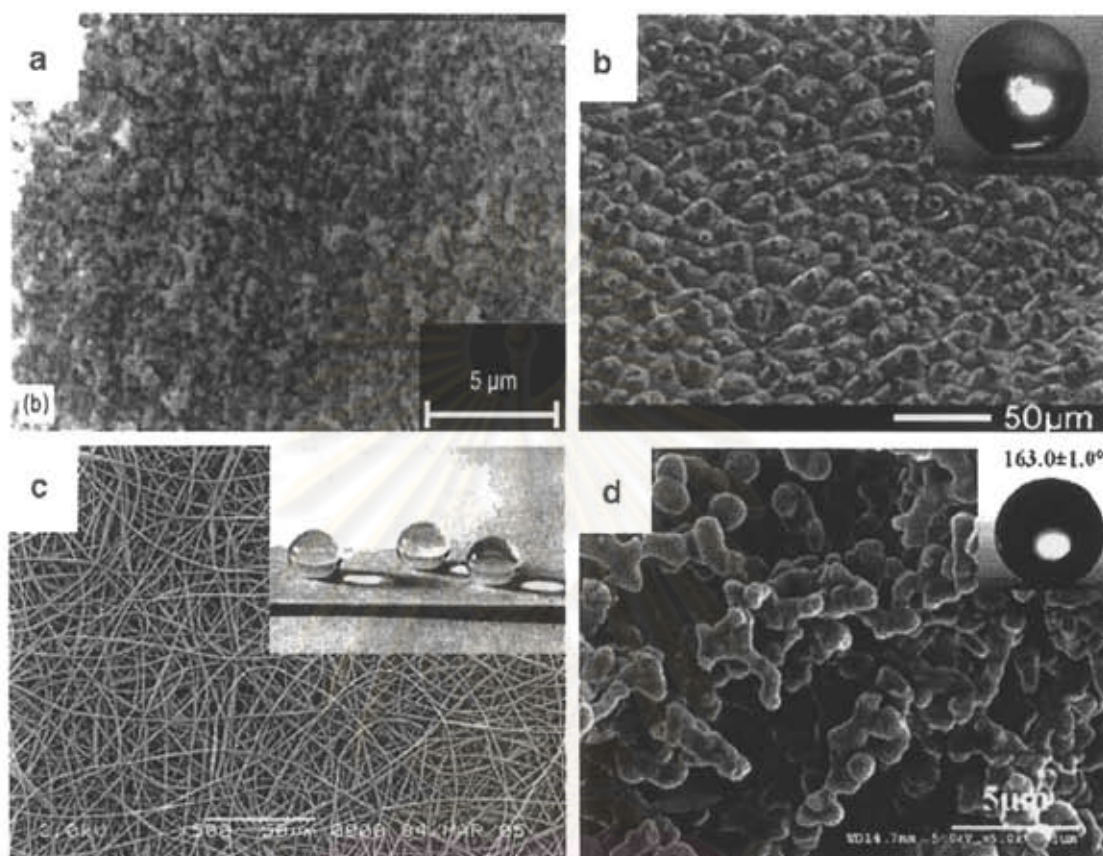


Figure 2.6 SEM images of superhydrophobic surfaces made by roughening PDMS-based materials. (a) PDMS surface treated by CO_2 -pulse laser [64], (b) lotus leaf-like PDMS surface by nanocasting [66], (c) PS-PDMS/PS electrospun fiber mat and the droplet on it [67], and (d) PS-PDMS surface cast from a 5 mg/ml solution in dimethylformamide in humid air [68].

The methods to make superhydrophobic surfaces by roughening low surface energy materials are mostly one-step processes and have advantage of simplicity. Many techniques reported by a totally different strategy such as making rough surface (not necessarily from low surface energy materials) and subsequent modifications of the surface chemistry or mixing roughening material with low surface energy matrix. Among these methods, the simple way to obtain hydrophobic surface is

hybrid organic/inorganic method. Moreover, the hybrid organic/inorganic materials are interested with possesses unique properties such as flexibility, thermal stability and environment stability because of synergistic properties between the inorganic and organic material [25]. The hybrid organic/inorganic films were prepared by low surface energy as organic polymer and surface roughness materials as inorganic particle. To enhance surface roughness, the matrix was mixed with inorganic particle as a direct particulate form or suspension form.

Previous studies have focused on preparation of a transparent organic/inorganic film and improve their mechanical property. Yamada et. al. have synthesized transparent PDMS-base hybrids using inorganic sources as metal alkoxides of Al (III), Ti (IV), Zr (IV), Nb (V) and Ta (V) and chemically modified with ethyl acetoacetate [23]. Ethyl acetoacetate bonded to metal alkoxides remained in hydrolyzed solutions and gels to prevent the rapid growth of large inorganic particles. The refractive index increased in the order of Al (III) < Zr (IV) \leq Ti (IV) < Ta (V) \leq Nb (V). Iketani et. al. prepared transparent TiO₂/poly(dimethylsiloxane) hybrid films by the same method. The films were highly transparent at transmittance > 90%, and amorphous TiO₂ in the films crystallized to anatase upon treatment at 100 °C for 1 h at an atmosphere [24]. They showed good photocatalytic activity for the decomposition of methylene blue and acetaldehyde, although the reactivity exhibited a slightly decreasing trend with the increase of PDMS content. Figure 2.7 shows SEM images of the TiO₂/PDMS hybrid films with various PDMS contents.

In order to perform indentation and scratch experiment, Douce et. al. prepared organic/inorganic hybrid films using silica colloids and polysiloxane. The objective is to find a compromise between an increasing in Young's modulus deduced from nanoindentation measurements and a deterioration of the scratch resistance observed in scratch test. The results showed that adding fillers increased the Young's modulus of the coatings in a significant way but decreased the scratch resistance [22].

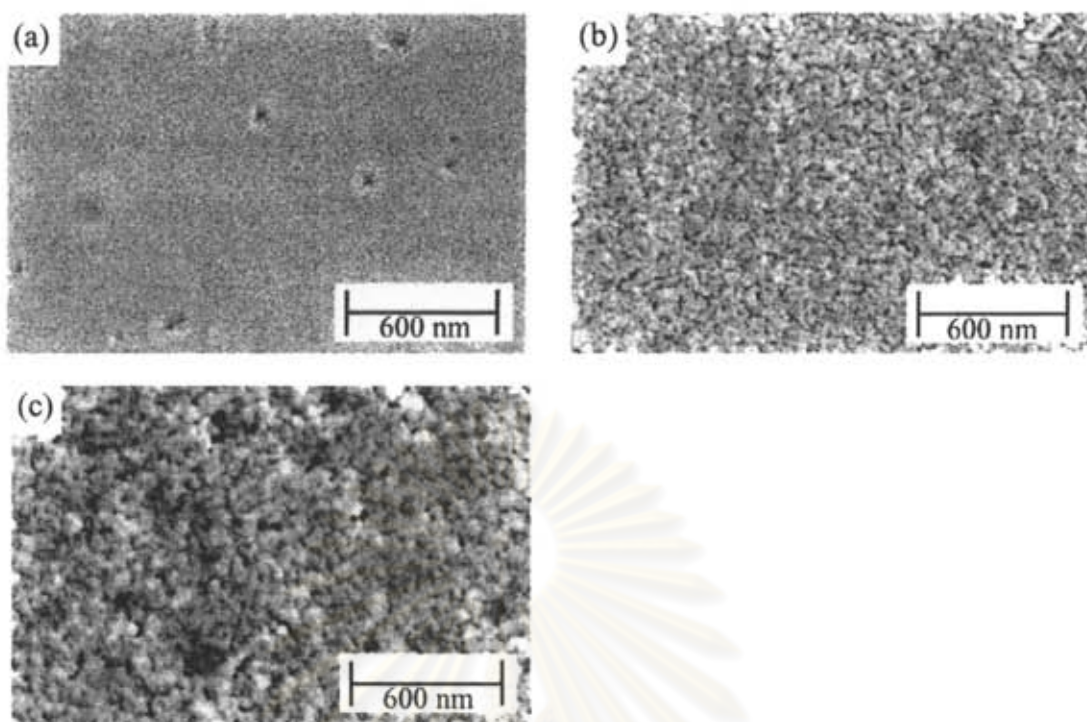
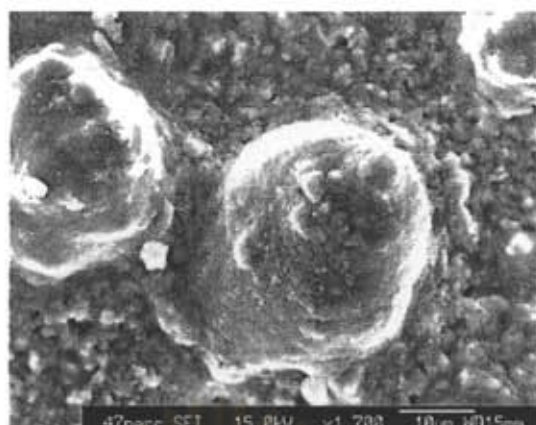
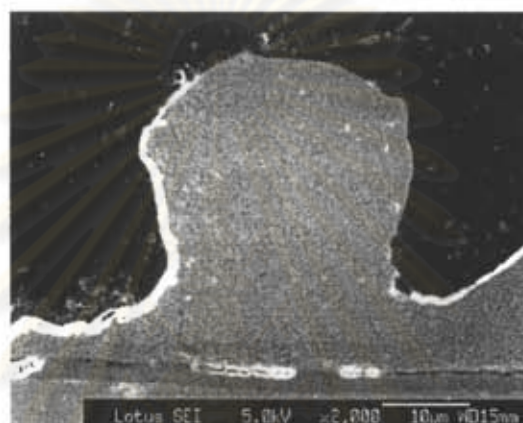


Figure 2.7 SEM images of TiO₂/PDMS hybrid films with various PDMS contents: (a) 0 (b) 40 and (c) 60 wt% [22].

However, for the previous studies of hybrid organic/inorganic method, the superhydrophobic surface was not obtained. The water contact angle was lower than 150 degrees. In recent years, the high contact angle just was obtained by modified chemical and physical routes. Wu et. al. reported an increasing hydrophobicity via chemical and morphological modification [16]. They modified surface morphology of the coating, a long side-chain alkyltrialkoxysilane, by adding a silica filler. The silica filler particles increased solid content of the coating, resulting in rough surface with a lotus-leaf-like structure (Figure 2.8). The silica filler improved the hydrophobic properties by increasing contact angles by 123 degrees. Then, they prepared hydrophobic coating by polydimethylsiloxane and tetraisopropoxide precursor and chemically modified with ethyl acetoacetate [26]. The water contact angle increased to a maximum of 133 degrees. The hardness was obtained by colloid silica with particles size of 20 nm. The hardness of coating increased with silica filler content and curing temperature. They optimized hydrophobic property and coating hardness at the same time.



(a)



(b)

Figure 2.8 FE-SEM micrographs of (a) top-view and (b) cross-section of 47% v/v silica. This microstructure analogous to that of the lotus leaf gives hydrophobic property [16].

Shindou et. al. prepared hybrid organic/inorganic films by polydimethylsiloxane and titanium tetra-isopropoxide precursor [25]. They focused on study an effect of composition on the film surface properties. The surface properties were discussed on the basis of the change of micro-domain structure with polydimethyl siloxane/titanium tetra-isopropoxide molar ratio. After heat treatment at 300 °C, the water contact angle was 115 degrees.

Many researchers have attempted to improve films' hydrophobic. Nakajima et. al. reported hard coating thin films that prepared by a phase separation of tetraethyl orthosilicate combined with an acrylic polymer and subsequent fluoralkylsilane coating [12]. The dominant mechanism of the hydrophobicity of the film was changed from Wenzel's mode to Cassie's mode with increasing surface roughness. The water

contact angle achieved was about 152 degrees. The film has high transmittance and its hardness was almost at the same level as normal silica-based hard coatings.

Zhang et. al. prepared the superhydrophobic materials by using fumed silica, alkyltrialkoxysilane and polysiloxane [20]. The water contact angle obtained was 169 degrees. It was utilized to control marine biofouling. Detail analysis indicated virtually no micro-organism attached to the superhydrophobic surfaces in the first week of immersion, while the uncoated smooth substrates exhibited fouling within a day. Chang et. al. reported the superhydrophobic films that prepared by TA-N fluoroalkylate and methyl methacrylate copolymer as water-repellent materials. Silica powder was added as surface roughness enhancer [17]. The contact angles obtained were greater than 160 degrees but the transmittance of the films was only 90%. The superhydrophobic films can be obtained by introducing roughening materials on the hydrophobic surface. Figure 2.9 shows SEM image of the films prepared by one-step method with various weight of SiO_2 .

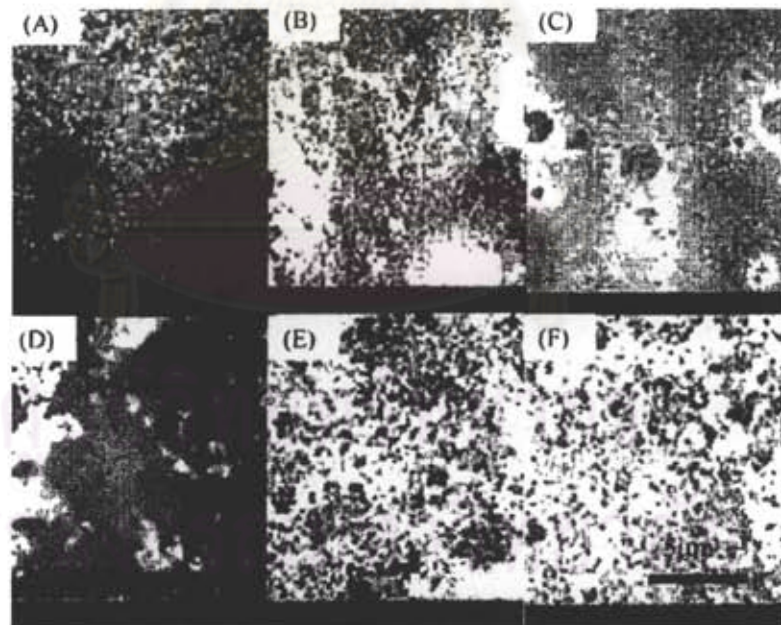


Figure 2.9 SEM images of the films prepared by one-step method with various weight of SiO_2 A200 (a) 14.4% (b) 37.6 % (c) 75.2 % and SiO_2 H70 (d) 14.4% (e) 37.6 % and (f) 75.2% [17].

Hsieh et. al. demonstrated the superhydrophobic surfaces that prepared from a perfluoralkyl methacrylic copolymer and titanium nanoparticles [19]. The influence of surface roughness on the performance of water-repellence was investigated. The maximum water contact angle was 164 degrees. To have super-repellency, the surface with more micropores is favorable because it consists of more air against wettability. Lin et. al. investigated the enhancement of water-repellency by the Taguchi and analysis of variance (ANOVA) methodologies [15]. The superhydrophobic surface was prepared by fluoromethylic copolymer and metal oxide nanoparticles. Seven operating factors including type of nanoparticle, solid ratio, dispersion time, F-binder, distance between nozzle and substrate, spray direction and layer number were considered. The contact angle of 161 degrees was obtained from the optimal condition.

The challenge in this field still remains the facile and cheap production of the superhydrophobic coatings with stability under the condition of use. To obtain films' stability for practical use, Nakajima et. al. reported that the addition of only a few percent of TiO_2 photocatalyst effectively provided a self-cleaning property to the superhydrophobicity films and maintained high contact angles during long period of outdoor exposure [13]. However, one of the problems is the stain accumulating on the rough surface. The most plausible driving force for the initial contamination of the surface coated with fluorocarbon is the electrostatic effect. Thus, the decrease of static electricity by lowering surface electric resistance to superhydrophobic films is one of the fundamental approaches to improve durability of the superhydrophobic film. Sasaki et. al. have prepared the superhydrophobic films with a low surface electric resistance through the use of an original process, then evaluated its property including durability during outdoor exposure [14]. Ming et. al. presented the superhydrophobic films that were stable under exposition of the surfaces to water overnight [29]. The superhydrophobic films were prepared from silica-based raspberry-like particles that were covalently bonded to an epoxy-based polymer matrix. The roughened surface was chemically modified with a layer of polydimethylsiloxane. The obtained contact angle was 165 degrees.

The use of a layer-by-layer deposition method for thin film has very recently been reported for making superhydrophobic surfaces [8, 35]. These studies address the critical issue of inducing surface roughness, which is required for superhydrophobic behavior. Seono et. al. described a multilayer polyelectrolyte/silica nanoparticles system. The film was heated to sinter the particles and burn off the polymer, and then treated with a fluorosilane to meet the required superhydrophobicity [8]. The film had a contact angle of large than 160 degrees. They found that nanostructured surface affected wettability and water-repellency generated due to rough structure at the nanoscale that caused the low contact between water and surface on liquid-solid interface. Therefore, it was shown that surface wettability was controllable by designing surface nanostructures. Figure 2.10 shows photograph of water droplets placed on the film, and AFM image of the surface.

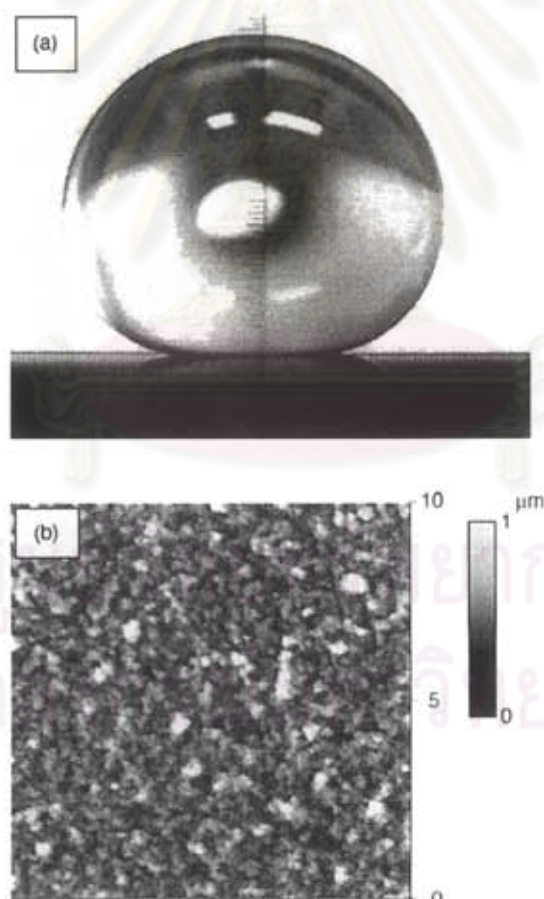


Figure 2.10 (a) Photograph of water droplet and (b) AFM image of the superhydrophobic SiO_2 nanoparticle films [8].

Some studies reported the methods for preparation of the superhydrophobic films by combination of a polyelectrolyte multilayer with other technique. For instance, Zhang et. al. reported the use of the polyelectrolyte multilayer as a performed matrix in electrochemical deposition of gold cluster onto the indium tin oxide (ITO). After chemisorption of a self-assembled monolayer of n-dedecanethiol, the superhydrophobic surface was obtained [32]. They combined the layer-by-layer and electrochemical deposition to fabricate the superhydrophobic surface. The water contact angle obtained was about 160 degrees. Zhao et. al. also combined the layer-by-layer and electrochemical deposition to fabricate the superhydrophobic surface [9]. They deposited Ag aggregated on the multilayer, on which further chemisorption of a monolayer of n-dodenethiol took place to make the superhydrophobic surface. The obtained water contact angle was 154 degrees. Morphology of the Ag aggregates can be adjusted by electrodeposition time and potential. Harris et. al. described a cross-linking of layered poly(allylamine hydrochloride)(PAH)/poly(acrylic acid)(PAA) films via heat induced amide formation [31]. Unlike many layered polyelectrolyte films, these cross-linking, nylon-like films were stable over a wide pH range and highly impermeable. Results of cyclic voltammetry and impedance spectroscopy analysis showed that film permeability decreased dramatically after cross-linking and it also depended on heating condition.

Zhai et. al. reported the formation of a pH-sensitive multilayer which underwent a porosity-inducing phase transition in acidic solutions [35]. Additional treatment steps, including cross-linking, deposition of silica nanoparticles, fluorosilane treatment, and thermal annealing, yielded stable superhydrophobic materials. They focused on reproducing the lotus effect, whereby micrometer-sized surface features were decorated with nanometer-sized wax particles. Jirs et. al. demonstrated a method of generating the superhydrophobic surfaces from a novel combination of fluorinated polyelectrolytes and natural nanorods [34]. They created surface roughness on two scales; micrometer and nanometer but using particles inserted as layers in a multilayer process. This surface had a contact angle of 168 degrees. However, the immobile

droplets were very hard to obtain. They believed that the droplet had been loosely pinned by a defect.

Hou et. al. fabricated the superhydrophobic surface on zinc substrate [7]. A superhydrophobic ZnO nanorod films were fabricated from zinc metal and subsequent modified with a monolayer of n-octadecyl thiol. The water contact angle was 153 degrees. The results confirmed that both the surface roughness and the low surface energy coating were the two cooperative factors in making the superhydrophobicity. Han et. al. presented a process for fabrication of a superhydrophobic coating via a multilayer polyelectrolyte and ZrO_2 nanoparticles [36]. After deposition of silica nanoparticles and a simple fluorination of the surface, superhydrophobic behavior was observed. Moreover, the chemical stability of the film was greatly increased by heat-induce cross-linking of the film. The incorporation of ZrO_2 nanoparticles in the superhydrophobic films improved mechanical properties. Figure 2.11 shows the films containing ZrO_2 particles with two different particle diameters, 5 and 100 nm.

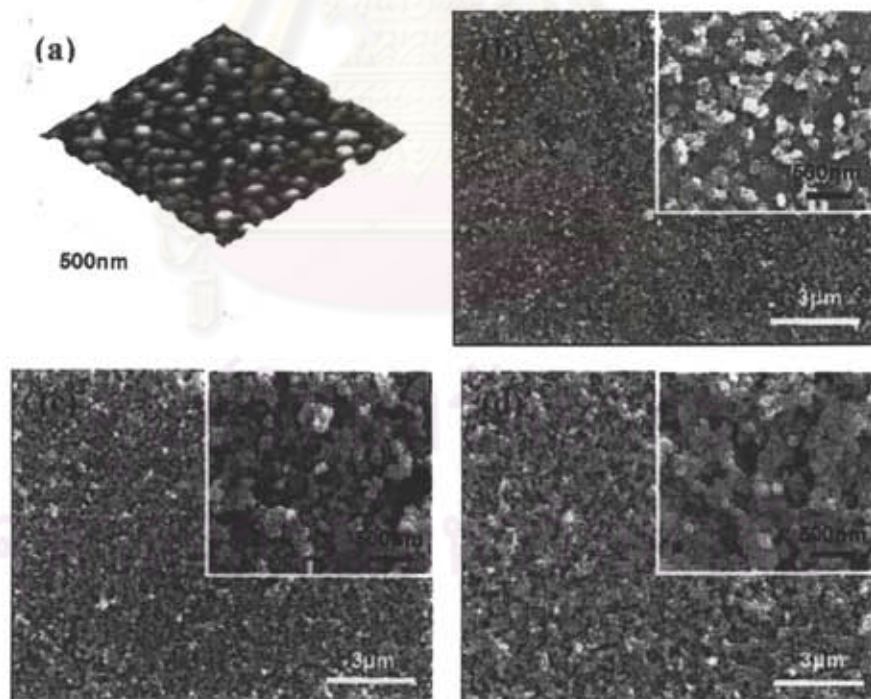


Figure 2.11 (a) AFM image of the PAH/PAA-coated ZrO_2 multilayer film with 5 nm ZrO_2 nanoparticles, and SEM images of the films with deposited cycles of (b) 5 (c) 10 and (d) 20, respectively. Insets in (c) and (d) show higher magnification images [36].

Many efforts have been made to theoretically evaluate the design criteria for optimizing the superhydrophobic effect in terms of contact angle, contact angle hysteresis and surface energy. Pullin et. al. presented surface energy characteristics of poly(1H, 1H, 2H, 2H-perfluorodecanoyl diitaconate) film structures as calculated from a contact angle measurement on droplets of water, diiodomethane and ethylene glycol [69]. The contact angle measurement demonstrated that the films had good hydrophobicity. However, for biofouling application, the films showed limited resistance to colonization by marine organism.

Chibowski calculated surface energy of a solid surface from contact angle hysteresis [70]. The contact angle hysteresis was discussed basing on the literature data of dynamic advancing and receding contact angles of n-alkanes and n-alcohols on surface of FC-732 film deposited on a silicon plate. Dispersion free energy and total surface free energy determined from the advancing contact angle and the hysteresis, respectively. For further studies, Chibowski et. al. reported that polymethyl methacrylate films adhering to glass surface could show hydrophobic effect [71]. In order to vary roughness of the films, different fillers such as titanium dioxide, alumina, silica, glass beads, Teflon and polypropylene grains were used. The results showed that the contact angles on films containing the polypropylene were around 140 degrees. The calculated surface energy was only 5-8 mJ/m^2 which was low. Figure 2.12 shows surface free energy of the PMMA/filler films.

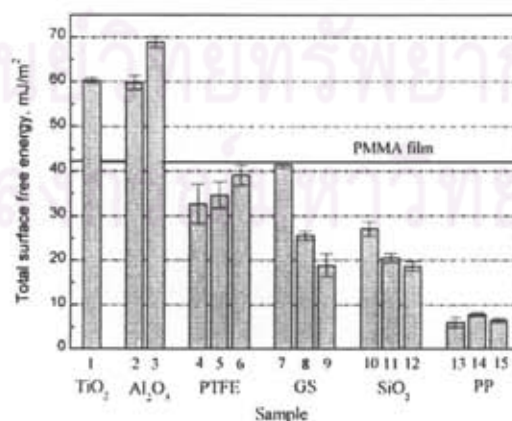


Figure 2.12 Surface free energy of the PMMA/filler films calculated from contact angle hysteresis. The solid line marks the energy value for filler-free PMMA film [71].

Extrand reported the wetting behavior of a series of polyamides surface [72]. The polyamides with varying amide content and polyethylene were molded against glass to produce rough surface. It was found that contact angle decreased with amide content while the hysteresis increased. Free energies of hysteresis were calculated from contact angles. He et. al. reported a quantitative investigation of the hysteresis of the Cassie and Wenzel droplets on a given rough surface [58]. The Cassie droplet showed much less hysteresis compared to a Wenzel droplet, and it was therefore preferred for application involving moving the droplets. Results from experimental measurements were compared with the results from various theoretical models for the contact angles, and recommendations were made. Li and Amirfazli studied a free energy thermodynamic analysis that significantly simplified calculation of free energy barrier associated with contact angle hysteresis [73]. They demonstrated that the predicted contact angle hysteresis and equilibrium contact angles were consistent with experimental observations and predictions of Wenzel's and Cassie's equations, respectively. Although a large number of fabrication techniques for superhydrophobic coatings have been published. Relationship between hydrophobicity, surface roughness and surface energy was scarcely reported.



ศูนย์วิทยทรัพยากร
จุฬาลงกรณ์มหาวิทยาลัย

CHAPTER III

EXPERIMENTAL PROCEDURE

As mentioned in chapter 2, degree of hydrophobicity can be controlled by modifying the surface roughness and surface energy. For the hydrophobic materials such as silicone, polyethylene, polystyrene, etc., the superhydrophobic surface can be obtained by enhancing a surface roughness. For other materials such as glass, ceramic, wood, etc., the superhydrophobic surface can be obtained either by creating a rough surface followed by coating with low-surface energy layer, or coating the flat surface with low-surface energy layer possessing a suitable surface roughness.

In this research, the superhydrophobic films were deposited on glass slide substrates. Since an optical transparency of the glass must be retained, the superhydrophobic surface cannot be achieved by creating a surface roughness directly on the glass surface since it will become translucent. Instead, the transparent films containing low surface energy substance and roughness enhancing filler were deposited. Based on this concept, the superhydrophobic films were prepared by two methods: layer-by-layer (LBL) deposition and organic/inorganic hybrid method. Details of film preparation by each method are described below.

3.1 Film deposition by layer-by-layer (LBL) method

The use of the LBL deposition for thin film has recently been reported for making the superhydrophobic surfaces [8, 35]. These studies address the critical issue of inducing surface roughness, which is required for true superhydrophobic behavior. In this present study, the deposition method was modified from the work of Zhai et. al. which employed a dip coating for the deposition of polyelectrolyte bilayer and a chemical vapor deposition (CVD) for the deposition of the outermost silane layer [35]. This present study employs only a dip coating in all steps which makes it easier to apply

the technique for larger substrate. More importantly, the dip coating has no limitation on line of sight as the CVD technique has.

3.1.1 Reagents

All of reagents used in the experiment were analytical grade or equivalent. They were used without any further purification. The reagents employed for preparation of precursor solutions were poly(allylamine hydrochloride) (PAH, MW = 70,000, Aldrich), poly(acrylic acid) (PAA, MW = 100,000, Aldrich), trichloro(1H, 1H, 2H, 2H-perfluorooctyl) silane (97%, Aldrich), hydrochloric acid (37%, Merck) and hexane (99%, Lab scan).

Three types of SiO₂ particles were employed to modify surface roughness: Aerosil[®] 200 (JJ degussa, average particle size of 12 nm), Aeroperl[®] 300/30 (JJ degussa, average particle size of 30 μm) and Aeroperl[®] 806/30 (JJ degussa, average particle size of 30 μm). Both the Aerosil[®] 200 and Aeroperl[®] 300/30 are hydrophilic, while the Aeroperl[®] 806/30 is hydrophobic. Almost all solutions were prepared using de-ionized water. Only Aeroperl[®] 806 was dispersed in hexane.

3.1.2 Film deposition

The glass slide substrate cut into 2.5 cm x 4.0 cm in size was cleaned by ultrasonication in ethanol, acetone and de-ionized water, respectively and then dried at 100°C. The first layer which was the PAH was deposited by dipping the cleaned substrate in 0.01 M PAH solution (adjusted to pH of 8.7 using 1 M NaOH) for 15 min, withdrawing at a speed of 0.1 mm/sec and rinsing twice with de-ionized water. Then, the PAA layer was deposited by dipping the PAH-coated substrate in 0.01 M PAA solution (pH = 3.3) for 15 min, withdrawing at a speed of 0.1 mm/sec followed by rinsing twice with de-ionized water. This dipping cycle gave 1 bilayer of the PAH/PAA. The dipping cycle was repeated several times to achieve several PAH/PAA bilayers. Desired surface roughness was created by etching the PAH/PAA film with HCl solutions at pH of 2.3 and 1.1, respectively, each for 180 min. The etched film was heated at 180°C for 2 h. Then, SiO₂ particles were deposited onto the etched film by dipping the sample into a suspension of SiO₂ particle. Finally, the sample was dipped into the PAH then solution of

0.01 M trichloro(1H, 1H, 2H, 2H-perfluorooctyl) silane followed by cross-linking at 180 °C for 2 h. The flow chart of film deposition is shown in Figure 3.1.

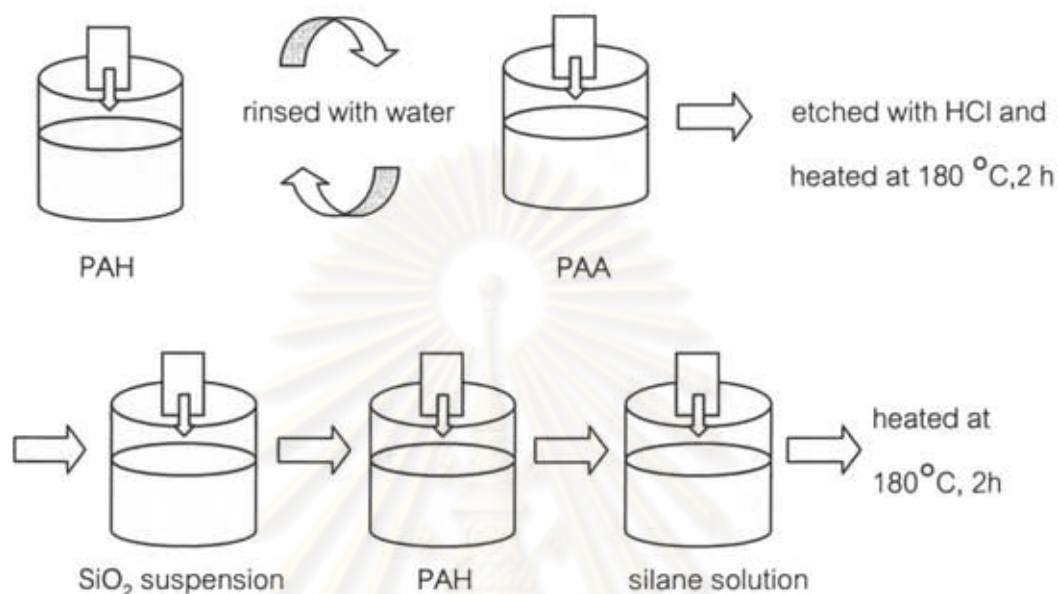


Figure 3.1 Flow chart of film deposition by a LBL method.

3.1.2.1 Effect of etching condition

Since etching of the PAH/PAA bilayers film resulted to open porosity for subsequent deposition of the SiO₂ particles which in turn affected surface roughness of the final film, it is noteworthy to study an effect of etching condition on film's property. Three PAH/PAA bilayers films were etched with HCl solutions at various conditions: pH of 1.1 for 180 min, pH of 2.3 for 180 min, and combination of pH 2.3 and 1.1, for 1.5 h each. The etched PAH/PAA films were heated at 180 °C for 2 h. Then, SiO₂ particles were deposited onto the etched films by dipping them into a suspension of Aerosil® 200 SiO₂. Finally, the samples were dipped in solutions of PAH and trichloro(1H, 1H, 2H, 2H-perfluorooctyl) silane followed by cross-linking at 180 °C for 2 h.

3.1.2.2 Effect of particulate types

As mentioned that surface roughness was created by deposition of SiO₂ particles, three types of SiO₂ particles having different particle size as well as

surface functionality were utilized to make a SiO₂ suspension to study their effects on film's roughness. They were the Aerosil® 200 having average particle size of 12 nm and bearing hydrophilic functionality, the Aeroperl® 300/30 having average particle size of 30 µm and bearing hydrophilic functionality, and the Aeroperl® 806/30 having average particle size of 30 µm and bearing hydrophobic functionality. These SiO₂ particles were deposited onto 3 PAH/PAA bilayers etched with HCl solutions at pH of 2.3 and 1.1, respectively, each for 1.5 h as described in section 3.1.2.

3.1.2.3 Effect of number of PAH/PAA bilayer

To study an effect of number of PAH/PAA bilayers (i.e. effect of thickness) on the film's property, the PAH/PAA bilayers was deposition for 1, 3, 5, 10 and 20 cycles to obtain 1, 3, 5, 10 and 20 bilayers, respectively. To obtain desirable roughness, they were etched with HCl solutions at pH of 2.3 and 1.1, respectively, each for 180 min. Finally, the Aerosil® 200 SiO₂ particles and trichloro(1H, 1H, 2H, 2H-perfluorooctyl) silane were deposited onto the etched PAH/PAA layers as described in section 3.1.2.

3.2 Film deposition by organic/inorganic hybrid method

The hybrid organic/inorganic materials are of interest since they possess unique properties such as flexibility, thermal stability and environment stability because of synergistic properties between the inorganic and organic material. Hybrid organic/inorganic films were prepared from low surface energy polymer matrix and surface roughness enhancer metal oxide particle. The polymer matrix was mixed with oxide particle which was used either as particulate form or sol form.

3.2.1 Organic/inorganic hybrid film containing oxide particulate

3.2.1.1 Reagents

All of reagents used in the experiment were analytical grade or equivalent. They were used without any further purification. The reagents employed for preparation of organic/inorganic hybrid film containing oxide particulate were MH1107

(> 60 wt% methyl hydrogen siloxane and 1-5 wt% methyl hydrogen cyclosiloxanes, Dow corning), hexane (99%, Lab scan) and trichloro(1H, 1H, 2H, 2H-perfluorooctyl) silane (97%, Aldrich).

Five types of oxide fillers were used to modify surface roughness. They were Aerosil[®] 200 SiO₂ (average particle size 12 nm, JJ degussa), Aeroperl[®] 300/30 SiO₂ (average particle size 30 μm, JJ degussa) and Aeroperl[®] 806/30 SiO₂ (average particle size 30 μm, JJ degussa). Cotiox TiO₂ (average particle size 250 - 300 nm, Cosmochemical Industrial) and P25 TiO₂ (average particle size 20-30 nm, JJ degussa).

3.2.1.2 Film deposition

Coating solution was prepared by dissolving 1 g of MH1107 in hexane. Then, oxide particle was dispersed in the coating solution at a ratio of 0.01, 5 and 10 wt%. Finally, 1 ml of simifluorosilane solution prepared by dissolving 0.12 ml of trichloro(1H, 1H, 2H, 2H-perfluorooctyl) silane in isopropanol was added into the suspension. The film was deposited by dipping glass substrate in coating solution and withdrawing at a speed of 0.1 mm/sec. Finally, the film was heated at 180°C for 1 h.

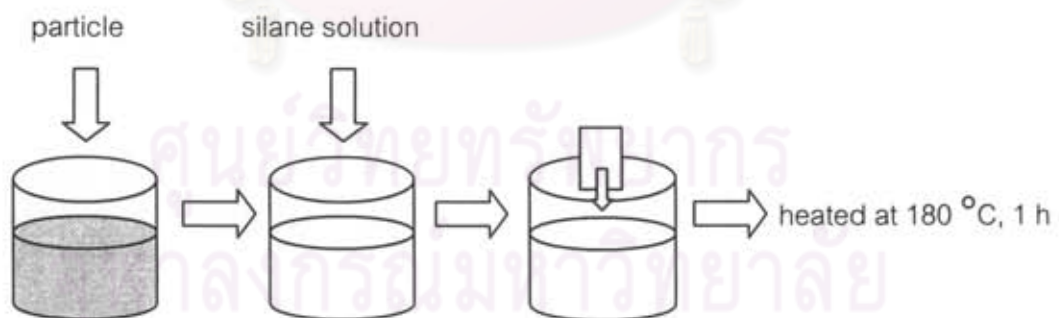


Figure 3.2 Flow chart of film deposition for the organic/inorganic hybrid film containing oxide particle.

3.2.1.3 Optimization of parameter by Taguchi method

For film deposition by layer-by-layer method, synthesis parameter in each layer can be optimized separately. However, the organic/inorganic hybrid film containing oxide particle was deposited by only 1 dipping step from one single precursor. Therefore, it is essential to find the optimum condition for some important parameters which in this case are types and amount of oxide particle, and withdrawing speed of the dip coater. To reduce a number of experimental run, an experimental design called "Taguchi's design of an experiment method (Taguchi's DOE)" was adopted. All factors affecting the film's property was divided into two types; control factor and noise factor. Three controlling factors; type of particulate, solid ratio and withdrawing speed were considered to play significant effect on hydrophobicity.

The ranges of parameters were selected based on the previous knowledge. Five types of oxide particle, three solid ratios and three withdraw speeds were selected. Therefore, fifteen experiments were operated. The ratio of signal-to-noise (S/N ratio) is defined according to the Taguchi method:

$$\eta = S / N = -10 \log \left[\frac{1}{n} \sum_{i=1}^n Y_i^2 \right] \quad (3.1)$$

where η denotes the observed S/N value, and Y_i represents the contact angle according to the experimental results. Table 3.1 summarizes the three parameters that were varied at several levels selected based on previous studies. Table 3.2 shows the controlling factors with different levels that were designed by using the Taguchi's DOE.

Table 3.1 Factors and the correspondent level of the factors.

Controlling Factors (units)	Level 1	Level 2	Level 3	Level 4	Level 5
A: Type of nanoparticle	Cotiox	Aerosil [®] 200	Aeroperl [®] 300/30	Aeroperl [®] 806/30	TiO ₂ P25
B: Solid ratio (%wt)	0.01	5	10		
C: Withdrawing speed (mm/sec)	0.01	0.5	1		

Table 3.2 Designed controlling factors with different levels by the Taguchi's DOE.

There is 15 conditions were employed to find optimum condition.

Oxide types	Solid ratio	Withdrawing speed (mm/sec)
Cotiox	0.01	0.01
Cotiox	5	0.5
Cotiox	10	1
Aerosil® 200	0.01	0.5
Aerosil® 200	5	1
Aerosil® 200	10	0.01
Aeroperl® 300/30	0.01	1
Aeroperl® 300/30	5	0.01
Aeroperl® 300/30	10	0.5
Aeroperl® 806/30	0.01	0.5
Aeroperl® 806/30	5	1
Aeroperl® 806/30	10	0.01
TiO ₂ P25	0.01	1
TiO ₂ P25	5	0.01
TiO ₂ P25	10	0.5

3.2.2 Organic/inorganic hybrid film containing oxide sol

3.2.2.1 Reagents

All of reagents used in the experiment were analytical grade or equivalent. They were used without any further purification. For organic/inorganic hybrid film containing oxide particle derived from liquid precursors, the following reagents were

employed. A hydroxyl-terminated polydimethylsiloxane (PDMS, MW = 4,392, Aldrich) was employed as organic matrix. A titanium tetraisopropoxide (TIP, 98%, Merck) was employed as an inorganic precursor for TiO_2 nanoparticle. 1-propanol (99%, Fisher scientific) was employed as a medium. Ethyl acetoacetate (EAcAc, 98%, Merck) was used to suppress hydrolysis reaction of titanium tetraisopropoxide.

3.2.2.2 Film deposition

Coating solution was prepared by dissolving TIP in 1-propanol and stabilized by addition of ethyl acetoacetate (EAcAc). Then, the PDMS dissolved in 1-propanol was added into the TIP solution at a molar ratio of PDMS:TIP being 1:1.5. Small amount of DI water was added into the resulting mixture to hydrolyze the TIP to form titanium oxide nanoparticle. Film deposition on glass substrate was performed by dip coating at a withdrawal speed of 0.01 mm/sec. The film was subjected to heat treatment at various temperatures for 2 h.

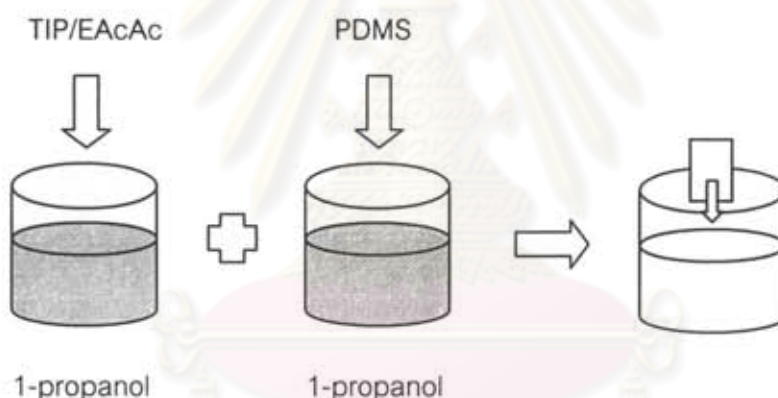


Figure 3.3 Flow chart for deposition of organic/inorganic hybrid film containing oxide particle derived from liquid precursors

3.2.2.3 Effect of TIP:PDMS ratio

To study the effect of TIP:PDMS ratio on film's property, the coating solution was prepared by dissolving TIP in 1-propanol and stabilized by addition of ethyl acetoacetate. Then, the PDMS dissolved in 1-propanol was added into the TIP solution having TIP: PDMS molar ratios of 1.0:0.5, 1.0:1.0, 1.0:1.5 and 1.0:2.0. Film deposition on glass substrate was performed by using a dip coater operated at a withdrawing speed of $0.01 \text{ mm}\cdot\text{sec}^{-1}$.

3.2.2.4 Effect of heat treatment condition

The effect of heat treatment on films' hydrophobicity was investigated. The films containing TIP: PDMS molar ratios of 1.0:1.5 were heat-treated at different 60, 100 and 200 °C for 2 h in ambient air.

3.3 Characterization

3.3.1 Thermal property

To study thermal stability of the PDMS, it was subjected to thermogravimetric (TGA) analysis (TGA7 Perkin Elmer) performed in the temperature range of room temperature to 600 °C at a heating rate of 10 °C·min⁻¹. A sample was placed in alumina pans left to hand in the furnace. The analysis was carried out under a nitrogen inert atmosphere.

3.3.2 Surface topology and films' thickness

Surface topological analysis was performed by using an atomic force microscopy (AFM, SPA 400 Seiko instruments) in a non-contact mode. The software provided by the manufacture was used to calculate a root-mean-square (*RMS*) roughness of the chosen scanned area.

The *RMS* roughness was chosen to quantify the film's surface roughness. The roughness profile has been filtered from the raw data and the mean line has been calculated as follow:

$$RMS = \sqrt{\frac{1}{n} \sum_{i=1}^n y_i^2} \quad (3.2)$$

where *RMS* is the root-mean-square roughness, *n* is spaced point along the trace, and *y_i* is the vertical distance from the mean line to the *ith* data point.

The AFM was also used to measure the film thickness. Steps were produced on the film. The thickness was determined by scanning The AFM tip across the revealed step between the film and glass substrate. A height was assigned to be positive in the up direction away from the bulk material.

3.3.3 Surface morphology

The films' morphology was examined by using a scanning electron microscope (SEM, Hitachi S-3200N) operated at a 5.0 kV acceleration voltage. To prepare the sample for SEM observation, the glass substrate coated with film was attached to a standard SEM stub. The film was gold coated by using a gold coater (JEOL JFC-1200) to reduce electric charge.

3.3.4 Films' hydrophobicity

The films' hydrophobicity was measured at room temperature by using a goniometer (ramé-hart). The static contact angle measurement was repeated at least five times at different locations on the film's surface using a microsyringe. Images of water droplets on the film's surface were recorded using a CCD camera and then a curvature profile at the left and right contact angles was created using the software provided by the manufacturer. Finally, the contact angle was measured.

The dynamic contact angle was measured in terms of water advancing and receding contact angle. Advancing and receding contact angle measurements were performed using the same apparatus as in the case static contact angle. All the advancing and receding angle values was recorded during drop volume increase and decrease, respectively.

3.3.5 Film adhesion

For practical application, the hydrophobic films must adhere to the substrate for the expected service life. With the proceeding hydrophobicity, the excellent adhesion exists between the coating and substrate that was desired. To study the adhesion property between the coating and glass substrate, A standard ASTM: D

3359 – 02 tape test was used to measure the adhesion based on percent area removed. This test method covers a procedure for the adhesion of coating film to metallic or glass substrates by applying and removing a pressure – sensitive tape over cuts made in the film (Appendix A). It is the most appropriate method that was designed to assess the adhesion of coating films to substrates by applying and removing an adhesive tape over the films. Images of these films before and after tape testing were taken by using an optical microscope to evaluate the films' adhesion. Adhesion was rated based on the amount of coating removed by the tape. It is reported as percent of the squares remaining on the films.

3.3.6 Optical properties

Films' Transparency was measured by using a UV-visible spectrophotometer (Ocean optics, USB4000) against air in a transmittance mode. The optical transmittance was measured in the wavelength of 300 – 700 nm. The bare glass substrate was used as a reference. The brightness transmitted through the film was evaluated.

3.3.7 Film stability

The films' stability was evaluated by placing the samples at ambient condition and measuring the static contact angle over a time span of nearly 4 weeks (in December 2008). The static contact angle measurement was measured at room temperature and repeated at least five times at different locations on the film's surface.

3.3.8 Surface free energy

Surface free energy is an importance parameter in evaluating chemical properties of solid surfaces and represents a measure of the solid wettability. Solid surface free energy can be determined only indirectly by measuring dynamic or static contact angles of different liquids. Many experimental methods for contact angle measurements and theoretical methods for solid surface free energy determination have been reported [58, 69-73]. For porous solids, the thin layer was recommended by van Oss et.al [49] and Chibowski [70-71], where the solid surface free energy components

can be determined from the results of liquid penetration rate under the appropriate conditions. The important limitation of this method is its application only to the substrates that are wettable by common liquids and low contact angles. In the case of the low surface energy substrates, their repellency to a majority of polar as well as non-polar liquids prevents their penetration into the solid porous structure restricting the method application. In this case, Owen - Wendt method is still the most appropriate for the liquid contact angle determination with the use of a sessile drop deposited on the solid surface.

In this research, two methods which are Owen - Wendt and Chibowski were used to measure surface free energy of the films. It is noteworthy to compare the surface free energy calculated from the Owen – Wendt and Chibowski methods. For the Owen – Wendt method, the surface free energies were calculated by the contact angle data taken with water and diiodomethane (99%, Aldrich) using the following equations[28, 74-75];

$$1 + \cos\theta = \frac{2\sqrt{\gamma_S^D \gamma_L^D}}{\gamma_{LV}} + \frac{2\sqrt{\gamma_S^P \gamma_L^P}}{\gamma_{LV}} \quad (3.3)$$

and
$$\gamma_S = \gamma_S^D + \gamma_S^P \quad (3.4)$$

where θ is contact angle, γ_s^o and γ_l^o are the dispersion component of solid and liquid, γ_s^p and γ_l^p is the polar component of solid and liquid, γ_{lv} is surface free energy of liquid and γ_s is total surface free energy of solid. Table 3.3 shows surface free energy and dispersion and polar components of liquid [75].

Table 3.3 Surface free energy and dispersion and polar components of liquid.

Liquid	γ_{lv} (mJ/m ²)	γ_l^o (mJ/m ²)	γ_l^p (mJ/m ²)
Water	72.6	21.6	51
Diiodomethane	50.8	50.8	0

For Chibowski method, an apparent surface energy was calculated from a contact angle hysteresis which is a different between an advancing and receding contact angles by using the equation below [74-75]:

$$\gamma_s^{tot} = \frac{\gamma_l(1 + \cos \theta_a)^2}{2 + \cos \theta_r + \cos \theta_a} \quad (3.5)$$

where γ_s^{tot} is the apparent surface energy, γ_l is the liquid surface tension, and θ_a and θ_r are advancing and receding contact angles, respectively.



ศูนย์วิทยทรัพยากร
จุฬาลงกรณ์มหาวิทยาลัย

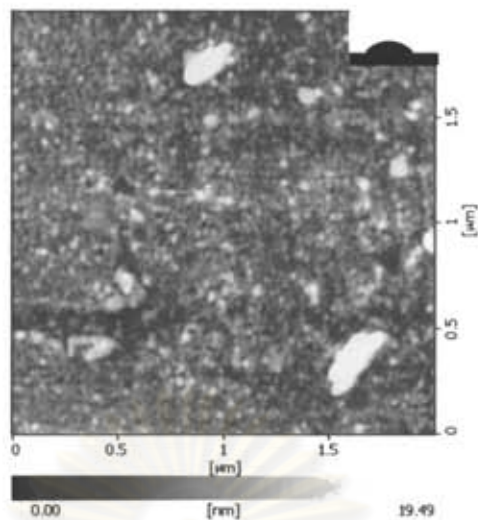
CHAPTER IV

RESULTS AND DISCUSSION

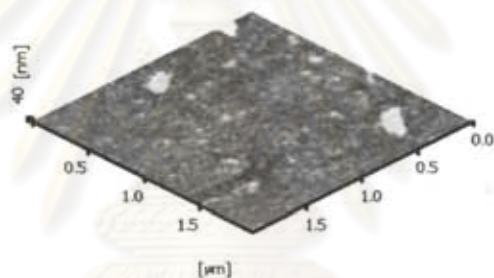
It is well realized that glass surface is hydrophilic since it contains surface hydroxyl groups. To reduce its surface wettability and maintain its transparency, coating it with a transparent superhydrophobic film is a practical method. To deposit the superhydrophobic film on glass substrate, two deposition methods were employed in this research: a hybrid organic/inorganic method and a layer-by-layer method. In this chapter, the experimental results are reported and discussed. Film properties such as degree of hydrophobicity (wettability), surface roughness, morphology, adhesion, stability and surface free energy are characterized. A relationship between surface roughness and surface free energy is also addressed to further understand factors that influence the degree of hydrophobicity.

4.1 Surface characterization of glass substrate

Since all the films possess very fine-scaled surface roughness, the AFM was employed as a primary tool for surface analysis since it has proven itself to be a suitable tool for investigating the structure on a nanometer scale of solid surfaces. Figure 4.1 is an AFM topographical image of a cleaned, bare glass substrate. It is seen as a uniform flat surface having RMS surface roughness of 3.55 nm. Irregular ripples are also observed. The ripple patterns have been found also for other glasses [76]. The flat glass surfaces can be discerned from atomically flat crystal terraces by a ripple pattern which has been found by AFM researchers on many glass surfaces and labeled features, hillocks, waves, entities and so on. Although varying in its dimensions, this pattern is common. This topography is referred to as 'the glass pattern'. The bare glass substrate had a water drop contact angle of 53 ± 0.65 degrees which is in a hydrophilic regime.



2-dimensional image



3-dimensional image

Figure 4.1 AFM topographical mapping and water droplet image of bare glass substrate.

4.2 Film deposition via layer-by-layer (LBL) method

4.2.1 Effect of etching condition

The film deposited by this method consisted of SiO_2 particles that were deposited onto dimples or open porosity previously created on the PAH/PAA 3 bilayers by acid etching. To study an effect of etching condition, the rough surface was created by etching the poly(allylamine hydrochloride) (PAH) and poly(acrylic acid) (PAA) bilayers with HCl solutions of three different conditions: pH = 1.0 for 3 h, pH = 2.3 for 3 h, and pH = 2.3 for 1.5 h followed by pH = 1.0 for 1.5 h. Figure 4.2 are SEM images of the PAH/PAA 3 bilayers after etching with HCl solution. The polyelectrolyte bilayers etched with HCl solution of pH 1.0 consisted of articulated worm features. Open porosity or dimples are not clearly seen in this image. The polyelectrolyte bilayers etched with HCl solution of pH 2.3 had slightly different feature. The articulated worm features were not observed as they were etched with a stronger acid. However, the dimples were still not created. In contrast, the polyelectrolyte bilayers etched with the combined acid of pH = 1.0 and 2.3 each for 3 h consisted of dimples or open porosity of a size as large as 500 nm.

Figure 4.3 shows AFM images of the polyelectrolyte bilayers before and after etching with HCl solution having a pH = 1.0 for 3 h, pH = 2.3 for 3 h, and pH = 2.3 for 3 h followed by pH = 1.0 for 3 h. These bilayers had surface roughness of 1.8 ± 0.09 , 2.8 ± 0.14 , 2.0 ± 0.09 and 5.0 ± 0.25 nm, respectively, and the water contact angle of 50 ± 0.58 , 79 ± 0.90 , 61 ± 0.60 and 87 ± 0.85 degrees, respectively. Obviously, the polyelectrolyte bilayers were hydrophilic. According to the previous study [77], when the PAA is the outermost layer, the film surface is rich in free, unpaired acid (COOH groups). This characteristic results to a hydrophilic property because of an interaction between the COOH group of the PAA and the -OH group of water.

The surfaces obtained by etching the polyelectrolyte bilayers with HCl solutions of pH 1.0 and 2.3 had similar roughness, while the one etched with the acid of pH 1.0 followed by the acid of pH 2.3 had dimples or open porosity. The porosity of the etched polyelectrolyte bilayers had two size ranges. The smaller porosity had diameter

of about 0.1 – 0.25 μm , while the larger porosity has diameter of about 0.5 – 1.0 μm . These AFM results are in good agreement with the result of SEM analysis.

As describes in chapter 2, the surface of a lotus leaf consists of a combination of a two-scaled roughness: one of around 10 μm (roughness structure) and the other of around 100 nm (fine structure) [1]. These surfaces are also referred as hierarchical micro- and nano-structure. To mimic the lotus leaf effect, it is necessary to create surface texture with both micron- and nano-scaled surface roughness. Thus, the combination of two pH treatments (pH = 2.3 and 1.0) was selected to create template for deposition of oxide particles. The surface roughness of such films made them ideally suited for use as the roughness template of a superhydrophobic surface. As addressed by Zhai et. al. [35] concerning etching the polyelectrolyte with acid, two keys processing elements enables the fabrication of rough surfaces. First, it is important that the polyelectrolyte bilayers not be rinsed with water after etching with the low-pH acid solution, and second, a multi-stages low pH treatment is better than a single low pH treatment.

Figure 4.4 shows AFM images of the Aerosil[®] 200 SiO_2 particles deposited on the polyelectrolyte bilayers etched with HCl of pH 1.0, 2.3, and pH 2.3 followed by pH 1.0. These surfaces had surface roughness of 36.1 ± 1.80 , 40.0 ± 2.00 and 44.4 ± 2.22 nm, and water contact angle of 50 ± 0.72 , 42 ± 0.52 and 54 ± 0.45 degrees, respectively. It was observed that film etched by pH 2.3 exhibited low surface coverage, while films etched by pH 1.0 and combination of pH 1.0 and 2.3 were too closely packed. The deposition of silica nanoparticles onto the polyelectrolyte surface resulted to the increase of surface roughness and decrease of water contact angle as the Aerosil[®] 200 is hydrophilic.

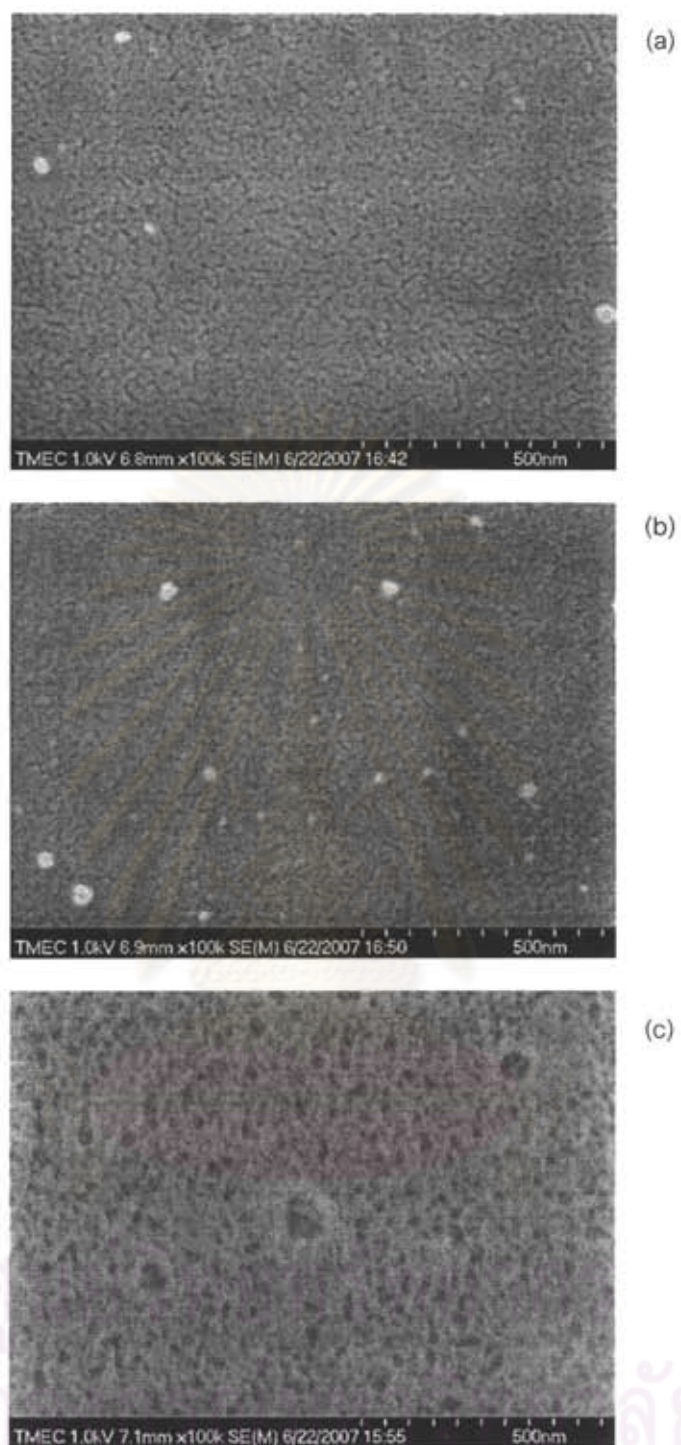


Figure 4.2 SEM images of 3 polyelectrolyte bilayers etched with HCl solution (a) pH 1.0 for 3 h, (b) 2.3 for 3 h and (c) pH 1.0 for 1.5 h followed by pH 2.3 for 1.5 h.

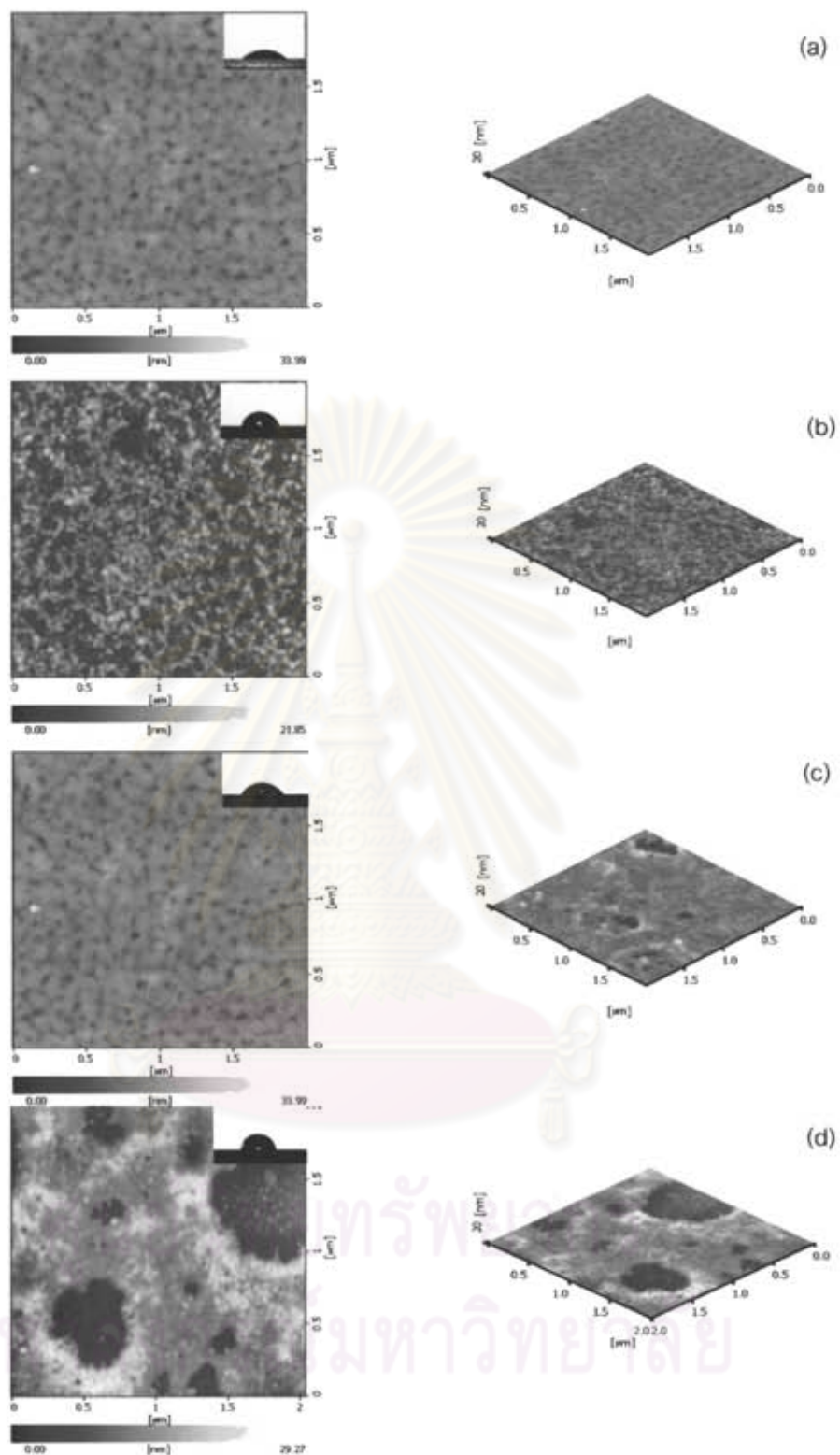


Figure 4.3 AFM topographical mapping and water droplet image of polyelectrolyte 3 bilayers (a) before, and after etching with HCl solution having a pH of (b) 1.0, (c) pH 2.3 for 3 h and (d) combination between pH 1.0 and 2.3 each 1.5 h, respectively.

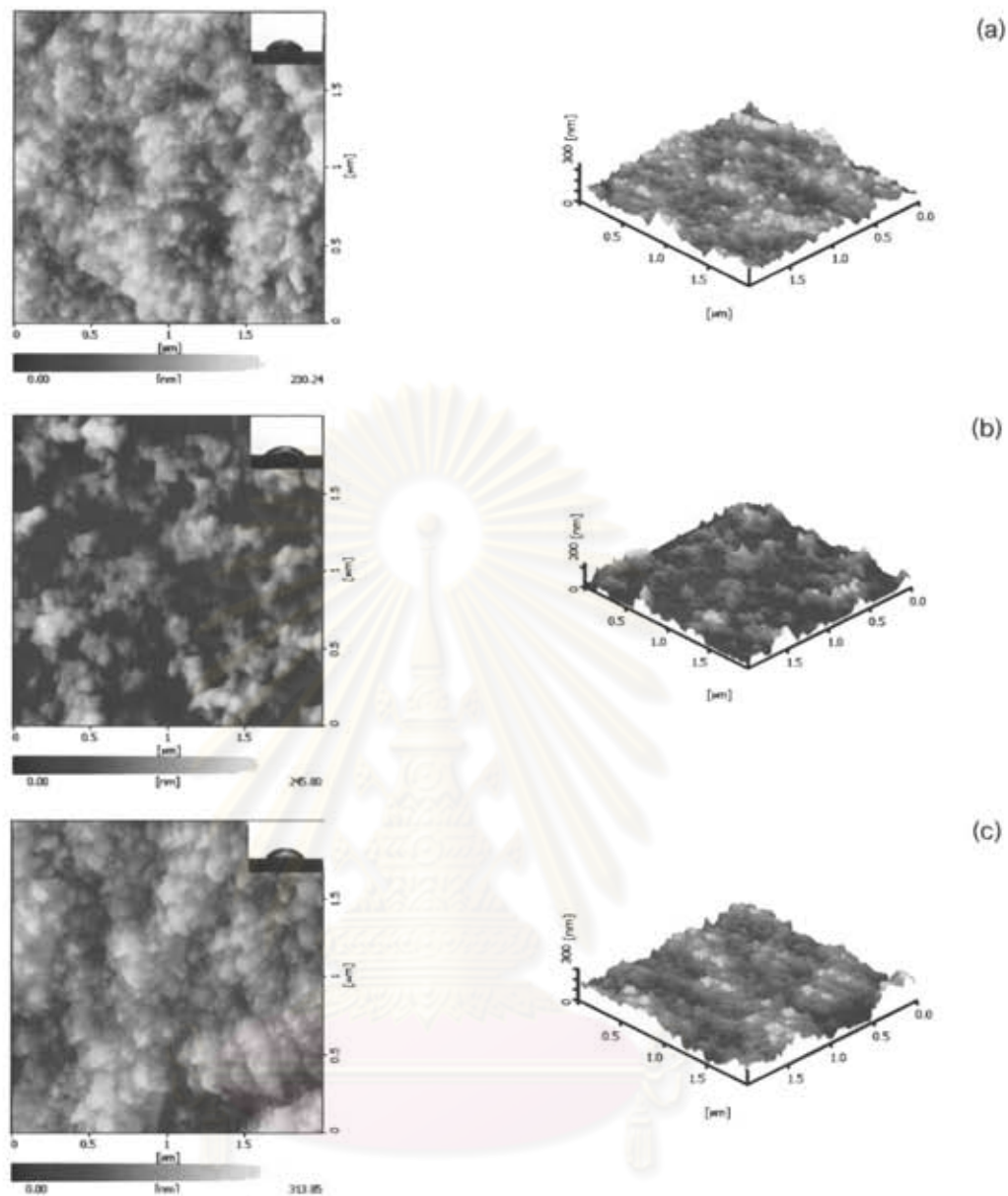


Figure 4.4 AFM topographical mapping and water droplet image of deposited nanosilica Aerosil® 200 on etched polyelectrolyte 3 bilayers by HCl solution (a) pH 1.0, (b) pH 2.3 for 3 h and (c) combination between pH 1.0 and 2.3 each 1.5 h, respectively.

Figure 4.5 shows AFM images of the final film prepared by deposition of Aerosil[®] 200 SiO₂ particles on the etched PAH/PAA 3 bilayers followed by deposition of semifluorinated silane. Surface roughness of the etched PAH/PAA polyelectrolyte was 5.0 ± 0.25 nm, and increased to 40.3 ± 2.01 nm after deposition with SiO₂ nanoparticles and silane. The film wettability changed from hydrophilic (contact angle of 87 degree) to superhydrophobic (contact angle of 172 degree) after deposition of silica nanoparticle and silane molecules. Moreover, it was found that the water droplets pinned in the uncoated surface after sitting on surface for a couple minutes. In contrast, the water droplets on the coated surface freely roll off the surface without becoming pinned. Values of water contact angle and surface roughness of each layer are summarized in Table 4.1.

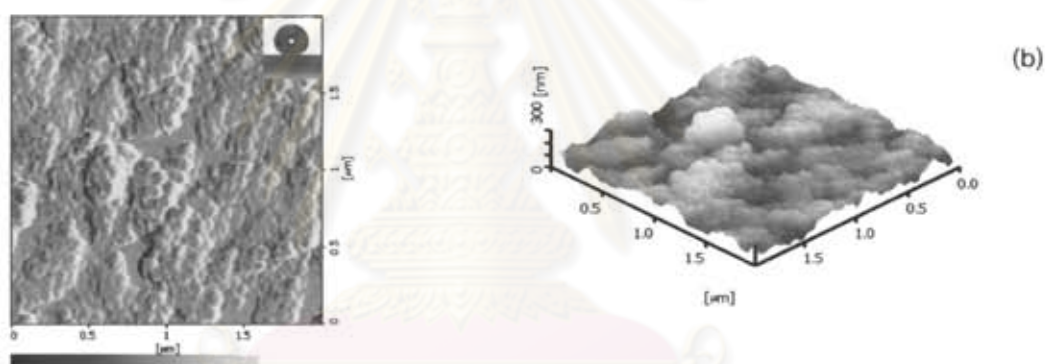


Figure 4.5 a) Before and (b) after deposition of Aerosil[®] 200 and silane treatment.

Table 4.1 Summary of the water contact angle and surface roughness of each layer.

Sample	Contact angle (degree)	Roughness (nm)
Bare glass	53 ± 0.65	3.6 ± 0.18
PAH_PAA 3 bilayer	50 ± 0.58	1.8 ± 0.09
Etched PAH_PAA with pH 1.0	79 ± 0.90	2.8 ± 0.14
Etched PAH_PAA with pH 2.3	61 ± 0.60	2.0 ± 0.01
Etched PAH_PAA with combination pH 1.0 and 2.3	87 ± 0.85	5.0 ± 0.25
Etched PAH_PAA with pH 1.0/Aerosil® 200	50 ± 0.72	36.1 ± 1.80
Etched PAH_PAA with pH 2.3/Aerosil® 200	42 ± 0.52	40.0 ± 2.00
Etched PAH_PAA with combination pH 2.3 and 1.0/ Aerosil® 200	54 ± 0.45	44.4 ± 2.22
Etched PAH_PAA with combination pH 2.3 and 1.0/ Aerosil® 200/silane	172 ± 0.19	40.3 ± 2.01

ศูนย์วิทยทรัพยากร
จุฬาลงกรณ์มหาวิทยาลัย

4.2.2 Effect of particulate type

In order to vary surface roughness and hydrophobicity of the films, three types of SiO_2 suspensions, Aerosil[®] 200 (hydrophilic surface), Aeroperl[®] 300/30 (hydrophilic surface) and Aeroperl[®] 806/30 (hydrophobic surface) with concentrations ranging from 0.05 to 5 wt.%, were used as the precursor for dip coating. Figure 4.6 shows TEM images of the oxide fillers. The Aerosil[®] 200 (Figure 4.6(a)) which is a fumed SiO_2 has an average particle size of around 12 nm. The Aeroperl[®] 300/30 (Figure 4.6(b)) which is a granulated fumed SiO_2 is seen as a combination of $\sim 1\text{-}10\ \mu\text{m}$ SiO_2 aggregates and much finer SiO_2 particles. The Aeroperl[®] 806/30 (Figure 4.7(c)) which is a hydrophobized granulated fumed SiO_2 also has similar feature. According to the specification provided by the manufacturer, the average size of both the Aeroperl[®] 300/30 and Aeroperl[®] R806/30 granules is 30 μm . However, a much finer size and broader size distribution was obtained in the suspension due to vigorous stirring that broke up the agglomerates. Therefore, it was anticipated that the size of both Aeroperl[®] fillers in the suspension was much finer than their specifications.

Figure 4.7(a) shows SEM image of the etched PAH/PAA polyelectrolyte bilayers. It is clearly seen that sub-micron sized dimples were created at the surface. These dimples then served as the sites for deposition of SiO_2 particles which enhanced the surface roughness. Prolong etching led to deteriorate of the polyelectrolyte bilayers. Figure 4.7(b)-(d) are SEM images of the water-repellent films containing various contents of the Aerosil[®] 200 particles deposited onto the etched polyelectrolyte bilayers. The film prepared from 0.05 wt.% suspension consisted of islands of agglomerated SiO_2 particles of 0.1-0.5 μm in size covering about half of the entire surface. The surface was fully covered when the SiO_2 was deposited from 5 wt.% suspension (Figure 4.7(d)). Figure 4.8 shows SEM images of the water-repellent films containing various amount of the Aeroperl[®] 300/30. The result is essentially similar to the films consisting of the Aerosil[®] 200 that the surface was covered with sub-micron, agglomerated SiO_2 particles, and the surface coverage increased with the increase of suspension concentration. However, some large particles of tens of microns were also found (insets). Note that

none of the 30 μm particles which is an average size of the Aeroperl[®] 300/30 was found since such large particle settled down to the bottom of the beaker during a dip coating step.

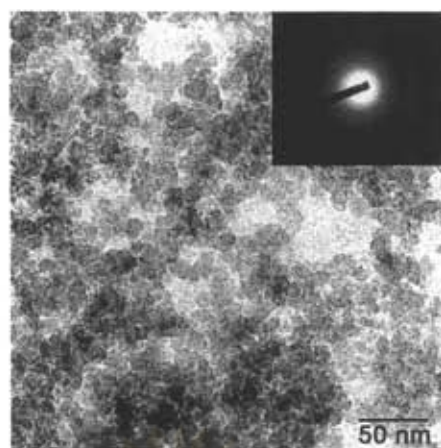
Table 4.2 shows relationship between content of SiO_2 nanoparticles employed and values of contact angle of the films. For a typical AFM analysis, an area of 5 μm x 5 μm was scanned. Regardless of the SiO_2 type, contact angle increased with increasing amount of the SiO_2 . However, the effect is not significant in the case of the Aerosil[®] 200 as the films had comparable values of contact angle within an experimental error. Moreover, the increase of contact angle (i.e. degree of hydrophobicity) did not in the same factor as the increase of the SiO_2 content. This result can be explained based on the amount of SiO_2 that was deposited onto the porous polyelectrolyte bilayers. The amount of deposited SiO_2 was limited by porosity of the polyelectrolyte bilayers rather than concentration of the SiO_2 suspension. At a certain amount of SiO_2 content, the film containing Aerosil[®] 200 gave the highest contact angle. The films containing the Aeroperl[®] 300/30 and Aeroperl[®] 806/30 showed similar hydrophobicity and lower than the films containing the Aerosil[®] 200. Basically, large particle deposited on the film should give rise to high surface roughness. Thus, much larger area of 100 μm x 100 μm scanning area was investigated for film containing the Aeroperl[®] 300/30. The results showed that larger scanning area has higher roughness. It may be caused by the presence of large particle size of 10 μm on the film's surface. However, it is believed that this surface roughness did not influence the hydrophobicity. Figure 4.9 shows drawing of water droplet on films containing the Aerosil[®] 200 and Aeroperl[®] 300/30. In case of films containing the Aeroperl[®] 300/30, it is most likely that water droplet sit between large particles which are far away apart based on SEM observation. Therefore, the roughness obtained from 5 μm x 5 μm is more reliable since it did not take into account the size of 10 μm particle. The effective roughness should be the one obtained from smaller scanned area.

Figure 4.10, 4.11 and 4.12 shows AFM images of the films containing various amounts of the Aerosil[®] 200, Aeroperl[®] 300/30 and Aeroperl[®] 806/30, respectively. It is clearly seen that the films were covered with SiO_2 nanoparticles, and

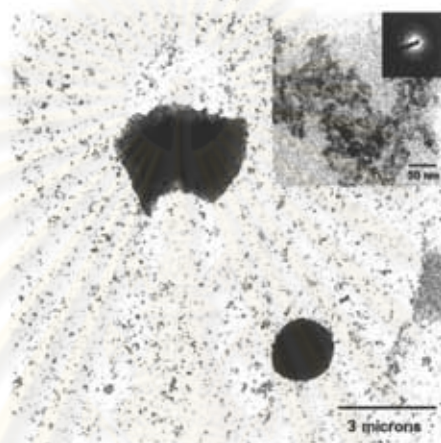
the coverage increased with increasing SiO₂ content in the suspension. In case of Aeroperl[®] 300/30 and Aeroperl[®] 806/30, it was observed that films fabricated from the low concentration solutions exhibited low surface coverage, while films fabricated from the high concentration solutions were densely packed. Therefore, as it was mentioned earlier that the amount of deposited SiO₂ did not increase by the same factor as concentration of the suspension. Surface roughness of these films was 37.9 ± 1.90, 41.7 ± 2.09 and 60.7 ± 3.03 nm for the films prepared from 0.05, 1 and 5 wt.% Aerosil[®] 200, respectively. Under the synthesis condition employed in this study, the maximum contact angle of 174 ± 0.90 degrees was obtained from the film possessing highest surface roughness as a result of highest SiO₂ content. Note that the film containing Aeroperl[®] 300/30 and Aeroperl[®] 806/30 exhibited similar hydrophobicity since they had similar particle size which resulted to similar surface roughness.

However, the real volume of SiO₂ content deposited onto etched multilayer polyelectrolyte films did not equal to the SiO₂ content in the suspension. It may be caused by limited size of porosity on etched multilayer polyelectrolyte films. Nevertheless, as shown in Table 4.2 it is not necessary that high surface roughness give high contact angle since surface free energy is another factor to be considered. This result demonstrates that the superhydrophobic template can be obtained from low content such as 0.05 wt.% for the Aerosil[®] 200, and 1wt.% for the Aeroperl[®] 300/30 and Aeroperl[®] 806/30, respectively.

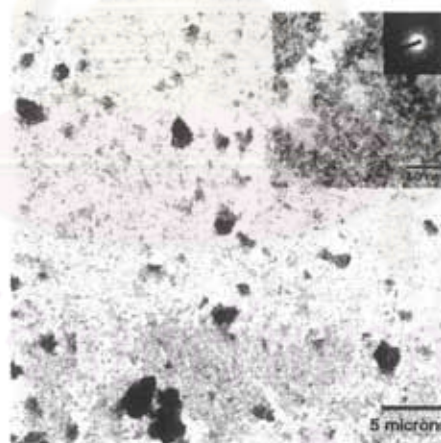
ศูนย์วิทยทรัพยากร
จุฬาลงกรณ์มหาวิทยาลัย



(a)



(b)



(c)

Figure 4.6 TEM images of (a) Aerosil[®] 200, (b) Aeroperl[®] 300/30 and (c) Aeroperl[®] R806/30.

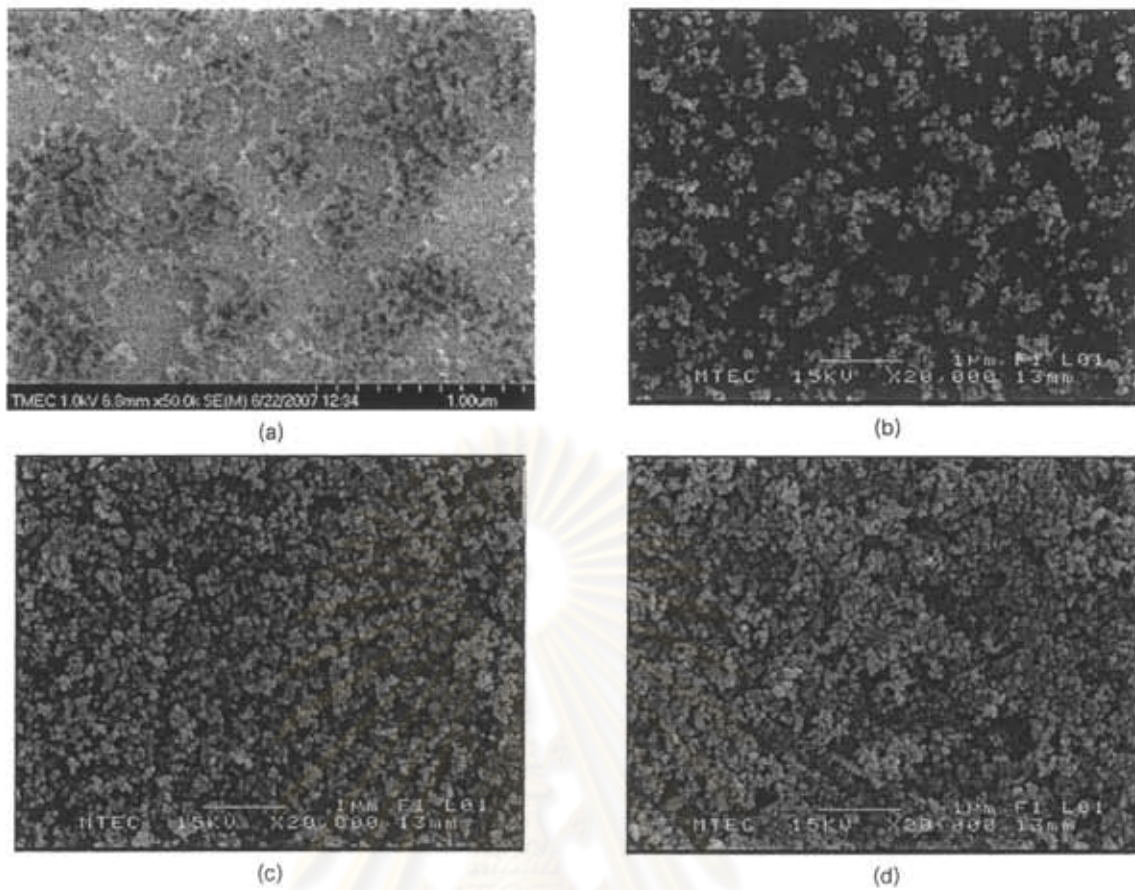
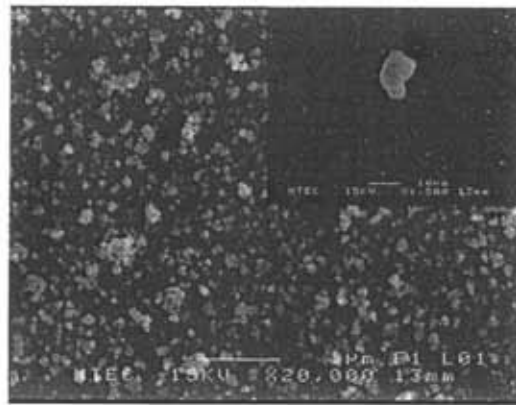
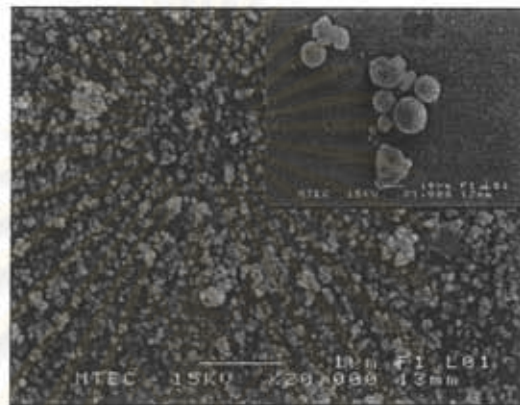


Figure 4.7 (a) SEM image of the etched polyelectrolyte bilayers, and (b-d) SEM images of the water-repellent films by which surface roughness was created by dipping into Aerosil[®] 200 suspension at a solid content of 0.05, 1 and 5 wt.%, respectively.

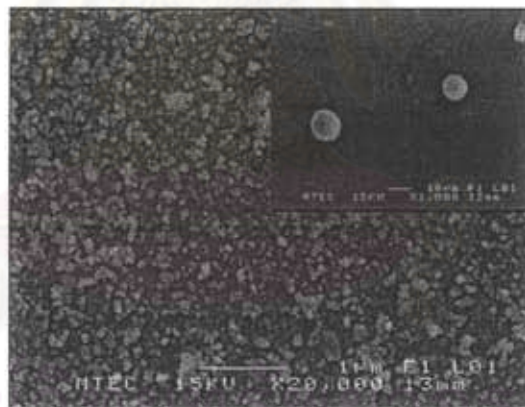
ศูนย์วิทยทรัพยากร
จุฬาลงกรณ์มหาวิทยาลัย



(a)



(b)



(c)

Figure 4.8 SEM image of the water-repellent films by which surface roughness was created by dipping into Aeroperl[®] 300/30 suspension at a solid content of (a) 0.05 wt.%, (b) 1 wt.% and (c) 5 wt.%.

Table 4.2 Contact angle and surface roughness (scanning area = 5 μm x 5 μm) of the films containing different type and amount of the SiO_2 nanoparticles. Numbers in parenthesis were obtained from a scanning area of 100 μm x 100 μm .

Type of SiO_2	SiO_2 content (wt.%)	Surface roughness (nm)	Contact angles (degrees)
Aerosil [®] 200 (particle size 12 nm, SSA = 200 m^2/g)	0.05	37.9 \pm 1.90	169 \pm 0.27
	1	41.7 \pm 2.09	171 \pm 0.69
	5	60.7 \pm 3.03	174 \pm 0.90
Aeroperl [®] 300/30 (particle size 30 μm , SSA = 300 m^2/g)	0.05	6.8 \pm 0.34 (67.2 \pm 3.36)	132 \pm 0.75
	1	15.0 \pm 0.75 (73.1 \pm 3.65)	150 \pm 0.33
	5	34.0 \pm 1.70 (88.3 \pm 4.41)	154 \pm 0.99
Aeroperl [®] 806/30 (particle size 30 μm , SSA = 300 m^2/g)	0.05	1.0 \pm 0.05	135 \pm 0.45
	1	17.1 \pm 0.85	151 \pm 0.19
	5	34.1 \pm 1.70	158 \pm 0.19

ศูนย์วิทยทรัพยากร
จุฬาลงกรณ์มหาวิทยาลัย

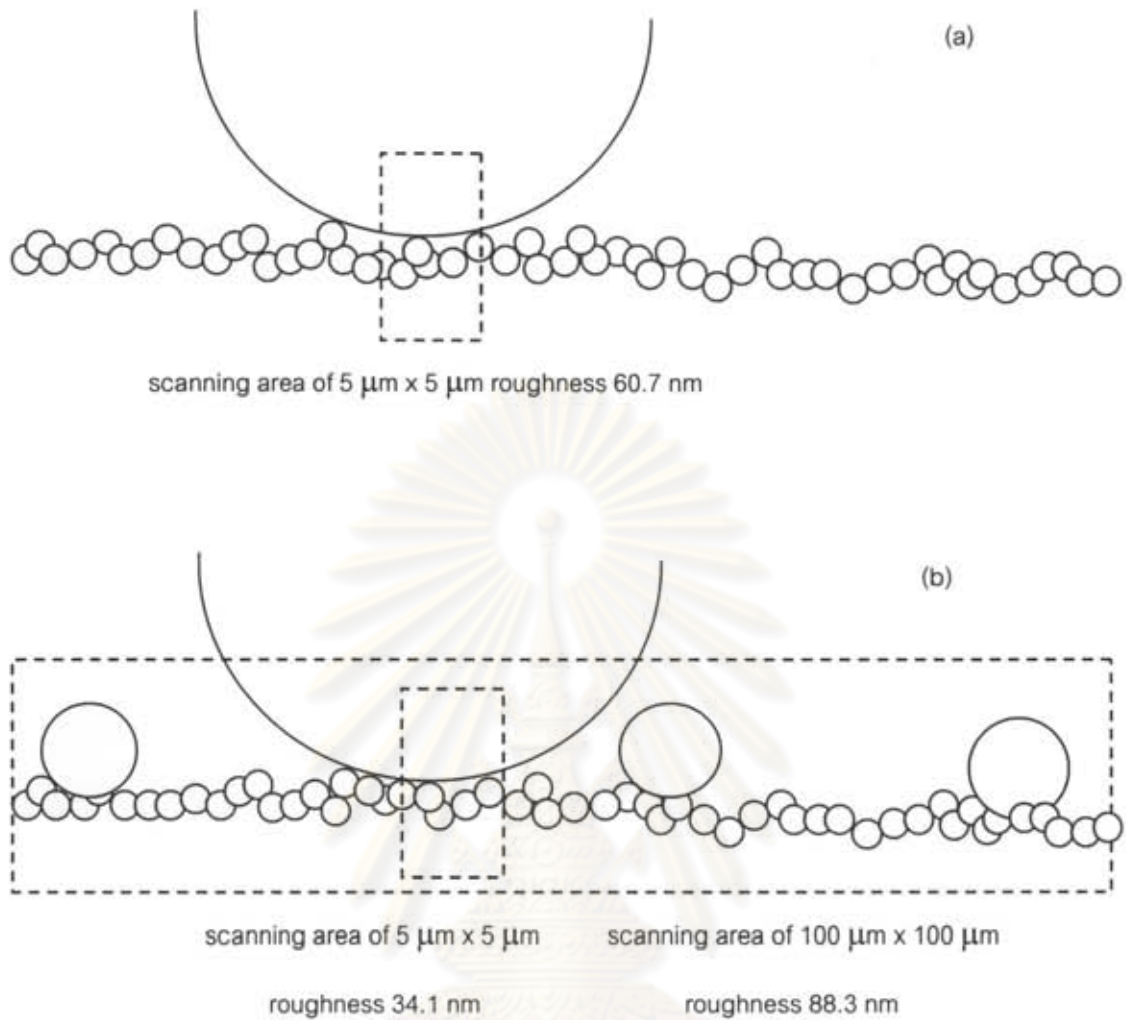


Figure 4.9 Drawing of water droplet on (a) films containing Aerosil[®] 200 and (b) Aeroperl[®] 300/30.

ศูนย์วิทยุโทรพยากร
จุฬาลงกรณ์มหาวิทยาลัย

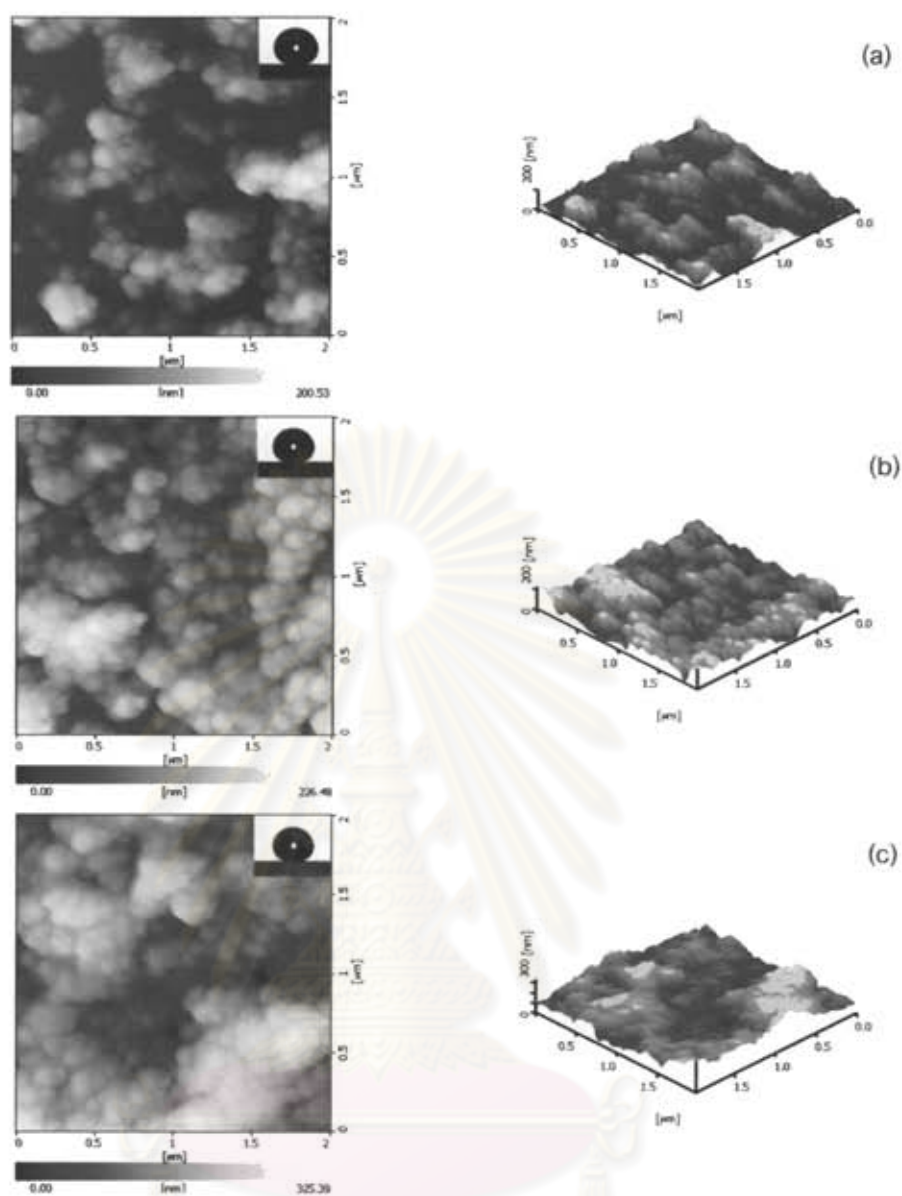


Figure 4.10 2-Dimensional (left) and 3-dimensional (right) topographical images of the films containing (a) 0.05, (b) 1 and (c) 5 wt.% of Aerosil[®] 200.

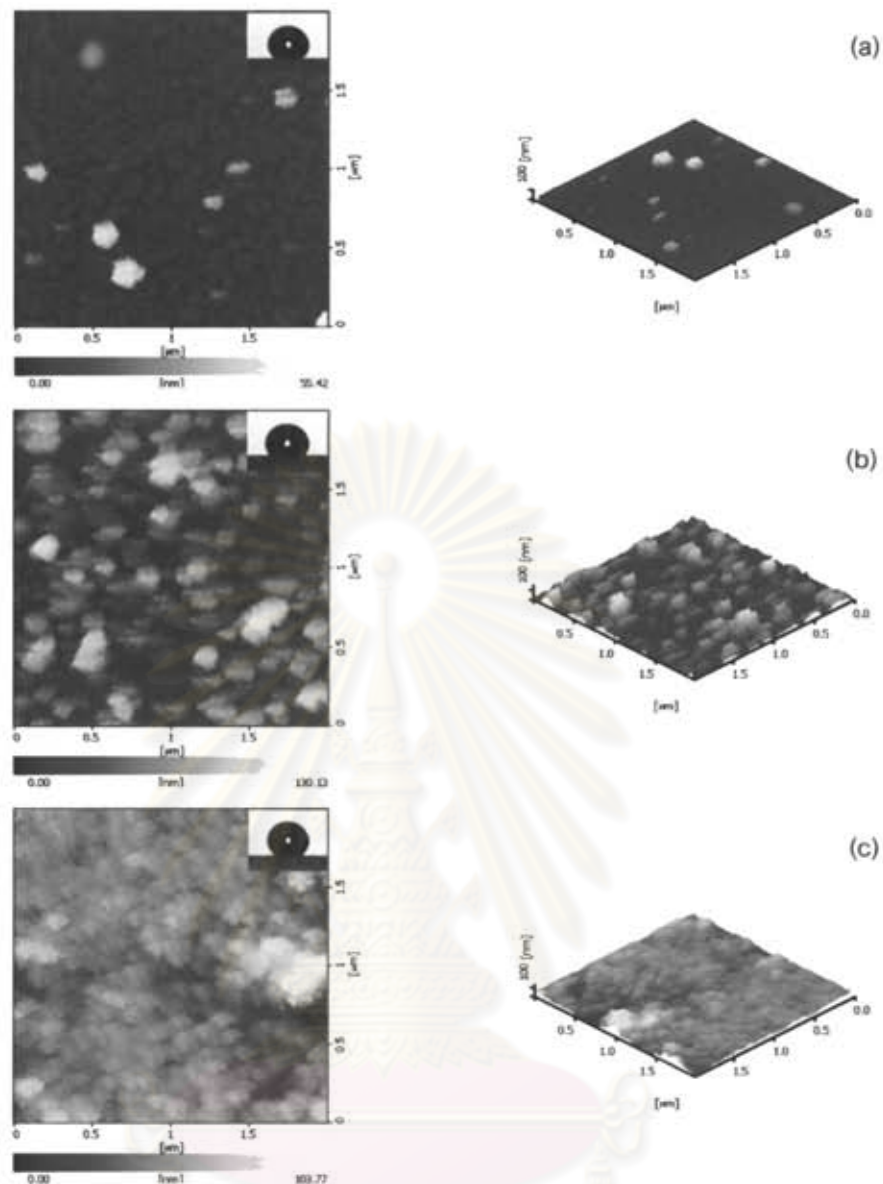


Figure 4.11 2-Dimensional (left) and 3-dimensional (right) topographical images of the films containing (a) 0.05, (b) 1 and (c) 5 wt.% of Aeroperl[®] 300/30.

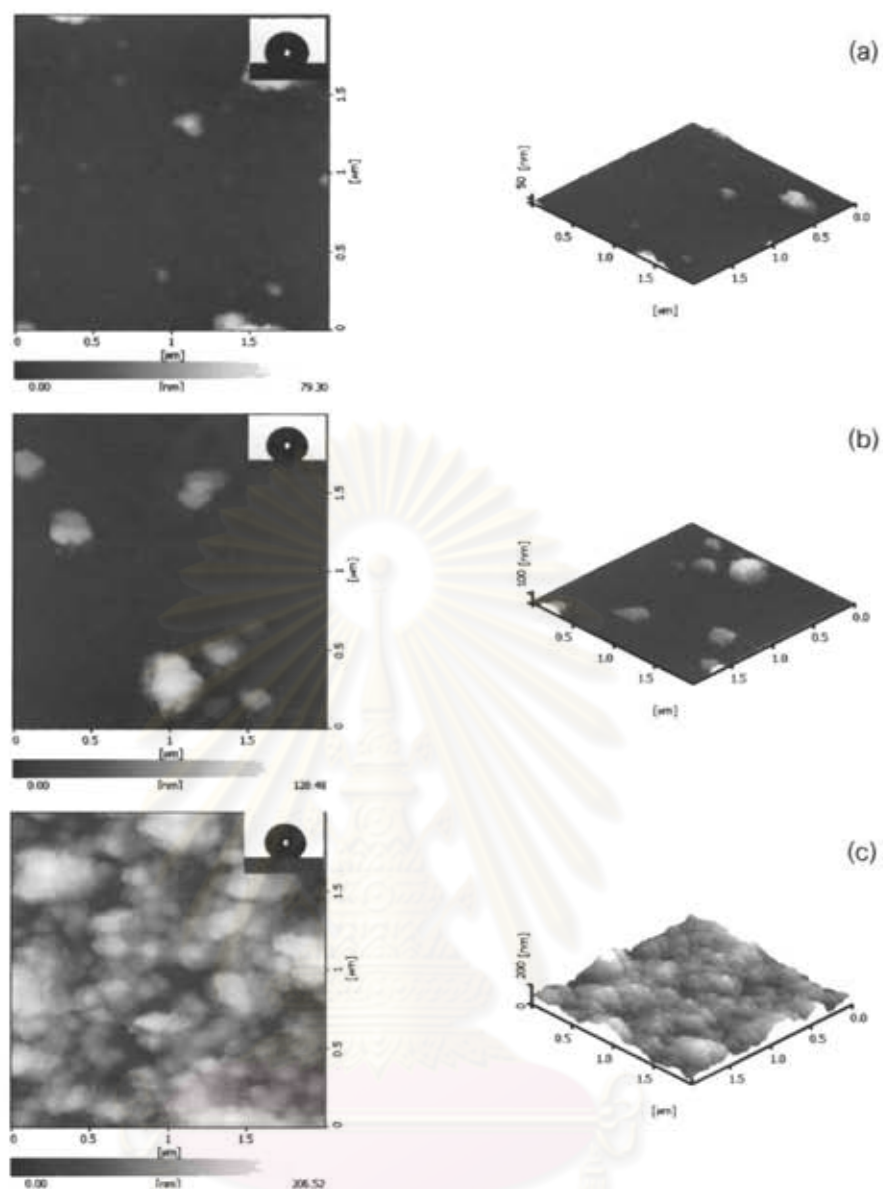


Figure 4.12 2-Dimensional (left) and 3-dimensional (right) topographical images of the films containing (a) 0.05, (b) 1 and (c) 5 wt.% of Aeroperl[®] 806/30.

In order to evaluate an optical property, transmittance of the films containing Aerosil[®] 200, Aeroperl[®] 300/30 or Aeroperl[®] 806/30 of various contents were measured. Figure 4.13 shows the optical transmittance spectra of the films at wavelengths ranging from 300 to 700 nm. The transmittance of the films decreased with increasing SiO₂ content. All the prepared films show good optical property about 90 % transmittance.

In case of films containing 0.05 and 1 wt.% Aerosil[®] 200, transmittance of film is higher than that of bare glass substrate. The reason is not well understood, but it is possible that the films with nanometer scale roughness may effectively reduce the reflection at the surface, resulting in an enhance transmittance. The SiO₂ nanoparticles may be present of more open space (porosity) with size close to wavelength of visible light, resulting in more scattering. It has been demonstrated that introducing of SiO₂ particles onto the etched polyelectrolyte multilayer exhibited significant roughness while maintaining the optical transparency. This property of film means that good visibility can be maintained for a coated glass substrate.



ศูนย์วิจัยทรัพยากร
จุฬาลงกรณ์มหาวิทยาลัย

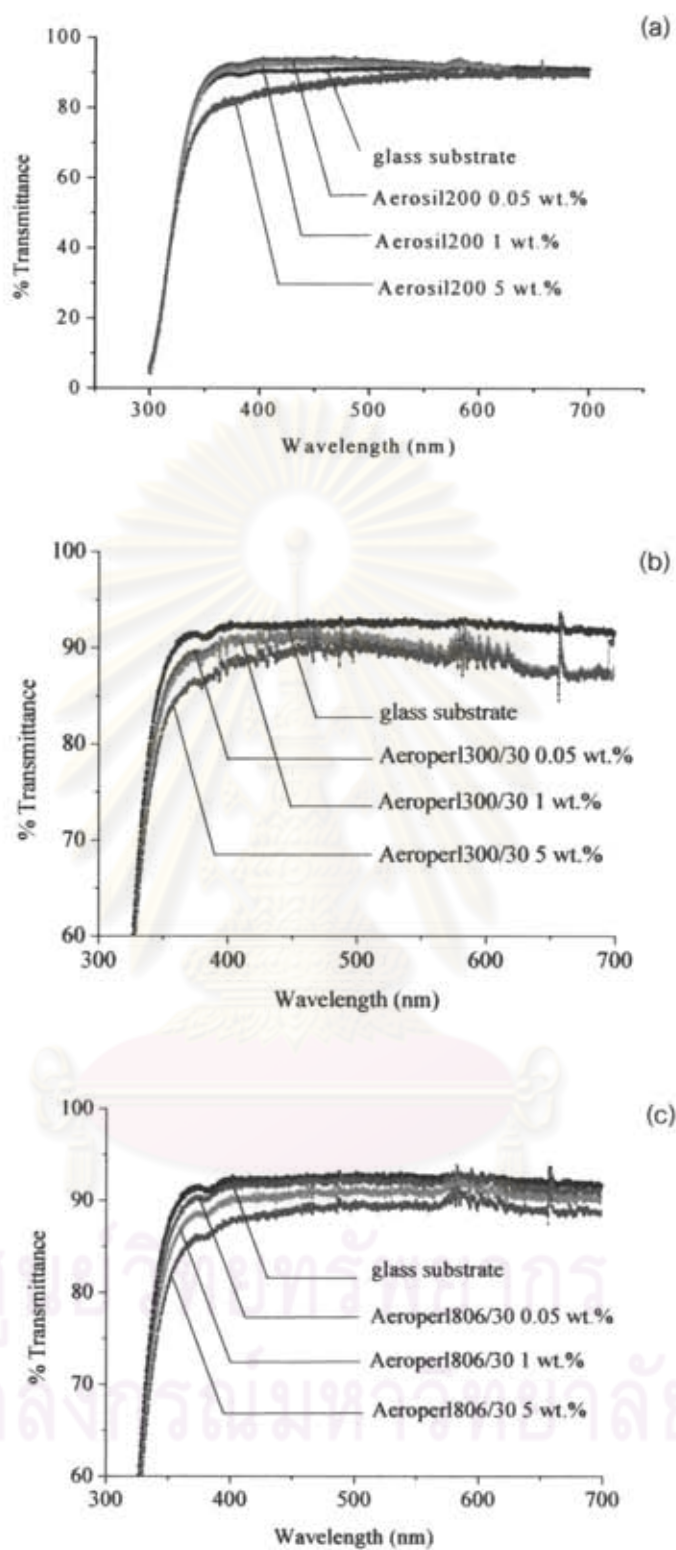


Figure 4.13 Transmittance of bare glass substrate and the glass substrate coated with films containing 0.05, 1 and 5 wt.% of (a) Aerosil[®] 200, (b) Aeroperl[®] 300/30 and (c) Aeroperl[®] 806/30.

4.2.3 Effect of number of polyelectrolyte bilayers

As mentioned previously that surface roughness is one of the two key parameters that affect degree of hydrophobicity. It is therefore worthy to investigate whether etching a thicker polyelectrolyte multilayer would result to rougher surface. In this respect, the polyelectrolyte multilayer films of various thicknesses were prepared. The thickness was varied by varying a number of layers to 1, 3, 5, 10 and 20 bilayers. That is, the dipping cycle was repeated several times to achieve the desired PAH/PAA bilayers. Then, the desired surface roughness was created by etching the PAH/PAA film with HCl solutions at pH of 2.3 followed by pH of 1.1, each for 1.5 h. The etched PAH/PAA film was heated at 180°C for 2 h.

Figure 4.14 shows the SEM images of the etched polyelectrolyte multilayer films containing 1, 3, 10 and 20 PAH/PAA bilayers. It is clearly seen from the images that the films containing only 1 bilayer was least porous. In contrast, the films containing 3-20 bilayers were more porous among them. However, there was no dramatic different porosity. Based on this SEM analysis, the polyelectrolyte multilayer film must be made of at least 3 PAH/PAA bilayers to gain sufficient thickness and porosity. It has also been learnt from this experiment that, by making the polyelectrolyte layer thicker it was easier to create porosity on its surface by means of chemical etching. High porosity is considered as an important property for templates for fabrication of superhydrophobic film by layer-by-layer deposition. This porosity then served as the site for deposition of the SiO₂ nanoparticles which in turn determined the surface roughness of the final film.

Since the 2-dimensional of SEM images did not provide quantitative result for determination of surface roughness. In order to gain better understanding of surface roughness, surface topology of the etched polyelectrolyte films was further investigated by AFM. The water contact angle was also measured by using a goniometer. Table 4.3 summarizes the water contact angle and surface roughness of the etched polyelectrolyte films of various number of PAH/PAA bilayers. It was observed that the contact angle did not vary dramatically with number of the bilayers. It was in a

range of 86 – 92 degrees with the maximum contact angle obtained in film containing 20 bilayers. Some of them can be viewed as the same value within an experimental error. This result is not beyond expectation since the water contact angle is determined by wettability of the outermost layer which is the PAA layer. The hydrophilicity was attributed to the hydrophilic carboxyl groups containing along the backbone of the PAA molecules. The previous work illustrated that the surface wettability of sequentially adsorbed polyelectrolyte bilayer was sensitive to the number of polyelectrolyte bilayer [84-85]. However, such relationship did not evidently observe in this study.

Values of surface roughness obtained from AFM analysis were 3.7 ± 0.18 , 5.0 ± 1.25 , 2.7 ± 0.13 and 7.63 ± 0.38 nm for the films containing 1, 3, 10 and 20 PAH/PAA bilayers, respectively. Obviously, the value of surface roughness did not vary significantly with the number of bilayers. Nevertheless, the AFM results showed that the number of polyelectrolyte bilayers affected surface roughness of film in some extent. That is, there was a tendency of increasing surface roughness with increasing number of polyelectrolyte bilayers. The result of AFM analysis corresponds well with the SEM result. It should be noted here that to obtain a superhydrophobic surface, the much more surface roughness is desirable. High surface roughness can be obtained by deposition of oxide particle onto the etched polyelectrolyte bilayers as previously mentioned in section 4.2.2. It is described later on that the existence of oxide particle on polyelectrolyte multilayer significant influenced the degree of hydrophobicity.

ศูนย์วิทยทรัพยากร
จุฬาลงกรณ์มหาวิทยาลัย

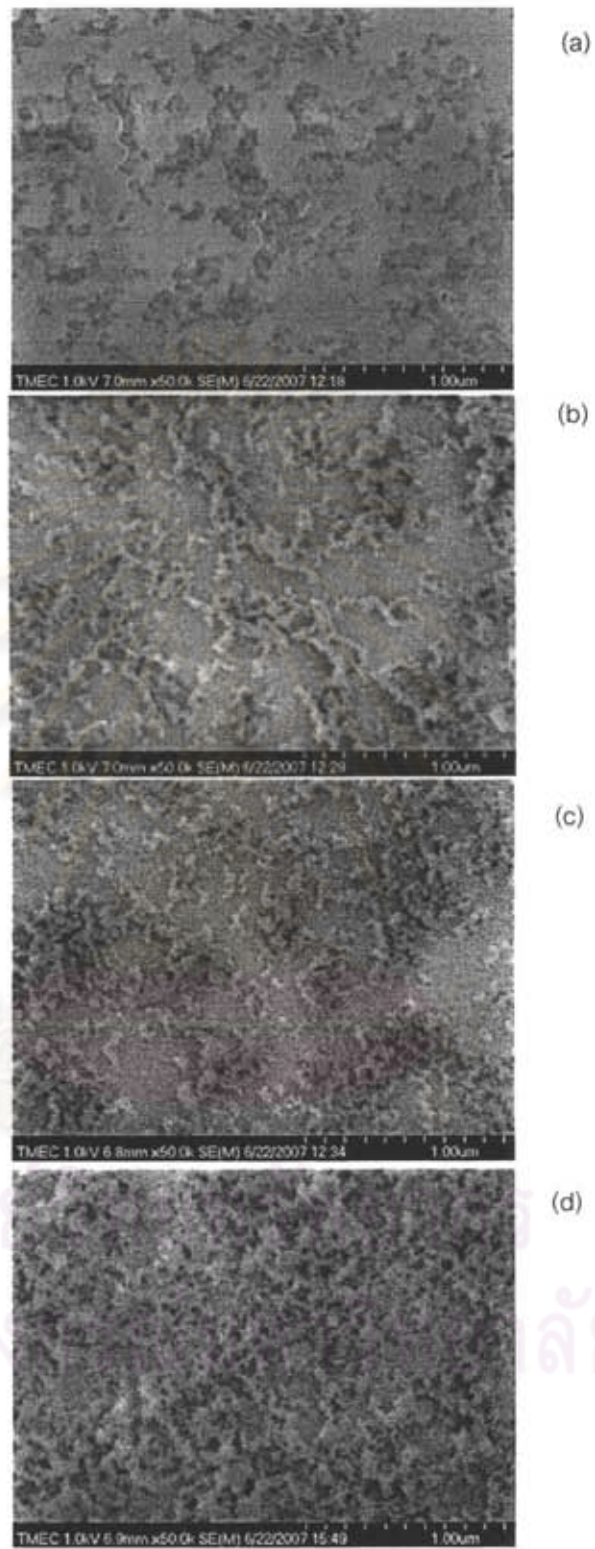


Figure 4.14 SEM images of etched PAH/PAA film with (a) 1, (b) 3, (c) 10 and (d) 20 bilayers.

Table 4.3 Summary of the water contact angle and surface roughness of etched polyelectrolyte bilayer.

Sample	Contact angle (degree)	Roughness (nm)
Etched PAH_PAA 1 bilayer	86 ± 0.62	3.7 ± 0.18
Etched PAH_PAA 3 bilayers	87 ± 0.85	5.0 ± 1.25
Etched PAH_PAA 10 bilayers	91 ± 0.52	2.7 ± 0.13
Etched PAH_PAA 20 bilayers	92 ± 0.70	7.6 ± 0.38

To determine a thickness of the polyelectrolyte film, the scratch was made across the film to create a step. The thickness was determined by scanning an AFM tip across the revealed step between the film and glass substrate. A height was assumed to be positive in the up direction, away from the bulk material. Figure 14.15 shows the AFM height images of the films containing 2 and 4 PAH/PAA bilayers. The thickness was 36.14 and 51.22 nm, respectively. This result indicates that the thickness did not linearly increase with number of dipping cycle. Nevertheless, this analysis gave an approximation of a thickness of 1 single PAH/PAA bilayer of 13 – 18 nm which is close to the value (12 nm) reported in the literature [83]. A small different can be attributed to a difference of solution's pH employed. In the reported work, the pH of PAH solution is 8.5 and the pH of PAA solution is 3.5.

The effect of number of polyelectrolyte bilayers to layer thickness has been studied by many researchers [83, 85-86]. Controlling of layer thickness can be achieved by simple adjustments of the pH of dipping solutions. The solution's pH controls the linear charge density of an adsorbing polymer as well as the charge density of the previously adsorbed polymer layer. In case of weak polyelectrolytes such as PAH and PAA, it was reported that dramatic changes in the thickness of an adsorbed layer can be induced by very small changes in the pH of the dipping solutions. The thickness of PAH/PAA bilayers building block is highly sensitive to solution's pH. By simply controlling the pH, it is possible to deposit unusually thick bilayers (>12 nm) or very thin bilayers (<1 nm). In this work, thick layer is desired.

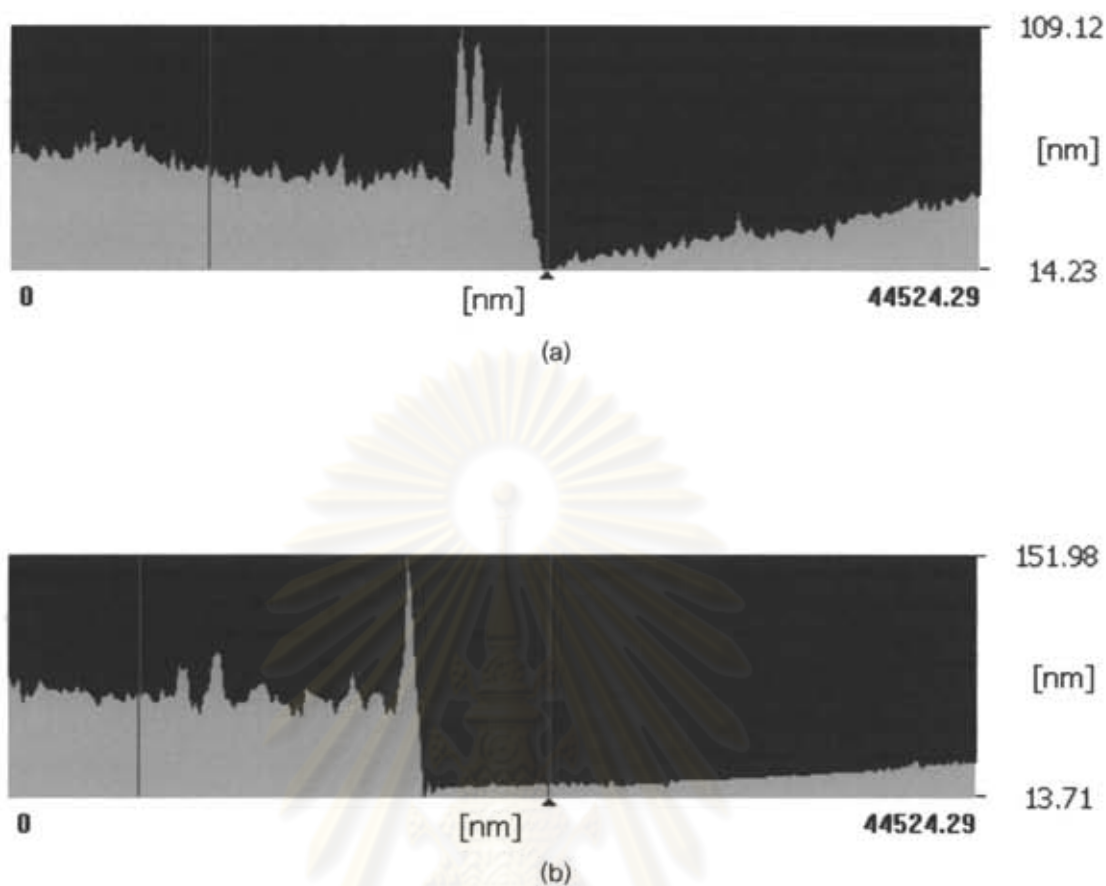


Figure 4.15 AFM height images of the film containing PAH/PAA (a) 2 bilayers and (b) 4 bilayers having thickness of 36 and 51 nm, respectively.

ศูนย์วิทยทรัพยากร
จุฬาลงกรณ์มหาวิทยาลัย

To create the superhydrophobic surface, the Aerosil[®] 200 SiO₂ was deposited onto the etched polyelectrolyte bilayers. Finally, the semifluorinated silane molecules were deposited by dipping the sample into silane solution followed by cross-linking at 180 °C for 2 h. Figure 4.16 shows a plot of contact angle of the final films versus number of polyelectrolyte bilayers. The contact angles were 171.6, 171.8, 172.6, 174.2 and 174.6 degrees for the films containing 1, 3, 5, 10 and 20 PAH/PAA bilayers, respectively. Obviously, all the films were superhydrophobic, and the films containing higher number of bilayers were slightly more superhydrophobic. This could be explained in term of the increase of surface roughness of etched the different number of bilayers films, which would allow suitable template for superhydrophobic surface.

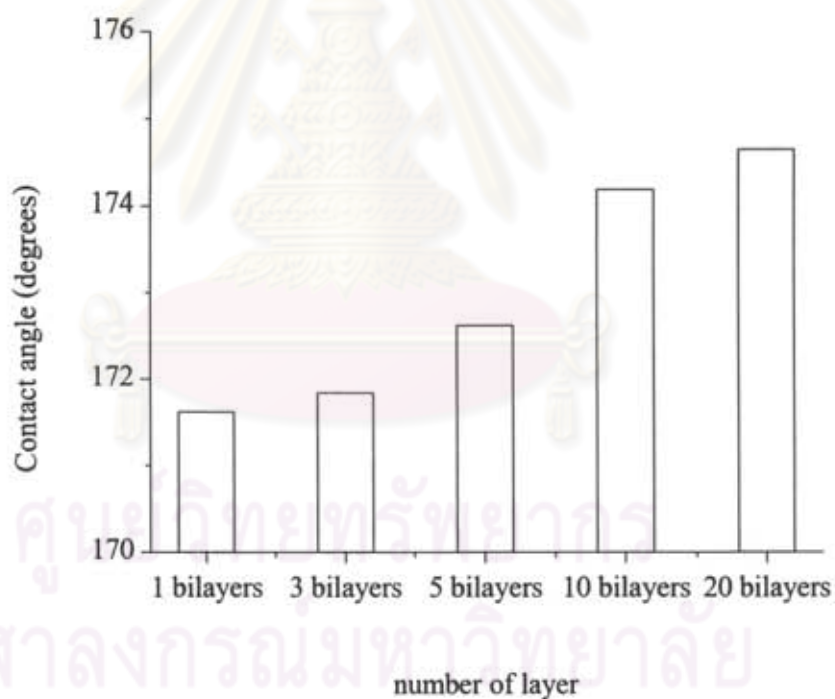


Figure 4.16 Relationship between hydrophobicity and number of PAH/PAA layers.

Figure 4.17 shows an optical transmittance of the uncoated and coated glass slides. The optical transmittance in a visible spectrum of all films was approximately 90% indicating that the films were transparent. At the wavelength of < 550 nm, the films transparency slightly decreased with the increase of film thickness, and the films were slightly less transparent compared to the bare glass slide. The slight decrease of the optical transparency of the thicker films may be attributed to more content of the silica and the presence of more open porosity with size close to the wavelength of visible light. Nevertheless, this result shows that the film prepared in this study satisfied the requirement of transparency. The transmittance of the films was closed to that of the optically transparent superhydrophobic films reported in the literature [6].

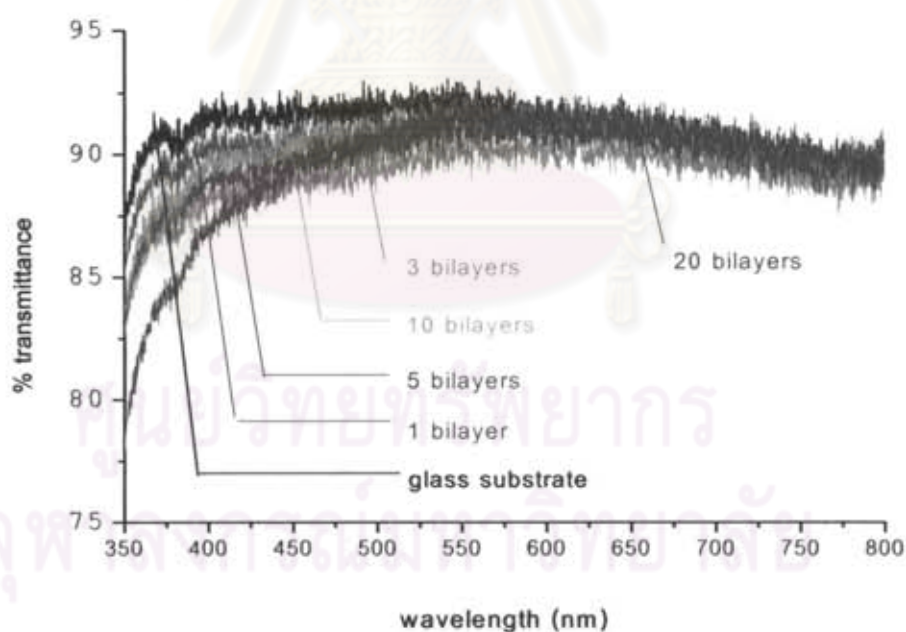


Figure 4.17 Relationship between wavelength and percent transmittance of glass substrate, of the film containing 1, 3, 5, 10 and 20 PAH/PAA bilayers.

In order for the superhydrophobic films to be practically applicable, it must exhibit satisfied stability. Aside from developing an inexpensive, easily applicable and versatile coating procedure, their stability is an important consideration which determines the technological success. Figure 4.18 shows the change of contact angle when the films were kept in open air in the laboratory at room temperature for about a month. The initial values of contact angles of the films containing 1, 3, 5, 10 and 20 PAH/PAA bilayers were 171.6, 171.8, 172.6, 174.2 and 174.6 degrees, respectively. Upon exposure to ambient atmosphere, the degree of superhydrophobicity was gradually decreased during the first 10 days, and tended to be constant afterward, regardless of number of the bilayers. However, all films still had superhydrophobicity after 24 days as the contact angle is > 150 degrees. The films containing higher number of bilayers were slightly more superhydrophobic. It is anticipated that the contact angle can be further decrease if the films are exposed outdoor. It is well known that the excellent hydrophobicity of an artificially constructed superhydrophobic surface gradually degrades over long periods of outdoor exposure. This is the fatal obstacle to be surmounted for practical application. Moreover, one of the causes of the degradation is the accumulation of stains that adhere to the surface [14].

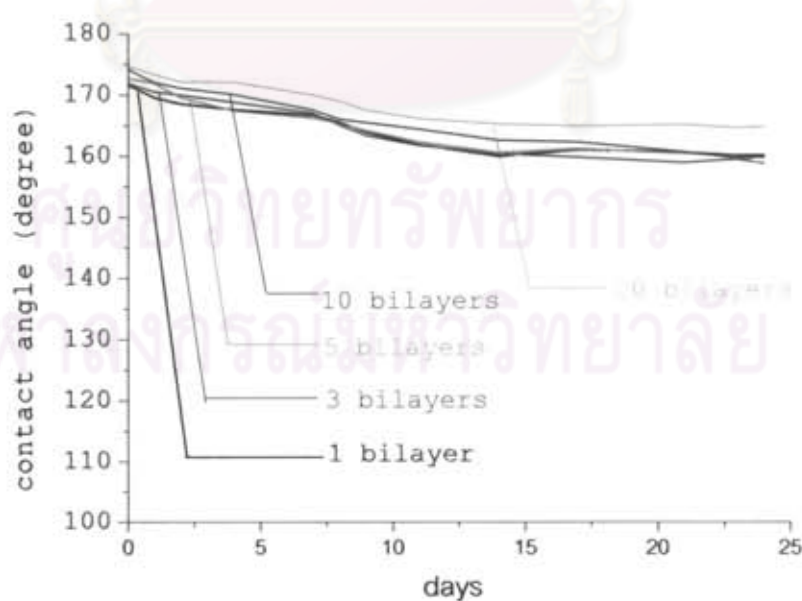


Figure 4.18 Relationship between number of bilayers and film stability.

4.2.4 Film adhesion

The results of adhesion testing for films containing the Aerosil[®] 200, Aeroperl[®] 300/30 and Aeroperl[®] 806/30 at various contents are presented in Table 4.4. The tape test result demonstrates the strong adhesion of the films containing 0.05 and 1 wt.% particle. However, the films containing 5 wt.% particle have flaked slightly along the cuts made in the coating and yielded rating of 4B for 5 wt.% Aerosil[®] 200 and Aeroperl[®] 300/30 containing film and 3B for Aeroperl[®] 806/30 containing film, respectively. Classification of adhesion test results is given in Appendix A. It was found that the content of particle in the suspension plays a critical role on the adhesion properties. At high percent content of particle in the suspension, the films tended to peel off from glass substrate easier. The tested samples were also analyzed under an optical microscope to provide a more critical look at the adhesion of each coating. The images of films containing 5 wt.% Aeroperl[®] 806/30 before and after measured by tape test are shown in Figure 4.19 and 4.20, respectively. The images of other samples are summarized in Appendix B.

Table 4.4 Adhesion test result by a standard ASTM: D-3359-02 tape test.

Types of particle	Ratio (%wt)	Percent area removed	Classification
Aerosil [®] 200	0.05	None	5B
	1	None	5B
	5	Less than 5%	4B
Aeroperl [®] 300/30	0.05	None	5B
	1	None	5B
	5	Less than 5%	4B
Aeroperl [®] 806/30	0.05	None	5B
	1	None	5B
	5	5 – 15%	3B

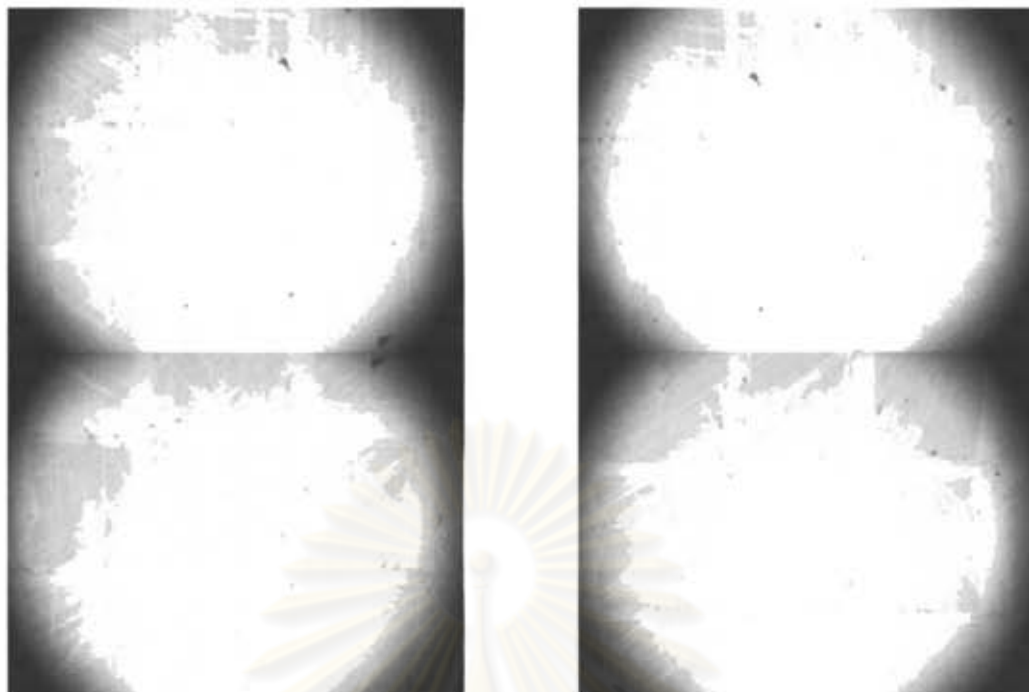


Figure 4.19 Film containing Aeroperl[®] 806/30 at 5 wt.% before tape test.



Figure 4.20 Film containing Aeroperl[®] 806/30 at 5 wt.% after tape test.

4.2.5 Surface energy

Table 4.5 summarizes values of the static contact angle of water and diiodomethane, and the surface free energy calculated by using the Owen – Wendt method which was the most widely used method for calculation of surface free energy of solids. The results show that the films containing the Aerosil® 200 have surface free energy in a range of about 1-12 mJ/m², depending on the SiO₂ content employed. The films containing Aeroperl® 300/30 shows similar surface free energy of about 1-13 mJ/m². However, the films containing the Aeroperl® 806/30 showed slightly lower surface free energy of about 1-9 mJ/m² that may be caused by the hydrophobic treated surface. Values of surface free energy obtained in this work following the Owen – Wendt's method were of comparable figure to the value reported in the literature [74]. According to the Fowkes theory [46], interactions between non-polar solid and liquid can be attributed to London dispersion forces. Owen – Wendt [47] suggested that the dispersive (d) and hydrogen (h) forces may be important across the interface for polar solid and liquid. In order to calculate the solid surface free energy, both of contact angle and the polarity of two liquid was used.

In addition to the Owen – Wendt method, the Chibowski method was also used to estimate surface free energy from dynamic contact angle. However, it is noticed that this method is applied for surface of low water contact angle (typically < 130 degrees). Table 4.6 shows a summary of the advancing and receding contact angles of water as well as the calculated surface free energy of the film. Regardless of the types of particle employed, the contact angle increased with increasing amount of the SiO₂ coverage which enhanced the surface roughness. The results shows that the films containing the Aerosil® 200 had the lowest surface free energy of about 0.03 – 0.5 mJ/m². The films containing the Aeroperl® 300/30 and Aeroperl® 806/30 showed much higher surface free energy of about 3 – 11 and 0.5 – 9 mJ/m², respectively. All the films had narrow hysteresis of only 3.0 – 9.0 degrees, indicating that water droplets can roll off easily on the tilted surface. Note that the surface free energy obtained in this work following the Chibowski's method was less than that reported in the literature because of very high contact angle obtained in this work [70-71].

By comparison the surface free energies calculated by using the Owen – Wendt and Chibowski methods, it was noticed that for the films containing the Aeroperl[®] 300/30 and 808/30 the calculated surface free energies were of similar values. Note that values of contact angle of these films were in a range of 132 - 158 degrees. However, for the films containing the Aerosil[®] 200 the surface free energies calculated from the two methods were significantly different. The values calculated from the Owen – Wendt method were around 20 times higher than the values calculated from the Chibowski method. Note that values of contact angle of these films were in a range of 169 - 174 degrees which are higher than the films containing the Aeroperl[®] SiO₂. A discrepancy between surface energy at higher contact angle calculated from the two methods can be explained based on the parameter used in the equation. For the Chibowski method, surface free energy is calculated solely from value of water contact angle. At very high value of contact angle as for the films containing the Aerosil[®] 200, the calculated free energy was very low. Unlike the Chibowski method, the Owen – Wendt method takes into account effect of polarity and dispersion of the liquid for calculation of the surface free energy. Thus, in case of high contact angle, the Owen – Wendt method is more suitable than the Chibowski method. Nevertheless, both methods gave similar trend of calculated surface free energy that it decreased with the increase of contact angle (hydrophobicity) and surface roughness which increased with the increased concentration of SiO₂ suspension employed. Figures 21 and 22 show relationship between water contact angle and surface roughness and surface free energy calculated by Owen – Wendt and Chibowski methods, respectively.

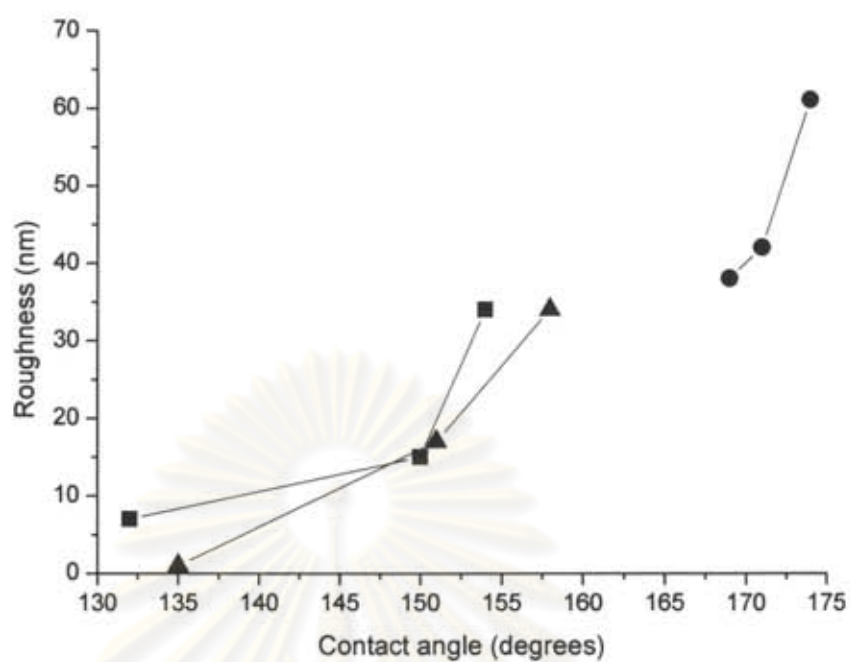
Table 4.5 Values of contact angle and Owen – Wendt method's surface energy of the films containing different type and content of SiO₂ particle.

Types of SiO ₂	Content (wt.%)	Contact angle (degrees)		γ_s^D (mJ/m ²)	γ_s^P (mJ/m ²)	Surface energy (mJ/m ²)
		Water	Diodomethane			
Aerosil [®] 200 (particle size = 12 nm, SSA = 200 m ² /g)	0.05	169 ± 0.27	99 ± 0.92	9.04	3.51	12.54
	1	171 ± 0.69	115 ± 2.42	4.23	1.65	5.88
	5	174 ± 0.90	138 ± 2.16	0.84	0.33	1.16
Aeroperl [®] 300/30 (particle size = 30 μm, SSA = 300 m ² /g)	0.05	132 ± 0.75	90 ± 1.57	12.70	0.35	13.05
	1	150 ± 0.33	105 ± 3.53	6.98	0.58	7.56
	5	154 ± 0.99	123 ± 2.04	2.63	0.26	2.89
Aeroperl [®] 806/30 (particle size = 30 μm, SSA = 300 m ² /g)	0.05	135 ± 0.45	99 ± 2.64	9.04	0.24	9.27
	1	151 ± 0.19	123 ± 2.7	2.63	0.18	2.82
	5	158 ± 0.19	134 ± 2.65	1.18	0.12	1.30

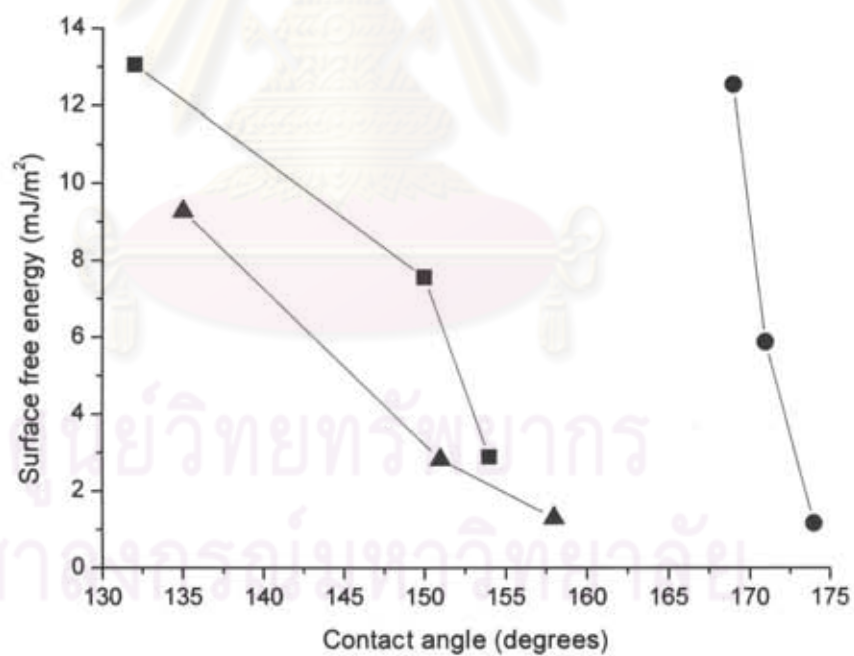
Table 4.6 Values of contact angle and Chibowski method's surface energy of the films containing different types and contents of SiO₂ particle.

SiO ₂ type	Content (wt.%)	Contact angles (deg.)		Hysteresis (deg.)	Surface energy (mJ/m ²)
		Advancing	Receding		
Aerosil [®] 200 (particle size = 12 nm, SSA = 200 m ² /g)	0.05	167 ± 1.4	158 ± 1.2	9.0	0.51
	1	172 ± 1.6	169 ± 1.7	3.0	0.30
	5	175 ± 0.7	170 ± 1.3	5.0	0.03
Aeroperl [®] 300/30 (particle size = 30 μm, SSA = 300 m ² /g)	0.05	132 ± 1.3	128 ± 2.1	4.0	11.29
	1	150 ± 1.3	146 ± 1.6	4.0	4.40
	5	154 ± 0.9	148 ± 1.2	6.0	3.07
Aeroperl [®] 806/30 (particle size = 30 μm, SSA = 300 m ² /g)	0.05	136 ± 0.69	134 ± 0.52	2.0	9.51
	1	154 ± 1.11	147 ± 1.48	7.0	2.97
	5	168 ± 0.89	164 ± 2.00	4.0	0.53

ศูนย์วิทยทรัพยากร
จุฬาลงกรณ์มหาวิทยาลัย



(a)



(b)

Figure 4.21 Relationship between (a) hydrophobicity and roughness and (b) hydrophobicity and surface energy from Owen – Wendt method of films containing Aerosil® 200 (●), Aeroperl® 300/30 (■) and Aeroperl® 806/30 (▲).

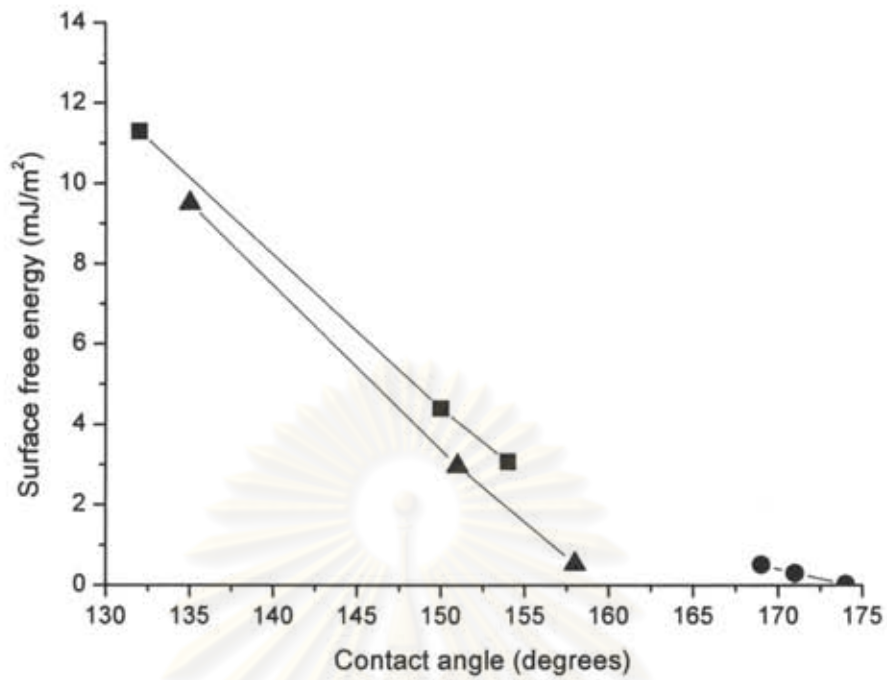


Figure 4.22 Relationship between (a) hydrophobicity and roughness and (b) hydrophobicity and surface energy from Chibowski method of films containing Aerosil[®] 200 (●), Aeroperl[®] 300/30 (■) and Aeroperl[®] 806/30 (▲).

ศูนย์วิทยทรัพยากร
จุฬาลงกรณ์มหาวิทยาลัย

On the other aspect, degree of wetting can be determined by the cohesive forces of liquid molecules among themselves and the adhesive forces that result from molecular interactions between the liquid and the solid as illustrated in Figure 4.23. As the contact angle decreases, wetting increases. Conversely as the contact angle approaches 180° , wetting decreases. Wettability can be explained by the relative strength of the cohesive (liquid/liquid) and adhesive (solid/liquid) forces. Strong adhesion with weak cohesion produces very low contact angles with nearly complete wetting. As the solid/liquid interactions weaken and the liquid/liquid interactions strengthen, wetting diminishes and contact angle increases. For a certain type of liquid, the adhesive force has constant value. Thus, the cohesive force between liquid and solid phase becomes influencing factor to wettability.

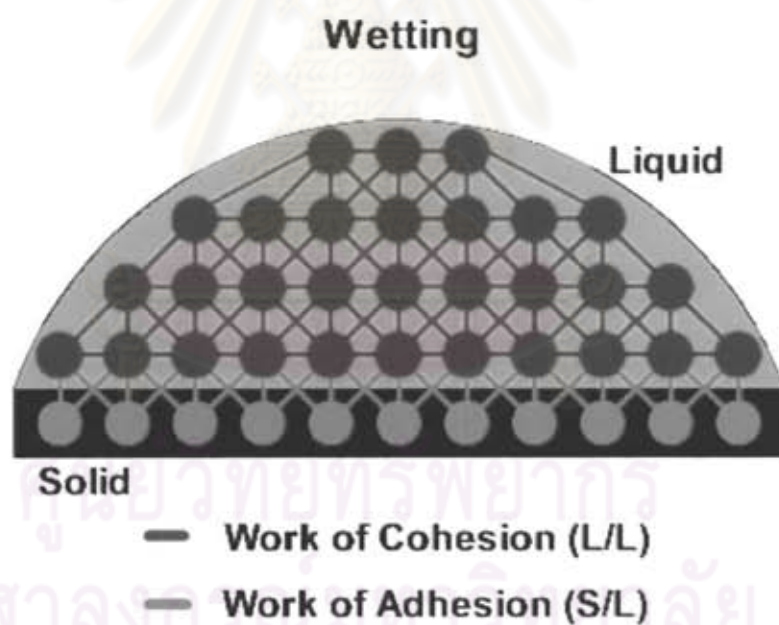


Figure 4.23 Diagram of work between liquid/liquid and solid/liquid.

Based on the work shown in Figure 4.23, the surface free energy between liquid and solid was calculated to explain work of adhesion between solid and liquid. The surface free energy of solid can be calculated from Owen – Wendt method as shown in Table 4.5. According to the drawing in Figure 4.24, surface free energy between liquid and solid can be express as:

$$\gamma_{sl} = \gamma_{sv} - \gamma_{lv} \cos\theta \quad (4.1)$$

where θ is contact angle, γ_{sl} is surface energy between solid and liquid, γ_{sv} is surface energy between solid and vapor and γ_{lv} is surface energy between liquid and vapor. Surface free energy between water and the films containing various type and content of silica particle can be calculated by this equation and the results are shown in Table 4.7.

Surface free energy between water and the films was in a range of about 60 – 83 mJ/m². The films containing the Aerosil[®] 200 have highest surface free energy between solid and liquid. Increasing of energy at the interface between liquid and solid means that the system becomes thermodynamically less stable. To be more thermodynamically stable, solid-liquid interface free energy must be minimized. That is, water will bead up to reduce this interface area, resulting to high water contact angle. Based on this analysis, the films containing the Aerosil[®] 200 (which had high surface free energy between liquid and solid) had high water contact angle. In case of the films containing the Aeroperl[®] 300/30 and Aeroperl[®] 806/30, free energy between solid and liquid was about 60 – 70 mJ/m² which is close to surface free energy of water (72 mJ/m² [75]). These films had lower values of water contact angle compared to that of the films containing the Aerosil[®] 200.

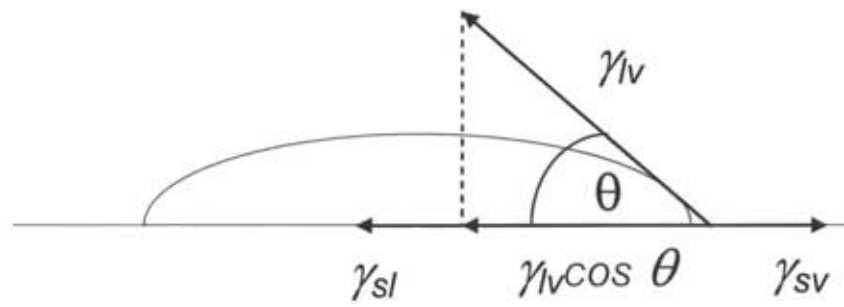


Figure 4.24 Schematic illustration of surface free energy between vapor, liquid and solid.

ศูนย์วิทยทรัพยากร
จุฬาลงกรณ์มหาวิทยาลัย

Table 4.7 Values of contact angle, surface energy of solid and surface free energy between solid and liquid obtained from the films containing different types and contents of SiO₂ particle.

SiO ₂ type	Content (wt.%)	Contact angle (degrees)	Surface energy of solid (mJ/m ²)	Surface energy between liquid and solid (mJ/m ²)
Aerosil [®] 200 (particle size = 12 nm, SSA = 200 m ² /g)	0.05	169 ± 0.27	12.54	83.41
	1	171 ± 0.69	5.88	77.19
	5	174 ± 0.90	1.16	72.96
Aeroperl [®] 300/30 (particle size = 30 μm, SSA = 300 m ² /g)	0.05	132 ± 0.75	13.05	61.36
	1	150 ± 0.33	7.56	70.09
	5	154 ± 0.99	2.89	67.78
Aeroperl [®] 806/30 (particle size = 30 μm, SSA = 300 m ² /g)	0.05	135 ± 0.45	9.27	60.32
	1	151 ± 0.19	2.82	65.97
	5	158 ± 0.19	1.30	68.24

ศูนย์วิจัยทรัพยากร
จุฬาลงกรณ์มหาวิทยาลัย

4.3 Film formation by organic/inorganic hybrid method

4.3.1 Organic/inorganic hybrid films containing oxide particulate

4.3.1.1 Optimization of parameter by Taguchi method

Table 4.8 lists 15 conditions and properties of the films prepared according to the condition obtained from the Taguchi's DOE method. The films prepared according to these conditions had various values of contact angle and transmittance (%T) as summarized in the table. From these experimental results, the Taguchi's DOE can get the best condition by using the Signal-to-Noise ratio (SNR or S/N). The larger-the-better approach was chosen for analysis of the contact angle. Figure 4.25 shows the charts of levels of all factors with respect to type of particle, solid ratio and withdraw speed of the dip coater. The rank of the type of particle is as follow: Aerosil[®]200 > Aeroperl[®] 300/30 > TiO₂ P25 > Aeroperl[®] 806/30 > Cotiox. For solid ratios, the rank is as follow: 5 ≥ 10 > 0.01. For the withdraw speed, the rank is as follow 0.01 > 1.00 > 0.50. The S/N ratio curves (Larger-the-Better) show that the best condition for getting the highest contact angle is the maximum S/N ratio for each parameter. The best condition in this study as follow: particle type: Aerosil[®] 200; solid ratio: 5; and withdraw speed: 0.01. The predicted contact angle is 169.72 degrees. Then the film was prepared from the best condition. The contact angle of this film was 166 ± 0.69 degrees which was close to the predicted value. Therefore, the maximum withdraw speed was chosen for economic reason. The optimum condition was as follow: type of particle: Aerosil[®] 200; solid ratio: 5; and withdraw speed: 1.00. As shown in Figure 4.25(c), low withdrawal speed would lead to better S/N ratio. However, such very low speed is not practical.

Table 4.8 The conditions obtained from the Taguchi DOE analysis (larger is better).

Type of particle	Solid ratio	Speed (mm/sec)	Contact angle (degrees)	% Transparent
Aerosil® 200	0.01	0.5	106 ± 0.75	91 ± 1.38
Aerosil® 200	5	1	166 ± 0.16	89 ± 1.64
Aerosil® 200	10	0.01	154 ± 0.18	61 ± 1.42
Aeroperl® 300/30	0.01	1	103 ± 0.44	95 ± 0.75
Aeroperl® 300/30	5	0.01	151 ± 0.78	93 ± 1.23
Aeroperl® 300/30	10	0.5	121 ± 0.38	92 ± 1.70
Aeroperl® 806/30	0.01	0.5	104 ± 0.82	97 ± 0.74
Aeroperl® 806/30	5	1	107 ± 0.22	94 ± 0.90
Aeroperl® 806/30	10	0.01	153 ± 0.92	93 ± 1.15
TiO ₂ P25	0.01	1	104 ± 0.68	96 ± 1.58
TiO ₂ P25	5	0.01	153 ± 0.96	91 ± 1.26
TiO ₂ P25	10	0.5	124 ± 0.90	94 ± 1.49
Cotiox	0.91	0.01	109 ± 0.80	72 ± 0.89
Cotiox	5	0.5	102 ± 0.22	94 ± 1.79
Cotiox	10	1	103 ± 0.24	88 ± 1.64

จุฬาลงกรณ์มหาวิทยาลัย

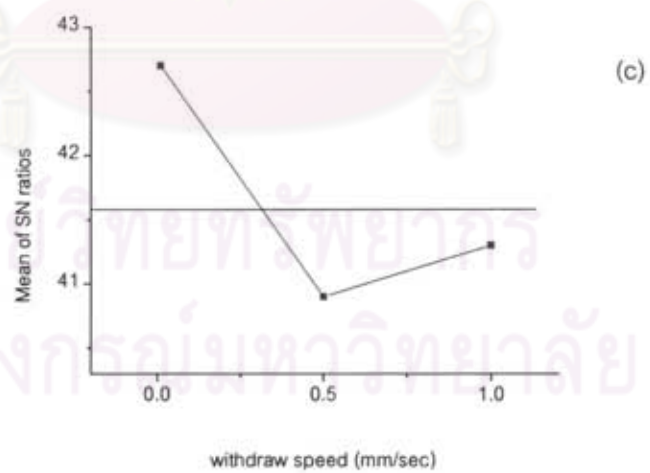
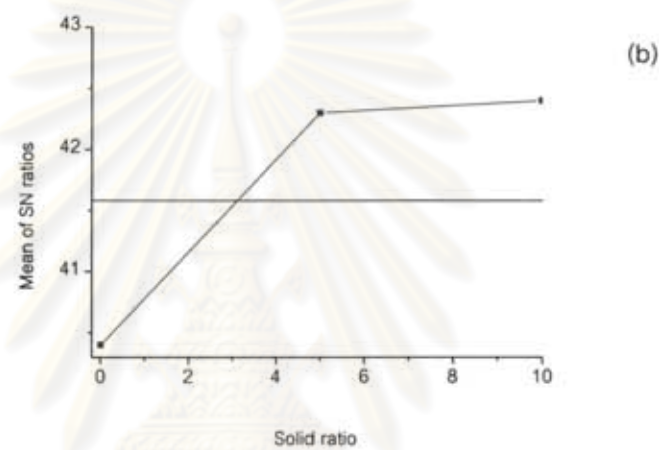
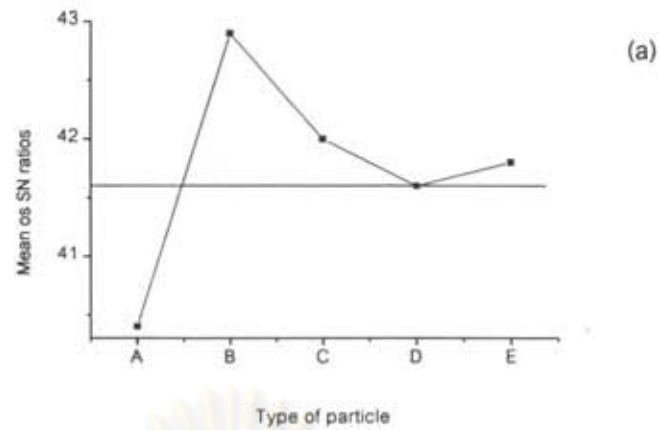


Figure 4.25 Main effects plot for S/N ratios to contact angle (A: Cotiox, B: Aerosil[®] 200, C: Aeroperl[®] 300/30, D: Aeroperl[®] 806/30 and E: TiO₂ P25).

4.3.1.2 Film topography

Figure 4.26 shows 2-dimension and 3-dimension AFM topological images of the hybrid organic/inorganic film prepared from the best condition obtained from the Taguchi's DOE method. Surface roughness is 60.05 nm. The Aerosil[®] 200 nanoparticles were seen as agglomerates having an average size of 1-2 μm . Each aggregated consists of several nanoparticles that gave rise to surface roughness at the nanoscale. On the rough surface, air can still be effectively trapped between the water droplet and the solid. Thus, the Cassie state can be maintained to achieve a superhydrophobic surface with high contact angle.

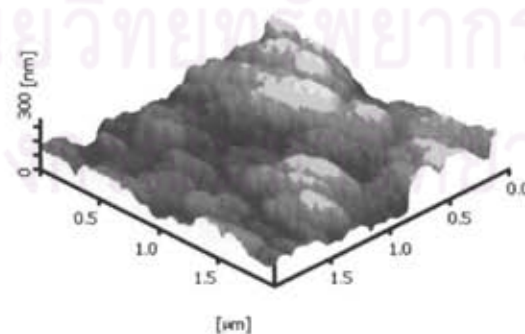
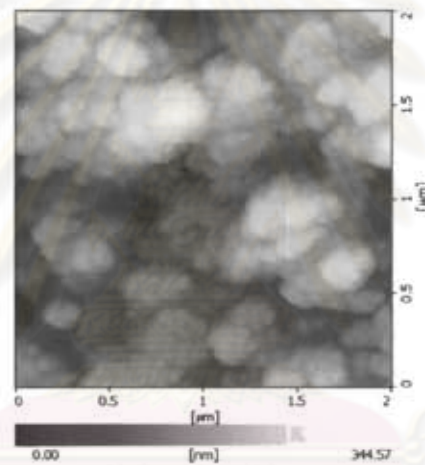


Figure 4.26 AFM topographical mapping of hybrid organic/inorganic film prepared from the optimum condition obtained by the Taguchi's DOE.

In order to determine thickness of the hybrid organic/inorganic film, AFM was employed as described in section 3.3.2. Figure 4.27 shows the AFM height image of the hybrid organic/inorganic film containing 5 wt.% Aerosil[®] 200. The film thickness was 690 nm. The thickness of this type of film was much higher than the thickness of the polyelectrolyte multilayer film. The simplicity of the process, and quality of the films obtained suggests that this hybrid film is the most appropriate way to obtain thick-films with controllable thickness in a sub-micron to micron range. Moreover, the method also opens-up possibilities for other potential applications [82-83]. However, since the transparent of film was desired for glass coating in this research, the transparent organic/inorganic hybrid film was prepared at thickness of less than 1 μm within a single dip coating process.



Figure 4.27 AFM height image of the hybrid film containing 5 %wt Aerosil[®] 200. The film's thickness was 692.5 nm.

4.3.1.3 Film stability

The usefulness of a superhydrophobic coating is determined by its stability. For practical use, the surface should retain its property. In order to study film stability, the hybrid organic/inorganic film was kept in ambient condition for about a month. Figure 4.28 shows contact angle of film versus duration. After keeping for about

one month, the contact angle decreased from 166 ± 0.71 degrees to 158 ± 0.62 degrees. When the film kept for over ten days, the contact angles gradually decrease. However, after twenty days the contact angles tended to be constant. After keeping for about one month, the contact angle was still higher than 150 degrees, exhibiting superhydrophobicity behavior. Comparing film stability of the hybrid organic/inorganic film and polyelectrolyte multilayer film, the polyelectrolyte multilayer film was slightly more stable than the hybrid organic/inorganic film.

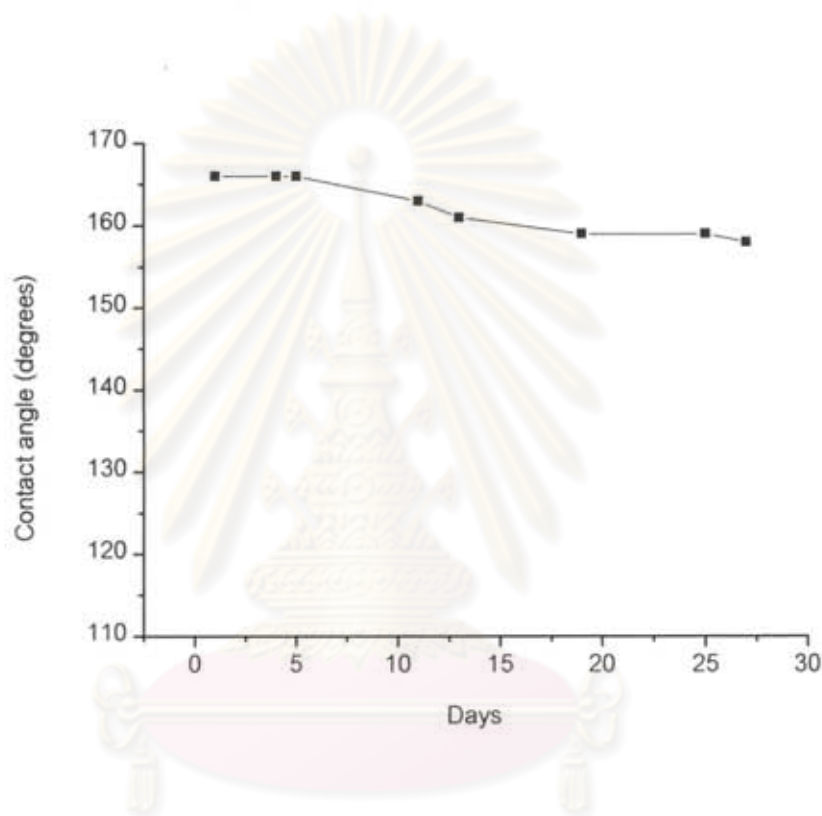


Figure 4.28 Relationship between contact angle and exposure duration.

4.3.1.4 Film adhesion

To study the adhesion property between coating and glass substrate, The tape test ASTM: D 3359 – 02 was used to measure adhesion by percent area removed. The images of films containing 5 wt.% Aerosil[®] 200 before and after the tape test are shown in Figure 4.29 and 4.30, respectively. The films containing the Aerosil[®] 200 5 wt.% had flakes slightly along the cuts made in the coating. The film removed by the tape test was less than 5% which was classified in a class 4B, demonstrating strong

adhesion between the film and substrate. The adhesion observed in the hybrid organic/inorganic film was slightly less than that in the polyelectrolyte multilayer film. It may be caused by its higher thickness.

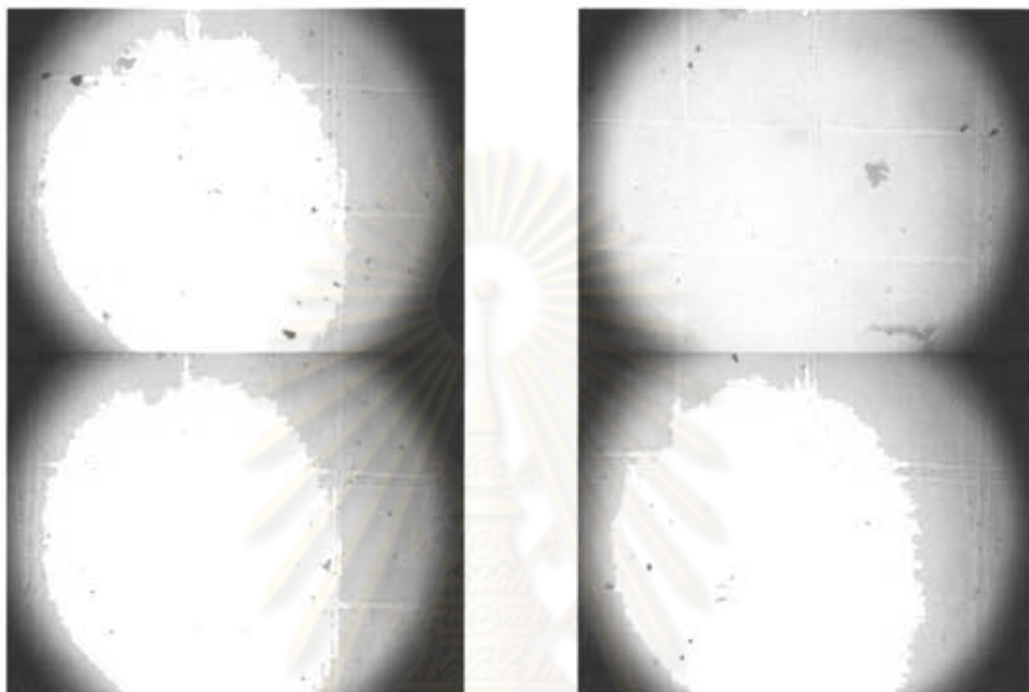


Figure 4.29 Film containing Aerosil® 200 at 5 wt.% before tape test.



Figure 4.30 Film containing Aerosil® 200 at 5 wt.% after tape test.

4.3.1.4 Surface free energy

Surface free energy of hybrid organic/inorganic film preparing from the optimum condition was calculated by Owens – Wendt method. The contact angle of water and diiodomethane were 166 ± 0.16 and 120 ± 0.85 degrees, respectively. The calculated data for γ_s^D , γ_s^P and γ_s were 3.18, 1.03 and 4.20 mJ/m^2 , respectively. The film shows low surface free energy of 4.20 mJ/m^2 which was in same range of surface free energy that obtained from the polyelectrolyte multilayer of about $1\text{-}13 \text{ mJ/m}^2$.

4.3.2 Organic/inorganic hybrid films containing oxide sol

4.3.2.1 Effect of TIP:PDMS ratio

Figure 4.31 shows the relationship between the value of contact angle and the TIP:PDMS ratio. Effect of heat-treated temperature on film's hydrophobicity is also illustrated. The precursor solutions used to prepare these films were aged for 2 days. At a given TIP:PDMS ratio, the contact angle decreased with increasing heat-treated temperature. The decrease of contact angle may be due to the effect of surface morphology as the surface changed from sharp to more rounded protrusion. The surface consisting large, round protrusion would have larger extend of contact area with water droplet and therefore exhibit lower contact angle. Partial decomposition of a low-energy PDMS to a higher-energy component was also another issue that could attribute to lower degree of hydrophobicity.

A maximum contact angle of 122° was obtained with TIP:PDMS molar ratio of 1.0:1.0, and heat-treated at 60°C . The effect of TIP:PDMS ratio on film's hydrophobicity was not well understand. It was expected that the hydrophobicity would increase with the increase of the PDMS content which was the constituent having low surface energy compared to the titanium hydrous oxide, provided that surface topography was unchanged at any TIP:PDMS ratio. However, this scenario might not be the case as surface topography might have changed. For instance, Iketani et.al.

reported that surface of the hybrid film became rougher and more porous with increasing PDMS content [24].

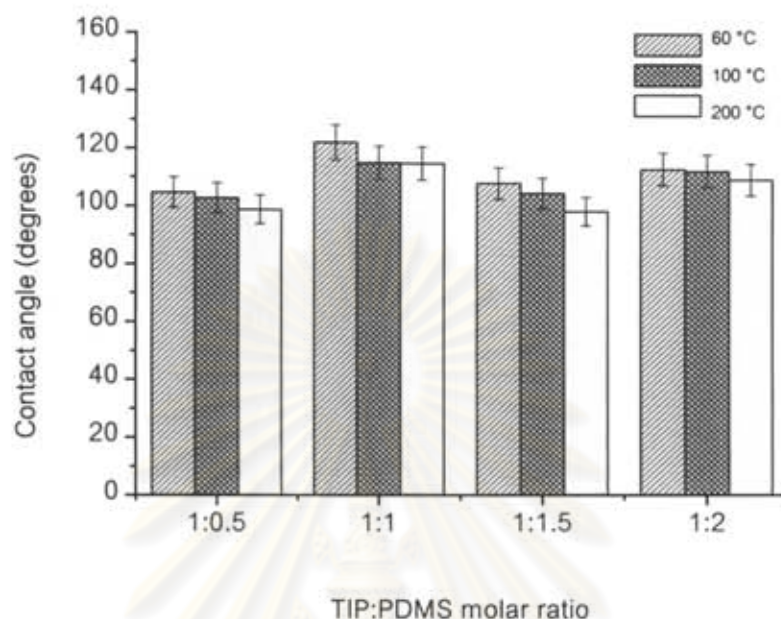


Figure 4.31 Effect of TIP:PDMS molar ratio on surface hydrophobicity.

4.3.2.2 Effect of heat treatment

The coating solution was investigated for thermal property by using TGA. Topology and hydrophobicity of films were studied by AFM and contact angle goniometer, respectively. Figure 4.32 shows the TGA profile of the prepared hybrid film. There was essentially no weight loss below 100 °C. Two distinct weight losses were observed at higher temperature. The first loss of 38% was in the temperature range of 200 - 400 °C while the second loss of 54% was in the temperature range of 400 - 550 °C. However, the residual mass was found after reaching 600 °C. The two weight losses were attributed to decomposition of organic constituent in the TIP and degradation of the PDMS, respectively [84-85]. Based on this thermal result, it is

recommended the film should be heat-treated to only 200 °C to preserve chemical nature of the PDMS.

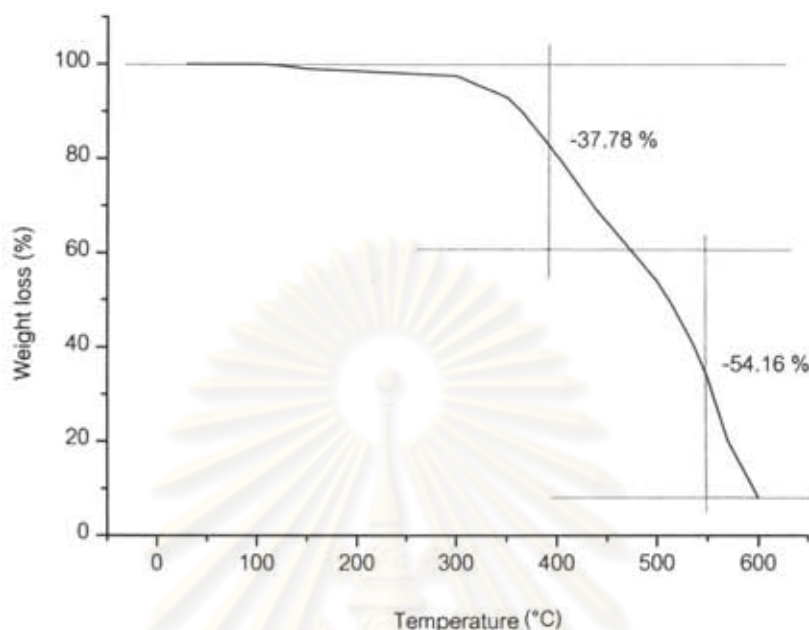


Figure 4.32 TGA profile of the sample prepared from the precursor having the TIP:PDMS ratio of 1.0:1.5, in N₂ atmosphere.

Figure 4.33 shows AFM topographical images of the films containing TIP:PDMS ratio of 1.0:1.5 heat-treated at 60, 100 and 200°C, respectively. The precursor solution was aged for 1 day before deposition. The films treated at 60 and 100°C had similar topographical feature that they consisted of fine protrusions (dimension of ~50 – 100 nm) and had surface roughness of 1.2 ± 0.06 nm and 3.0 ± 0.15 nm, respectively. The two films had water contact angle of ~100 degrees. Some bright features, ~0.3 - 0.5 μm in size, which might be titanium (hydrous) oxide particles were also observed. The film heated at 200°C consisted of large protrusions of ~0.1 – 0.3 μm, and had higher surface roughness of 8.7 ± 0.43 nm and lower contact angle of 91 degrees. Based on the TGA result which shows slight weight loss (few percents) at the temperature between 100 - 200 °C, it was believed that such large feature was

formed as a result of evaporation and/or partial decomposition of the organic constituents such as solvent or perhaps the PDMS molecules.

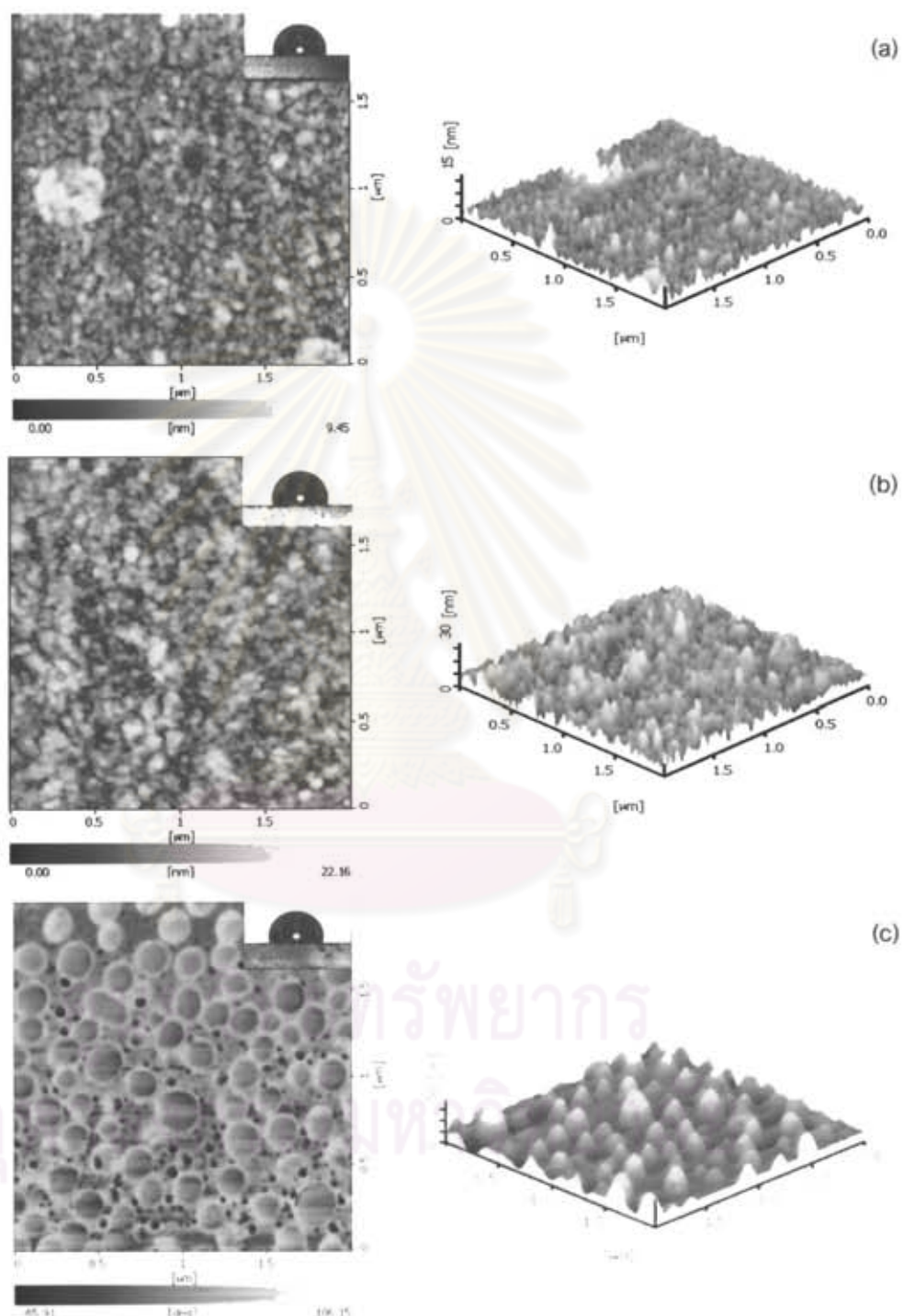


Figure 4.33 AFM topographical images of the PDMS-based hybrid films coated on glass substrate heat-treated at (a) 60 (b) 100 and (c) 200 °C.

Values of contact angle and surface roughness of the films heated at various temperatures are summarized in Table 4.9. It has been reported that hydrophobicity depends on both surface topography and chemical composition. High surface roughness usually gives rise to more hydrophobicity. Scale of roughness is also another important parameter to be taken into account. In this present study, it has been illustrated that fine protruding feature gave more hydrophobicity than larger, rounded feature although it has lower value of roughness, as well as lower contact angle area with water droplet.

Table 4.9 Values of contact angle and surface roughness of the films obtained at difference heating temperature.

Heating temperature (°C)	Contact angle (degrees)	Surface roughness (nm)
60	100 ± 0.2	1.2 ± 0.06
100	99 ± 0.2	3.0 ± 0.15
200	91 ± 0.3	8.7 ± 0.43

ศูนย์วิทยทรัพยากร
จุฬาลงกรณ์มหาวิทยาลัย

4.4 Comparison of the polyelectrolyte multilayer and hybrid organic/inorganic films

The methods for preparation of water-repellent, superhydrophobic films have been described. In this section, comparison of two types of superhydrophobic films - polyelectrolyte multilayer and hybrid inorganic/organic films – are summarized. Important aspects of the preparation method and film quality are shown in Table 4.10. Regarding the preparation procedure, the polyelectrolyte multilayer films prepared by layer-by-layer deposition method is more complicated than a method for preparation of the hybrid organic/inorganic films which can be deposited just by a single dipping because surface enhancing material and low surface free energy substance are mixed together. However, the layer-by-layer deposition gives more feasibility of designing roughness values.

Regarding the films' properties, both types of films show good optical transparency of about 90% transmittance for the optimum preparation condition. These films have good adhesion that is classified as class "4B" based on a standard tape test. They also exhibit good stability after prolong exposure in the laboratory for months. At the optimum preparation condition, the polyelectrolyte and hybrid organic/inorganic films are of 50 nm and 690 nm thick, respectively. Both of films show excellent water repellency as they have very high water contact angle of 166 degrees for hybrid organic/inorganic films and 174 degrees for the polyelectrolyte multilayer film which can be regarded as an "ultrahydrophobic" film (water contact angle of 170 degrees and higher).

ศูนย์วิทยทรัพยากร
จุฬาลงกรณ์มหาวิทยาลัย

Table 4.10 Comparison of the polyelectrolyte multilayer and hybrid films. The listed values are at the optimum condition for each coating method.

Properties	Polyelectrolyte multilayer	Hybrid organic/inorganic
1. Procedure	Complicate	Simply
2. Transparency	~90%	~90 %
3. Adhesion	Good	Good
4. Stability (in door)	Good	Good
5. Thickness	50 nm	690 nm
6. Water contact angle	174 degrees	166 degrees
7. Surface roughness	~60 nm	~60 nm
8. Surface free energy	1 mJ/m ²	4 mJ/m ²

CHAPTER V

CONCLUSIONS

Inspired by lotus effect found at surface of some plant's leaves, the superhydrophobic films were prepared by employing two different methods: layer-by-layer deposition of polyelectrolyte multilayer film and dip coating of organic/inorganic hybrid film. The films were prepared based on the same principle that the surface roughness was enhanced while the surface free energy was reduced.

For the layer-by-layer deposition method, the films were prepared by deposition of the transparent PAH/PAA polyelectrolyte bilayers, followed by the SiO₂ and silane layers. Three types of commercial silica particles - Aerosil[®] 200, Aeroperl[®] 300/30 and Aeroperl[®] 806/30 - were employed as surface roughness enhancer. It was found that film's preparation condition had dramatic effect on the film's hydrophobicity. Two-stage etching with HCl solutions of pH = 1.0 for 1.5 h followed by pH = 2.3 for 1.5 h was found to be more effective than one-step etching with either HCl solution of pH = 1.0 for 3 h or pH = 2.3 for 3 h. It was also found that the film having highest contact angle of 174 ± 0.90 degrees was obtained when the Aerosil[®] 200 was utilized as a surface roughness enhancer. The contact angle increased with the increase concentration of the SiO₂ particle employed regardless of the SiO₂ type, which can be related to the increased surface roughness. However, the surface roughness created by incorporation of the Aeroperl[®] 300/30 and Aeroperl[®] 806/30 which are tens of microns in size was slightly less than that created by the Aerosil[®] 200, probably due to less deposition of such large size particle during a dip coating step. All the films were about 90% transmittance which were transparent, and had good adhesion and stability.

For the organic/inorganic hybrid films, the organic matrix was a methyl hydrogen siloxane-based material which is a low surface energy material while the inorganic particles were incorporated in the form of either particulate or sol. The particulates employed were Aerosil[®] 200, Aeroperl[®] 300/30, Aeroperl[®] 806/30, P25 TiO₂

and Cotiox TiO₂. They were mixed with the methyl hydrogen siloxane matrix as a surface roughness enhancer. Since the film was coated by only 1 dipping cycle and many preparation conditions were concerned for film preparation, the experimental condition was optimized by using a Taguchi's DOE method. The optimum condition for film's preparation was as follow: the methyl hydrogen siloxane-based matrix consisting of the Aerosil[®] 200 having a solid ratio of 5 and coated at the withdrawal speed of 1 mm/sec. This film had the contact angle of 166 degrees. The film was transparent, had good adhesion and stability. The other type of organic/inorganic hybrid film was prepared from the polydimethylsiloxane base consisting of the TiO₂ sol derived from titanium tetraisopropoxide. The films prepared from this formulation had the maximum contact angle of only 122 degrees.

Degree of superhydrophobicity is dependent on two important factors: surface roughness and surface free energy. In this study, the highest surface roughness of 60 nm was achieved from the polyelectrolyte multilayer film containing Aerosil[®] 200. Surface free energy of the polyelectrolyte multilayer film calculated by using the Owen – Wendt method was in a range of 1 – 13 mJ/m², depending on the type and content of incorporated SiO₂ particle, while that of the hybrid film was 4.2 mJ/m². However, much lower surface free energy was obtained from the Chibowski's method. It was in a range of only 0.03 – 0.51 mJ/m² for the polyelectrolyte multilayer film containing the Aerosil[®] 200, and in a range of about 0.5 – 11 mJ/m² for the polyelectrolyte multilayer film containing the Aeroperl[®] SiO₂. It is concluded that the surface energy calculated from the Owen – Wendt method is more reliable since it takes into account the effect of polarity and dispersion of water. The correlation between degree of superhydrophobicity and surface roughness and surface free energy was also investigated. The film's hydrophobicity increased with the increase of surface roughness and the decrease of surface free energy.

Suggestions for Future Work

Although the superhydrophobic films were successfully prepared with satisfied properties, some suggestions are given below to further improve the film's property.

Other films' properties such as thermal stability, chemical stability as well as UV-resistant property should be investigated.

The films can be applied to other substrates such as wood, concrete or brick for practical use. Deposition on large or complex-shaped substrates should also be attempted.

Further investigation on the surface chemical groups is suggested. In this study, ATR – FTIR analysis was attempted but no reliable results were obtained since the films were too thin.

In case of the hybrid organic/inorganic film, particulate inorganic component such as the P25 TiO₂ gave interesting result at high water contact angle. As well known of its excellent photocatalytic property, it is attractive for further study.



ศูนย์วิทยทรัพยากร
จุฬาลงกรณ์มหาวิทยาลัย

REFERENCES

- [1] W. Bartholtt and C. Neinhuis. Purity of the sacred lotus, or escape from contamination in biological surfaces. Planta. 202 (1997) : 1-8.
- [2] C. Qian, C. Guang-hua, F. Yan and R. Lu-quan, Super-hydrophobic characteristics of butterfly wing surface. J. Bionic Eng. 1, 4 (2004) : 249-255.
- [3] M. Ma and R.M. Hill. Superhydrophobic surfaces. Curr. Opin. Colloid Interface Sci. 11 (2006) : 193-202.
- [4] X.M. Li, D. Reinhoudt, and M. Crego-Calama. What do we need for a superhydrophobic surface? a review on the recent progress in the preparation of superhydrophobic surfaces. Chem. Soc. Rev. 36 (2007) : 1350-1368.
- [5] A. Nakajima. Design of a transparent hydrophobic coating. J. Ceram. Soc. Japan. 112, 10 (2004) : 533-540.
- [6] H.M. Shang, Y. Wang, S.J. Limmer, T.P. Chou, K. Takahashi and G.Z. Cao. Optically transparent superhydrophobic silica-based films. Thin Solid Films. 472 (2005) : 37-43.
- [7] X. Hou, F. Zhou, B. Yu and W. Liu. Superhydrophobic zinc oxide surface by differential etching and hydrophobic modification. Mater. Sci. Eng. A. 452-453 (2007) : 732-736.
- [8] T. Soeno, K. Inokuchi and S. Shiratori. Ultra-water-repellent surface: fabrication of complicated structure of SiO₂ nanoparticles by electrostatic self-assembled films. Appl. Surf. Sci. 237 (2004) : 543-547.
- [9] N. Zhao, F. Shi, Z. Wang and X. Zhang. Combining layer-by-layer assembly with electrodeposition of silver aggregates for fabricating superhydrophobic surfaces. Langmuir. 21 (2005) : 4713-4716.
- [10] G. Zhang, D. Wang, Z.Z. Gu and H. Mohwald. Fabrication of superhydrophobic surfaces from binary colloidal assembly. Langmuir. 21 (2005) : 9143-9148.
- [11] M. Miwa, A. Nakajima, A. Fujishima, K. Hashimoto and T. Watanabe. Effects of the surface roughness on sliding angles of water droplets on superhydrophobic surface. Langmuir. 16 (2000) : 5754-5760.
- [12] A. Nakajima, K. Abe, K. Hashimoto and T. Watanabe. Preparation of hard super-

- hydrophobic films with visible light transmission. Thin Solid Films, 376 (2000) : 140-143.
- [13] A. Nakajima, K. Hashimoto and T. Watanabe. Transparent superhydrophobic thin films with self-cleaning properties. Langmuir, 16 (2000) : 7044-7047.
- [14] M. Sasaki, N. Kieda, K. Katayama, K. Takeda and A. Nakajima. Processing and properties of transparent super-hydrophobic polymer film with low surface electric resistance. J. Mater. Sci., 39 (2004) : 3717-3722.
- [15] T.S. Lin, C.F. Wu and C.T. Hsieh. Enhancement of water-repellent performance on functional coating by using Taguchi method. Surf. Coatings Tech., 200 (2006) : 5253-5258.
- [16] L.Y.L. Wu, A.M. Soutar and X.T. Zeng. Increasing hydrophobicity of sol-gel hard coating by chemical and morphological modifications. Surf. Coatings Tech., 198 (2005) : 420-424.
- [17] K.C. Chang, H. Chen, C.K. Huang and S.I. Huang. Preparation of super-hydrophobic film with fluorinated-copolymer. J. Appl. Polym. Sci., 104 (2007) : 1646-1653.
- [18] A. Fuchs, F. Kanoufi, C. Combellas and M.E.R. Shanahan. Wetting and surface properties of (modified) fluoro-silanised glass. Colloids Surf. A: Physicochem. Eng. Aspects, 307 (2007) : 7-15.
- [19] C.T. Hsieh, J.M. Chen, R.R. Kuo, T.S. Lin and C.F. Wu. Influence of surface roughness on water- and oil-repellent surfaces coated with nanoparticles. Appl. Surf. Sci., 240 (2005) : 318-326.
- [20] H. Zhang, R. Lamb and J. Lewis. Engineering nanoscale roughness on Hydrophobic surface-preliminary assessment of fouling behaviour. Sci. Tech. Adv. Mater., 6 (2005) : 236-239.
- [21] H.J. Jeong, D.K. Kim, S.B. Lee, S.H. Kwon and K. Kadono. Preparation of water-repellent glass by sol-gel process using perfluoroalkylsilane and tetraethoxysilane. J. Colloid Interface Sci., 235 (2001) : 130-134.
- [22] J. Douce, J.P. Boilot, J. Biteau, L. Scodellaro and A. Jimenez, Effect of filler size and surface condition of nano-size silica particles in polysiloxane coatings. Thin Solid Films, 466 (2004) : 114-122.

- [23] N. Yamada, I. Yoshinaga and S. katayama. Formation behavior and optical properties of transparent inorganic-organic hybrids prepared from metal alkoxides and polydimethylsiloxane. J. Sol-Gel Sci. Tech. 17 (2000) : 123-130.
- [24] K. Iketani, R.D. Sun, M. Toki, K. Hirota and O. Yamaguchi. Sol-gel-derived TiO₂/poly(dimethylsiloxane) hybrid films and their photocatalytic activities. J. Phys. Chem. Solids. 64 (2003) : 507-513.
- [25] T. Shndou, S. Katayama, N. Yamada and K. Kamiya. Effect of composition on surface properties of polydimethylsiloxane-based inorganic/organic hybrid films. J. Sol-Gel Sci. Tech. 30 (2004) : 229-237.
- [26] L.Y.L. Wu, G.H. Tan, X.T. Zeng, T.H. Li and X. Chen. Synthesis and characterization of transparent hydrophobic sol-gel hard coatings. J. Sol-Gel Sci. Tech. 38 (2006) : 85-89.
- [27] E. Burkarter, C.K. Saul, F. Thomazi, N.C. Cruz, L.S. Roman, W.H. Schreiner. Superhydrophobic electrosprayed PTFE. Surf. Coatings Tech. 202 (2007) : 194-198.
- [28] L. Laguardia, D. Ricci, E. Vassallo, A. Cremona, E. Mesto, F. Grezzi and F. Dellera. Deposition of super-hydrophobic and oleophobic fluorocarbon films in radio frequency glow discharges. Macromol. Symp. 247 (2007) : 295-302.
- [29] W. Ming, D. Wu, R.V. Benthem and G.D. With. Superhydrophobic films from raspberry-like particles. Nanoletters. 5, 11 (2005) : 2298-2301.
- [30] C. Sun, L.Q. Ge and Z.Z. Gu. Fabrication of super-hydrophobic film with dual-size roughness by silica sphere assembly. Thin Solid Films. 515 (2007) : 4686-4690.
- [31] J.J. Harris, P.M. DeRose and M.L. Bruening. Synthesis of passivating, Nylon-like coatings through cross-linking of ultrathin polyelectrolyte films. J. Am. Chem. Soc. 121 (1999) : 1978-1979.
- [32] X. Zhang, F. Shi, X. Yu, H. Liu, Y. Fu, Z. Wang. L. Jiang and X. Li. Polyelectrolyte multilayer as matrix for electrochemical deposition of gold clusters: toward super-hydrophobic surface. J. Am. Chem. Soc. 126 (2004) : 3064-3065.
- [33] J.Y. Shiu, C.W. Kuo, P. Chen and C.Y. Mou. Fabrication of tunables superhydrophobic surfaces by nanosphere lithography. Chem. Mater. 16, 4 (2004) : 561-564.

- [34] R.M. Jisr, H.H. Rmaile and J.B. Schlenoff. Hydrophobic and ultrahydrophobic multilayers thin films from perfluorinated polyelectrolytes. Angew. Chem. Int. Ed. 44 (2005) : 782-785.
- [35] L. Zhai, F.C. Cebeci, R.E. Cohen and M.F. Rubner. Stable superhydrophobic coatings from polyelectrolyte multilayers. Nanoletters. 4, 7 (2004) : 1349-1353.
- [36] J.T. Han, Y. Zheng, J.H. Cho, X. Xu and K. Cho, Stable superhydrophobic organic-inorganic hybrid films by electrostatic self-assembly. J. Phys. Chem. B. 109 (2005) : 20773-20778.
- [37] W. Li and A. Amirfazli. A thermodynamic approach for determining the contact angle hysteresis for superhydrophobic surfaces. J. Colloid Interface Sci. 292 (2005) : 195-201.
- [38] A.J. Kinloch. Adhesion and adhesives: science and technology. London : Chapman & Hall, 1987.
- [39] T. Fort and H.T. Patterson. A simple method for measuring solid-liquid contact angles. J. Colloid Sci. 18 (1963) : 217-222.
- [40] R.E. Johnson and R.H. Dettre. Advances in chemistry series. 43. Washington : American Chemical Society, 1964.
- [41] A.W. Neumann and R.J. Good. Thermodynamics of contact angles. I. Heterogeneous solid surfaces. J. Colloid Interface Sci. 38 (1972) : 341-358.
- [42] D.G. Rance. Industrial adhesion problems. Oxford : Orbital Press, 1985.
- [43] E. Pesonen-Keinonen. Determination of cleanability of plastic surfaces. Dissertation Department of Agrotechnology University of Helsinki, 2005.
- [44] P.K. Sharma and K.H. Rao. Analysis of difference approaches for evaluation of surface energy of microbial cells by contact angle goniometry. Adv. Colloid Interface Sci. 98, 3 (2002) : 341-463.
- [45] W.A. Zisman and H.W. Fox. The spreading of liquids on low-energy surfaces II. Moldified tetrafluoroethylene polymers. J. Colloid Sci. 7 (1952) : 109-121.
- [46] F.M. Fowkes. Attractive Forces at Interfaces. Ind. Eng. Chem. 56, 12 (1964) : 40-52.
- [47] D.K. Owen and R.C. Wendt. Estimation of the surface free energy of polymers. J.

- App. Poly. Sci. 13 (1969) : 1741-1917.
- [48] D.Y. Kwok and A.W. Neumann. Contact angle measurements and interpretation: wetting behavior and solid surface tension for poly(alkyl metacrylate) polymers. J. Adhesion Sci. Technol. 14, 5 (2000) : 719-743.
- [49] C.J. Van Oss, R.J. Good and M.K. Chaudhury. Additive and non-additive surface tension components and the interpretation of contact angles. Langmuir, 4, 4 (1988) : 884-891.
- [50] A.W. Neumann, R.J. Good, C.J. Hope and M. Sejpal. An equation-of-state approach to determine surface tensions of low-energy solids from contact angles. J. Colloid Interface Sci. 49, 2 (1974) : 291-304.
- [51] D. Li and A.W. Neumann. Equation of state for interfacial tensions of solid-liquid systems. Adv. Colloid Interface Sci. 39 (1992) : 299-345.
- [52] C.M. Castilho Pereira, A. Catarino Fernandes and B. Saramago. The surface tension of Cork from Contact Angle Measurements. J. Colloid Interface Sci. 156 (1993) : 195-201.
- [53] H.J. Jacobasch, K. Grundke E. Mader, K.H. Freitag and U. Panzer. Application of the surface free energy concept in polymer processing. Netherlands : VSP BV, 1993.
- [54] M.C. Michalski, S. Desobry, V. Babak and J. Hardy. Adhesion of food emulsions to packaging and equipment surfaces. Colloids Surf. A: Physicochem. Eng. Aspects. 149, 1-3 (1999) : 107-121.
- [55] E.F. Hare E.G. Shaffrin and W.A. Zisman. Properties of films of absorbed fluorinated acids. J. Phys. Chem. 58 (1954) : 236-239.
- [56] D.Y. Kwok and A.W. Neumann. Contact angle measurement and contact angle interpretation. Adv. Colloid interface Sci. 81 (1999) : 167-249.
- [57] S.H. Wu. Polymer interface and adhesion, Marcel Dekker Press, New York, 1982.
- [58] B. He, J. Lee and N.A. Patankar. Contact angle hysteresis on rough hydrophobic surfaces. Colloids Surf. A: Physicochem. Eng. Aspects. 248, 1-3 (2004) : 101-104.
- [59] T. Young. An Essay on the Cohesion of Fluids. Trans. Roy. Soc. 95 (1805) : 65-87.

- [60] R.N. Wenzel. Surface roughness and contact angle. J. Phys. Colloid Chem. 53 (1949) : 1466-1467.
- [61] K. Gjerde, R.T.R. Kumar, K.N. Andersen, J.K. Hansen, K.B.K. Teo, W.I. Milne, C. Persson, K. Molhave, H.G. Rubahn and P. Boggild. On the suitability of carbon nanotube forests as non-stick surfaces for nanomanipulation. soft matter, 4 (2008) : 392-399.
- [62] J. Li, J. Fu, Y. Cong, Y. Wu, L. Xue and Y. Han. Macroporous fluoropolymeric films templated by silica colloidal assembly: a possible route to superhydrophobic surfaces. App. Surf. Sci. 252 (2006) : 2229-2234.
- [63] T. Onda, S. Shibuchi, N. Satoh and K. Tsujii. Super-water-repellent fractal surfaces. Langmuir. 12 (1996) : 2125-2127.
- [64] M.T. Khorasani, H. Mirzadeh and Z. Kermani. Wettability of porous polydimethylsiloxane surface: morphology study. Appl. Surf. Sci. 242 (2005) : 339-345.
- [65] M.H. Jin, X.J. Feng, J.M. Xi, J. Zhai, K.W. Cho and L. Feng. Superhydrophobic PDMS surface with ultra-low adhesive force. Macromol. Rapid Commun. 26 (2005) : 1805-1809.
- [66] M.H. Sun, C.X. Luo, L.P. Xu, H. Ji, O.Y. Qi, and D.P. Yu. Artificial lotus leaf by nanocasting. Langmuir, 21 (2005) : 8978-8981.
- [67] M. Ma, R.M. Hill, J.L. Lowery, S.V. Fridrikh and G.C. Rutledge. Electrospun poly(styrene-block-dimethylsiloxane) block copolymer fibers exhibiting superhydrophobicity. Langmuir, 21 (2005) : 5549-5554.
- [68] N. Zhao, Q.D. Xie, L.H. Weng, S.Q. Wang, X.Y. Zhang and J. Xu. Superhydrophobic surface from vapor-induced phase separation of copolymer micellar solution. Macromolecules. 38 (2005) : 8996-8999.
- [69] R.A. Pullin, T.G. Nevell and J. Tsibouklis. Surface energy characteristics and marine antifouling performance of poly(1H, 1H, 2H, 2H-perfluorodecanoyl diitaconate) film structures. Mater. Lett. 39 (1999) : 142-148.
- [70] E. Chibowski. Surface free energy of a solid from contact angle hysteresis. Adv. Colloid Interface Sci. 103 (2003) : 149-172.
- [71] E. Chibowski, L. Holysz, K. Terpilowski and M. Jurak. Investigation of super-

- hydrophobic effect of PMMA layers with different fillers deposited on glass support. Colloid Surf. A: Physicochem. Eng. Aspects, 291 (2006) : 181-190.
- [72] C.W. Extrand. Water contact angles and hysteresis of polyamide surfaces. J. Colloid Interface Sci. 248 (2002) : 136-142.
- [73] W. Li and A. Amirfazli. A thermodynamic approach for determining the contact angle hysteresis for superhydrophobic surfaces. J. Colloid Interface Sci. 292 (2005) : 195-201.
- [74] T. YAbuta, K. Tsuru, S. Hayakawa and A. Osaka. Synthesis of blood compatible PDMS-based organic-inorganic hybrid coatings. J. Sol-Gel Sci. Tech. 31 (2004) : 273-276.
- [75] L.Q. Tang, Y.Y. Wang and L. Yin. Study of wettability and resin bonding strength of H-DLC coating on pure titanium. J. US-China Medical Sci. 4, 5 (2007) : 43-46.
- [76] E. Radlein and G.H. Frischat. Atomic force microscopy as a tool to correlate nanostructure to properties of glasses. J. Non-Cryst. Solids. 222 (1997) : 69-82.
- [77] J.D. Mendelsohn, S.Y. Yang, J. Hiller, A.I. Hochbaum and M.F. Rubner. Rational Design of cytophilic and cytophobic polyelectrolyte multilayer thin films. Biomacromolecules. 4 (2003) : 96-106.
- [78] S.S. Shiratori and M.F. Rubner. pH-dependant thickness behavior of sequentially adsorbed layers of weak polyelectrolytes. Macromolecules. 33 (2000): 4213-4219.
- [79] D.M. DeLongchamp and P.T. Hammond. Fast ion conduction in layer-by-layer polymer films. Chem. Mater. 15 (2003) : 1165-1173.
- [80] D. Yoo, S.S. Shiratori and M.F. Rubner. Controlling bilayer composition and surface wettability of sequentially adsorbed multilayers of weak polyelectrolytes. Macromolecules. 31 (1998) : 4309-4318.
- [81] J. Cho and K. Char. Effect of layer integrity of spin self-assembled multilayer films on surface wettability. Langmuir. 20 (2004) : 4011-4016.
- [82] B. Memaa, M. Takahashi, Y. Tokuda and T. Yoko. Preparation and properties of polyphenylsiloxane-based hybrid glass films obtained from a non-aqueous coating sol via a single-step dip coating. Optical Materials. 29 (2007) : 806-813.
- [83] Y.Y. Yu, C.Y. Chen and W.C. Chen. Synthesis and characterization of organic-

inorganic hybrid thin films from poly(acrylic) and nonodispersed colloidal silica. Polymer, 44 (2003) : 593-601.

[84] R. Vogel, P. Meredith and I. Krtini. Mesistructure dye-doped titanium dioxide for micro-optoelectronic application. Chem. Phy. Chem. 4 (2003) : 595-603.

[85] G. Camino, S.M. Lomakin and M. Lazzari. Polydimetylsiloxane thermal degradation part 1, kinetic aspects. Polymer, 42 (2001) : 2395-2402.



ศูนย์วิทยทรัพยากร
จุฬาลงกรณ์มหาวิทยาลัย



ศูนย์วิทยทรัพยากร
จุฬาลงกรณ์มหาวิทยาลัย

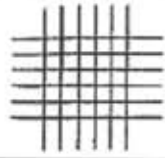
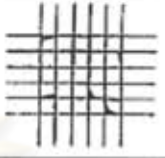
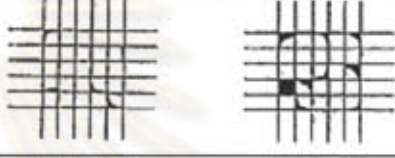

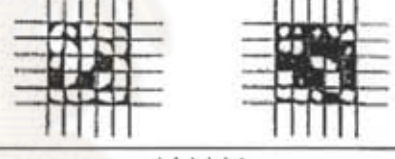
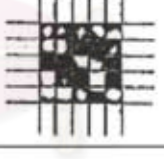


APPENDIX A


A CLASSIFICATION OF ADHESION TEST RESULTS

ศูนย์วิทยทรัพยากร
จุฬาลงกรณ์มหาวิทยาลัย

Table A.1 Classification of adhesion test results. Grid size is 1 mm x 1 mm.

Classification	Percent area removed	Surface of cross-cut area from which flaking have occurred for six parallel cuts and adhesion range by percent
5B	0% None	
4B	Less than 5%	
3B	5 – 15%	
2B	15 – 35%	
1B	35 – 65%	
0B	Greater than 65%	

ศูนย์วิทยทรัพยากร
จุฬาลงกรณ์มหาวิทยาลัย



APPENDIX B
ADHESION TEST RESULTS FROM TAPE TEST

ศูนย์วิทยทรัพยากร
จุฬาลงกรณ์มหาวิทยาลัย

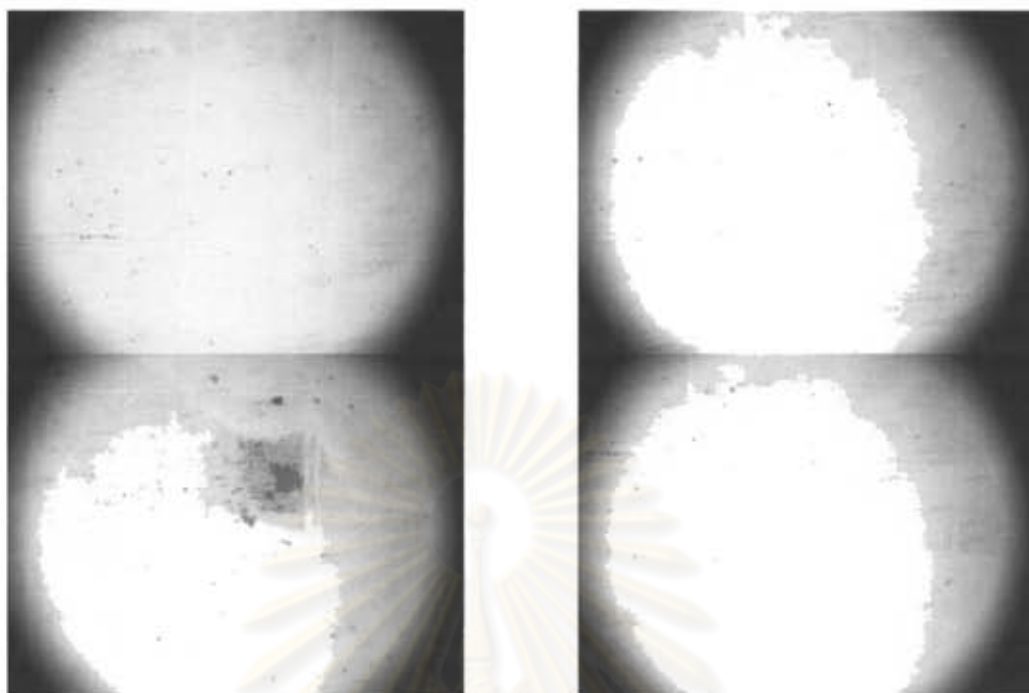


Figure B.1 Film containing Aerosil® 200 at 0.05 wt% before tape test.

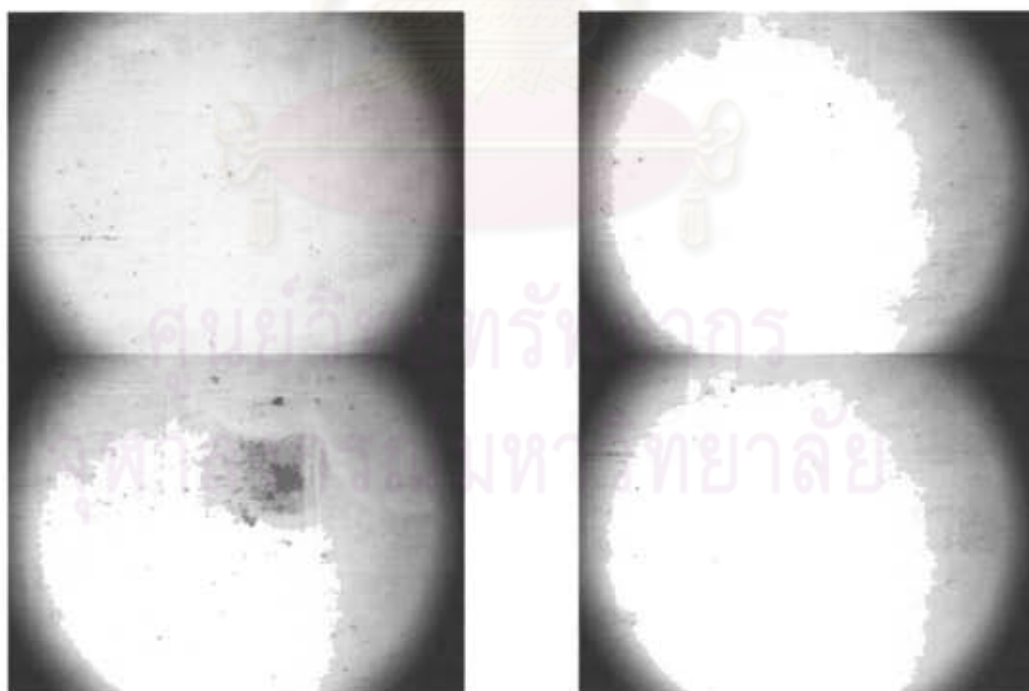


Figure B.2 Film containing Aerosil® 200 at 0.05 wt% after tape test.

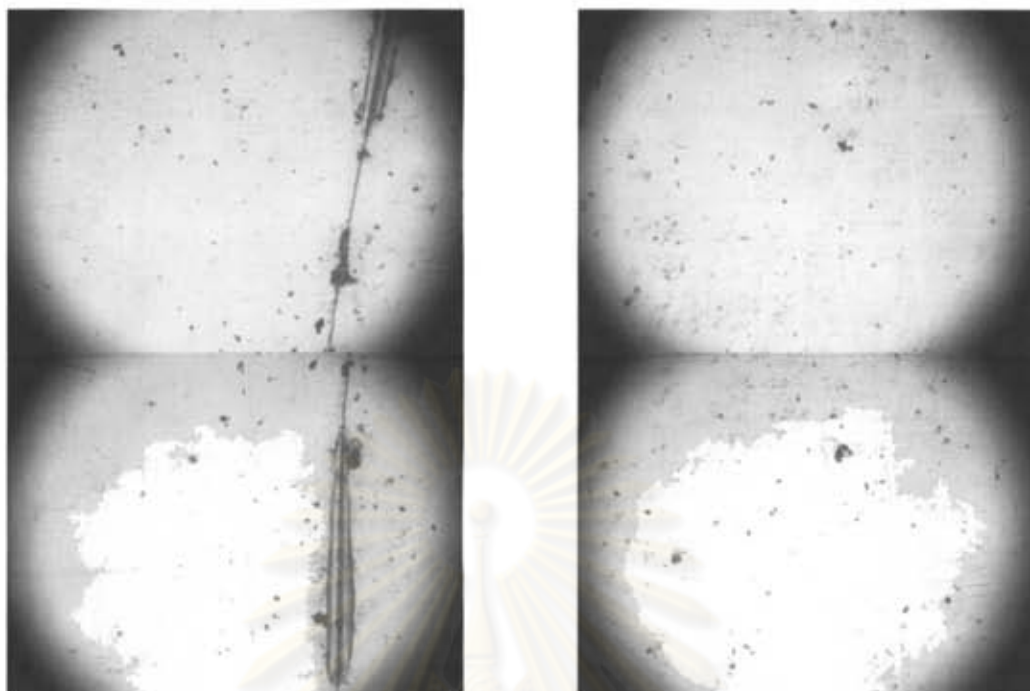


Figure B.3 Film containing Aerosil[®] 200 at 1 wt% before tape test.

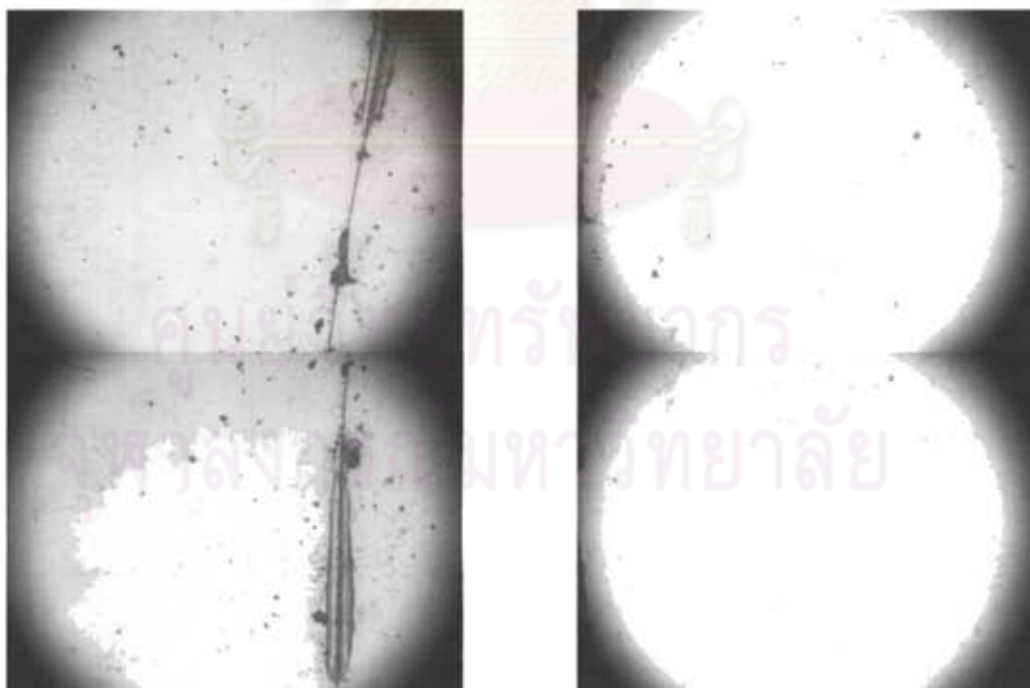


Figure B.4 Film containing Aerosil[®] 200 at 1 wt% after tape test.

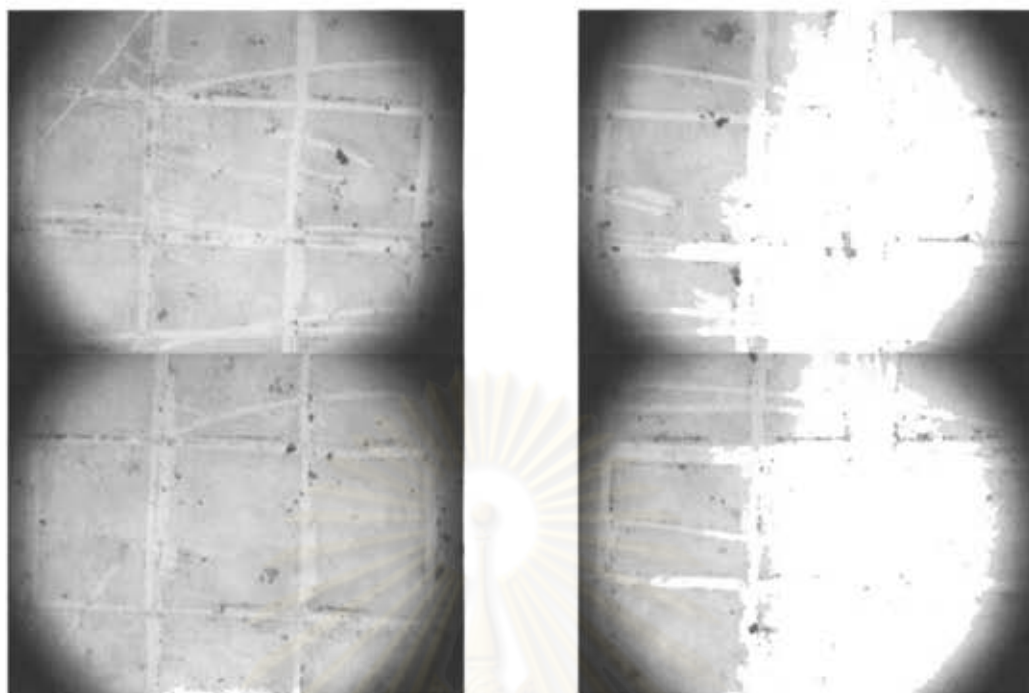


Figure B.5 Film containing Aerosil[®] 200 at 5 wt% before tape test.



Figure B.6 Film containing Aerosil[®] 200 at 5 wt% after tape test.



Figure B.7 Film containing Aeroperl[®] 300/30 at 0.05 wt% before tape test.



Figure B.8 Film containing Aeroperl[®] 300/30 at 0.05 wt% after tape test.



Figure B.9 Film containing Aeroperl[®] 300/30 at 1 wt% before tape test.



Figure B.10 Film containing Aeroperl[®] 300/30 at 1 wt% after tape test.



Figure B.11 Film containing Aeroperl[®] 300/30 at 5 wt% before tape test.



Figure B.12 Film containing Aeroperl[®] 300/30 at 5 wt% after tape test.



Figure B.13 Film containing Aeroperl[®] 806/30 at 0.05 wt% before tape test.



Figure B.14 Film containing Aeroperl[®] 806/30 at 0.05 wt% after tape test.



Figure B.15 Film containing Aeroperl[®] 806/30 at 1 wt% before tape test.



Figure B.16 Film containing Aeroperl[®] 806/30 at 1 wt% after tape test.



Figure B.17 Film containing Aeroperl® 806/30 at 5 wt% before tape test.



Figure B.18 Film containing Aeroperl® 806/30 at 5 wt% after tape test.

BIOGRAPHY

- Name: Sunisa Jindasuwan
- Birthday: 18 January 1979
- Education: 2000 Bachelor's degree in industrial chemistry, Faculty of Applied Science,
King Mongkut's Institute of Technology North Bangkok, Thailand
2003 Master's degree in material science, Graduate College,
King Mongkut's Institute of Technology North Bangkok, Thailand
- Publication: Hydrophobicity and topology analysis of polydimethylsiloxane-base
Organic/inorganic hybrid films., J. Microscopy Society of Thailand, Vol.21
(2007) : 282-283.
Relationship between chemical composition and hydrophobicity of sol-gel-
derived TiO₂/polydimethylsiloxane hybrid films., The 2nd International on
Advances in Petrochemicals and Polymers (2007).
Stability study of a transparent superhydrophobic self-cleaning glass.,
German-Thai Symposium on Nanoscience and Nanotechnology
Proceedings (2007).
Effect of SiO₂ content on superhydrophobicity and transparency of silica-
polyelectrolyte multilayer films., Pure and Applied Chemistry International
Conference (2008).
Surface characteristics of water-repellent polyelectrolyte multilayer films
containing various silica content., The 4th International conference on
Technological Advances of Thin Films & Surface Coating (2008), submitted
to Thin Solid Films.
Effect of heat treatment temperature on surface topography and
hydrophobicity of polydimethylsiloxane/titanium oxide hybrid films.,
Macromolecular Symposia., Vol.264 (2008), 90-94.
Influence of surface roughness and surface free energy on contact angle of
superhydrophobic films., The 2nd Thammasat University International
Conference on Chemical, Environmental and Energy Engineering (2009).